RV SONNE
CRUISE REPORT SO148
TECFLUX - II - 2000
TECTONICALLY-INDUCED MATERIAL FLUXES

VICTORIA - VICTORIA - VICTORIA
JULY 20 - AUGUST 15, 2000

Leg SO148-1: Victoria - Victoria
July 20 - August 3, 2000

Leg SO148-2: Victoria - Victoria
August 4 - August 15, 2000

Edited by
Peter Linke and Erwin Suess
with contributions of cruise participants

GEOMAR
Forschungszentrum
für marine Geowissenschaften
der Christian-Albrechts-Universität
zu Kiel

KIEL 2001

GEOMAR REPORT 98

GEOMAR
Research Center
for Marine Geosciences
Christian Albrecht University
in Kiel

Redaktion dieses Reports: Peter Linke und Erwin Suess

GEOMAR REPORT
ISSN 0936 - 5788

GEOMAR
Forschungszentrum
für marine Geowissenschaften
Wischhofstr. 1-3
D - 24148 Kiel
Tel. (0431) 600-2555, 600-2505

Editor of this issue: Peter Linke and Erwin Suess

GEOMAR REPORT
ISSN 0936 - 5788

GEOMAR
Research Center
for Marine Geosciences
Wischhofstr. 1-3
D - 24148 Kiel
Tel. (49) 431 / 600-2555, 600-2505

Table of Contents

PREFACE

E. Suess, P. Linke

The TECFLUX program (= TECtonically induced FLUXes) addresses geophysical, biogeochemical, and hydrographic processes associated with fluid venting from the Cascadia continental margin, specifically the processes resulting from the methane hydrate dynamics at Hydrate Ridge. An international group of scientists from institutions in Germany, the USA, Canada, and Japan (see list of participating institutions) established a long-term research program based on the initial discovery in 1996 of methane hydrate exposures. At this margin site mixed methane-sulfide hydrates and carbonates form a pavement along the crest of the ridge at water depths between 600–1000 m. Vent fields from which methane-charged, low-salinity fluids containing sulfide, ammonia, ^4He, and isotopically light CO_2 escape, are associated with these exposures. The fluid emissions characterize a newly recognized mechanism of dewatering at convergent margins. However, the rates of discharge, the fluctuations and frequency of pulses, as well as the mechanisms responsible for the modulations of flow are totally unknown. Also immediate and intriguing questions concerning the composition, depth distribution, interlayering with sediment, and physical properties of these near-surface gas hydrates were to be addressed during SONNE Cruise 148.

Initial results suggest that hydrate-related fluid emissions lead to local dewatering rates that are much higher than at other margins in the absence of hydrate. Discharge of fluids stimulates benthic oxygen consumption that is orders of magnitude higher than is normally found at comparable ocean depths. Extensive coverage of the seafloor by bacterial mats and hydrogen sulfide immediately below the seafloor suggest an intimate relationship between hydrate exposure, fluid discharge, biological community structure and activity, and total sediment respiration. During previous investigations (SO 110/ROPOS, RV ATLANTIS/ALVIN Cruise AT3-35b, SO143) vigorous discharge of methane bubbles was observed at the northern summit of the ridge at depths where hydrates are actually stable. The injection of methane from the ridge generates a plume hundreds of meters high and several kilometers wide. A large fraction of the methane appears to be oxidized within the water column and generates $\partial^{13}C$ anomalies of the dissolved inorganic carbon pool, although it remains unclear if, where, and how much methane escapes to the atmosphere.

The widespread carbonate pavement as well as the chemoherms result from bacterial methane oxidation and subsequent precipitation of a variety of carbonate mineral phases and fabrics leading to the recognition of a class of carbonates with considerable diagnostic features related to gas hydrates. The subsurface extent of the chemoherms, the detailed petrographic, isotopic, and structural relationship of the carbonates are presently unknown but contain enough information from which -in conjunction with rates of biogeochemical turnover- a budget of past and present carbon emissions may be derived.

The expedition and program of TECFLUX were jointly planned, coordinated and carried out by the GEOMAR Research Center for Marine Geosciences at Kiel and the College of Ocean and Atmospheric Sciences of Oregon State University, Corvallis with a large number of investigator groups from different institutions (see list of participating institutions). The projects were financed in Germany by the Federal Ministry of Science and Technlogy, Bonn. Project review and scheduling of the SONNE Cruise 148 was handled efficiently by the Projektträger Biologie, Energie und Umwelt, Jülich-Warnemünde. On behalf of all participants we wish to thank these agencies,

departments, and staff for their support. The ROPOS crew demonstrated that the ROV system ROPOS is a valuable and reliable work tool which ideally supplements the existing instrumentation on a research vessel like SONNE. The Reedereigemeinschaft Forschungsschifffahrt, RF Bremen, as always, provided technical support on the vessel in order to accommodate the variety of technological, electronic, and navigational challenges required for the complex sea-going operations. We would like to especially acknowledge the vessel's master H. Andresen (SO148) and H. Papenhagen (SO150) and their crews for their continued interest, flexibility, patience, and their contribution to provide an always pleasant and professional atmosphere aboard.

Scientific crew

Leg SO148-1: 20 July - 3 August, Victoria – Victoria

Appel, Frank	OKTOPUS, Hohenwestedt
Bannert, Bernhard	OKTOPUS, Hohenwestedt
Bock, Barbara	GEOMAR, Kiel
Boetius, Antje	MPI, Bremen
Bohrmann, Gerhard	GEOMAR, Kiel
Domeyer, Bettina	GEOMAR, Kiel
Heeschen, Katja	OSU/GEOMAR
Heuser, Alexander	GEOMAR, Kiel
Holland, Bob	CSSF, Sydney
Jung, Carmen	GEOMAR, Kiel
Karpen, Volker	GEOMAR, Kiel
Linke, Peter	**GEOMAR, Kiel**
Müller, Matthias	GEOMAR, Kiel
Murdock, Ian	CSSF, Sydney
Nakamura, Ko-ichi	GSJ, Ibaraki
Petersen, Asmus	K.U.M., Kiel
Rickert, Dirk	GEOMAR, Kiel
Shepherd, Keith	CSSF, Sydney
Teichert, Barbara	GEOMAR, Kiel
Treude, Tina	MPI, Bremen
Vaessen, Bernd	GEOMAR, Kiel
Vorhees, Andrea	OSU, Corvallis
Wallace, Kim	CSSF, Sydney
Yamazaki, Tetsuo	GSJ, Ibaraki

Leg SO148-2: 4 Aug - 15 August, Victoria – Victoria

Bock, Barbara	GEOMAR, Kiel
Bohrmann, Gerhard	GEOMAR, Kiel
Cremer, Axel	Biolab, Hohenwestedt
Dempsay, Michael	CSSF, Sydney
Domeyer, Bettina	GEOMAR, Kiel
Goergens, Rainer	BGR, Hannover
Grant, Nicholas	UVIC, Victoria
Heeschen, Katja	OSU/GEOMAR
Heuser, Alexander	GEOMAR, Kiel
Hohenberg, Hans-Jürgen	TU Berlin
Jung, Carmen	GEOMAR, Kiel

Karpen, Volker	GEOMAR, Kiel
Kudrass, Herrmann	BGR, Hannover
Müller, Matthias	GEOMAR, Kiel
Murdock, Ian	CSSF, Sydney
Petry, Daniel	Context TV, Berlin
Rickert, Dirk	GEOMAR, Kiel
Sahling, Heiko	GEOMAR, Kiel
Suess, Erwin	**GEOMAR, Kiel**
Steinmann, Rüdiger	BGR, Hannover
Tamburri, Keith	CSSF, Sydney
Teichert, Barbara	GEOMAR, Kiel
Vorhees, Andrea	OSU, Corvallis
Wallace, Kim	CSSF, Sydney
Yamazaki, Tetsuo	GSJ, Ibaraki

Personnel of the Reedereigemeinschaft Forschungsschiffahrt GmbH, Bremen

Callao - Victoria/Canada	Leg SO148-1	Leg SO148-2
Andresen, Hartmut	**Andresen, Hartmut**	**Andresen, Hartmut**
Bendin, Axel	Bendin, Axel	Bendin, Axel
Bierstedt, Torsten	Blohm, Volker	Blohm, Volker
Blohm, Volker	Boldt, Wieland	Boldt, Wieland
Boldt, Wieland	Braatz, Willy	Braatz, Willy
Braatz, Willy	Eller, Peter	Eller, Peter
Eller, Peter	Grund, Helmut	Grund, Helmut
Grund, Helmut	Gudera, Manfred	Gudera, Manfred
Gudera, Manfred	Guzman N., Werner	Hoffmann, Hilmar
Guzman N., Werner	Hoffmann, Hilmar	Isbrecht, Frank
Hoffmann, Hilmar	Isbrecht, Frank	Jahns, Winfried
Isbrecht, Frank	Jahns, Winfried	Kaiser, Reiner
Kaiser, Reiner	Kaiser, Reiner	Klein, Andreas
Klein, Andreas	Klein, Andreas	Konrath, Rolf
Konrath, Rolf	Konrath, Rolf	Köthe, Wolfgang
Köthe, Wolfgang	Köthe, Wolfgang	Löffler, Jörn
Löffler, Jörn	Löffler, Jörn	Lößnitz, Leonore
Lößnitz, Leonore	Lößnitz, Leonore	Mucke, Hans-Peter
Mischker, Joachim	Mucke, Hans-Peter	Neumann, Peter Gerhard
Mucke, Hans-Peter	Neumann, Peter Gerhard	Reichmacher, Wolfgang
Neumann, Peter Gerhard	Reichmacher, Wolfgang	Schade, Uwe
Reichmacher, Wolfgang	Stammer, Kurt	Stammer, Kurt
Stammer, Kurt	Stenzler, Joachim	Stenzler, Joachim
Stenzler, Joachim	Teichert, Klaus	Teichert, Klaus
Teichert, Klaus	Tiemann, Frank	Tiemann, Frank
Tiemann, Frank	v. Arronet, Johannes	v. Arronet, Johannes
v. Arronet, Johannes	Ventz, Günter	Ventz, Günter
Ventz, Günter	Vöhrs, Helmut	Vöhrs, Helmut
Vöhrs, Helmut	vom Berg, Götz	vom Berg, Götz
Wege, Andreas	Wege, Andreas	Wege, Andreas

Participating institutions

GEOMAR Forschungszentrum für marine Geowissenschaften der Christian-Albrechts-Universität zu Kiel
Wischhofstraße 1-3
24148 Kiel, Germany

College of Oceanic and Atmospheric Sciences
Oregon State University
Ocean Admin. Bldg. 104
Corvallis, Oregon 97331-5503
U.S.A.

School of Earth and Ocean Sciences
University of Victoria
P.O. Box 3050
Victoria, BC, V8W 2Y2, Canada

Marine Geology Department
Geological Survey of Japan
1-1-3 Higashi
Tsukuba, Ibaraki 305, Japan

Technische Universität Berlin
Maritime Technik
Müller-Breslau-Str.
10623 Berlin, Germany

Max Planck Institut für Marine Mikrobiologie
Celsiusstr.1
28359 Bremen, Germany

Bundesanstalt für Geowissenschaften und Rohstoffe
Stilleweg 2
30161 Hannover, Germany

Context TV
Lützowstr.92
10785 Berlin, Germany

OKTOPUS GmbH
Kieler Straße 51
24594 Hohenwestedt, Germany

K.U.M. Umwelt- und Meerestechnik Kiel GmbH
Wischhofstraße 1-3, Geb. D5
24148 Kiel, Germany

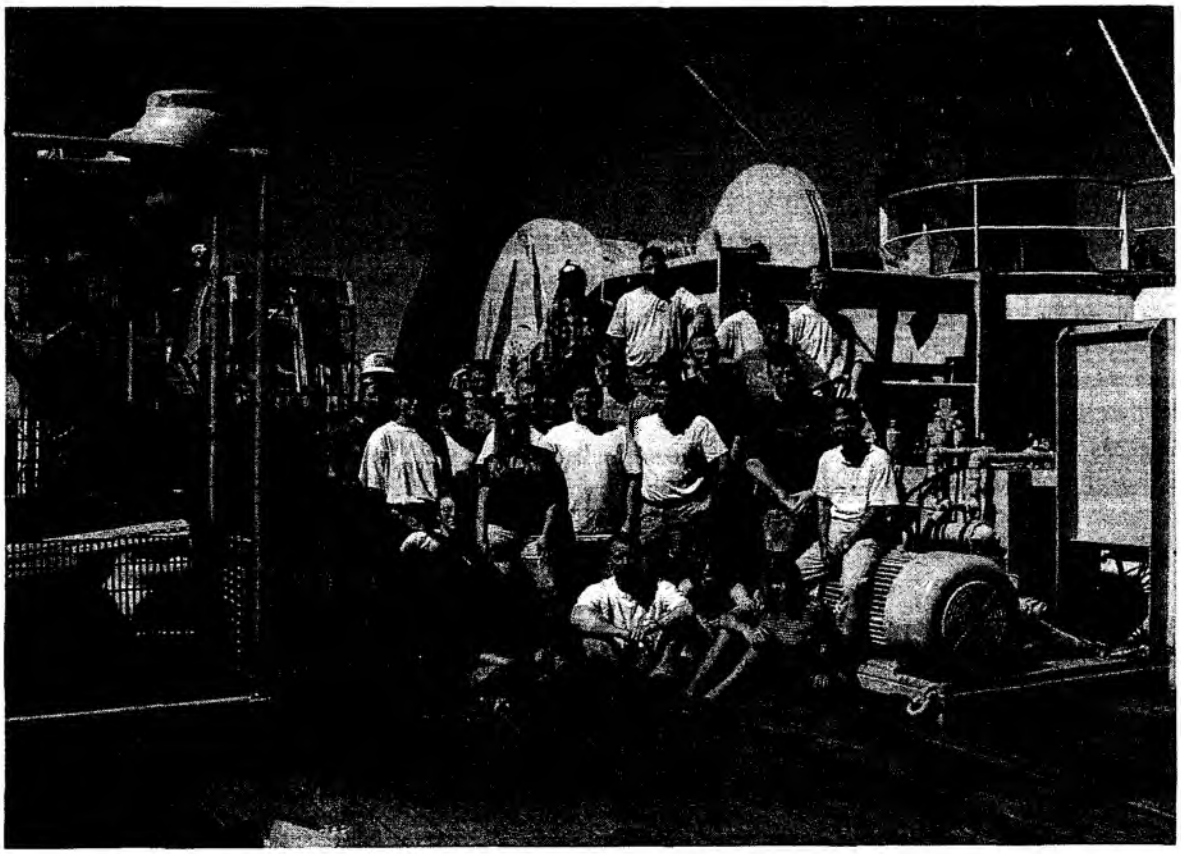

Fig. 1: Scientific crew of Leg SO148-1.

Fig. 2: Scientific crew of Leg SO148-2.

1 INTRODUCTION

E. Suess

1.1 Objectives

The fault pattern on Hydrate Ridge, generated by subduction of the Juan de Fuca Plate underneath the North American Plate is wellknown (Kulm et al., 1986; MacKay, 1995; MacKay et al., 1992) and is related to the evolution and growth of accretionary tectonics of the Cascadia convergent margin (Fig. 3). The faults extend through the accreted sediments to below the gas hydrate phase transition. At depth, they tap a fluid reservoir, which contains free methane. The faults serve as conduits and channel methane up to the seafloor where it either escapes into the water column or forms secondary gas hydrates. The secondary sea-floor hydrates are very porous and less dense than sea water. As the layers grow downward towards the rising stream of methane, their buoyancy eventually exceeds the lithostatic loading by sediments and chunks of hydrate detach and float to the sea surface. The scenario for the development of hydrate floats is reconstructed based on high-resolution small-scale mapping of vent fields and hydrate exposures and on sampling of the complete gas hydrate–pore water–sediment system which were the objectives of previous SONNE expeditions. In piecing together this scenario, which represents an efficient mechanism for this greenhouse gas to escape into the atmosphere, extensive new observations from ROPOS and sea floor video-surveys and sampling from aboard RV SONNE are required. With this background and the central objective of the TECFLUX campaign, to understand the dynamics of near-surface gas hydrates, the following scientific objectives were adressed during SONNE Cruise 148:

- Map and discover new vent sites, chemoherms, and hydrate carbonate occurrences by Ocean Floor Observation System;
- Obtain time-series of gas & fluid emissions: VESP lander, bubble camera & mirror camera;
- Sample „pristine" vent fluids from hydrate reservoirs (fresh/salty) with ROPOS suction sampler/vent funnel;
- Maintain hydrates at *in situ* conditions;
- Determine "pristine" hydrate properties using specific sampling protocol: (density, fabric, total gas composition, total gas content; hydrate water);
- Ascertain „water limitation" and „salt exclusion" hypotheses for subsurface hydrate formation using piston cores;
- Ascertain and recover „styrofoam" fabric in order to understand occurrence of „hydrate floats";
- Determine composition, structure and plumbing of pinnacles/chimneys from carbonate lithologogies and fabric;
- Determine methane bubble behavior in the water column from visual observations by ROV, CTDs & methane sensor & hydroacoustics;
- Quantify relationship between microbial biomass and nitrate storage capacity in bacterial mats;
- Determine rates of microbial sulfate reduction and methane oxidation;
- Recover Autoclav-sampler.

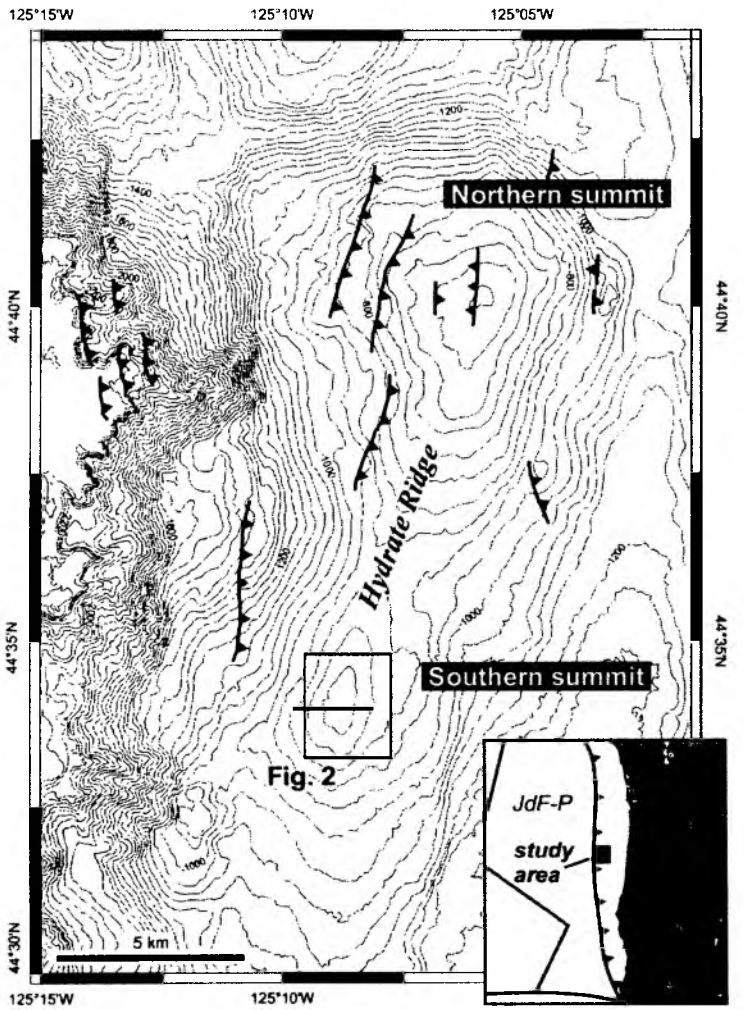

Fig. 3: Bathymetry of Hydrate Ridge, the second accretionary ridge and area of TECFLUX-work: box = southern summit; E-W line = 18 kHz section; inset = plate tectonic setting of the Cascadia convergent margin.

1.2. Background

More than a decade of research on the Cascadia convergent margin has documented active venting of fluids and gases and exposures of methane hydrates at the seafloor. Hydrates were recognized in seismic reflection data (McKay et al., 1994; Tréhu et al., 1999). Hydrates were encountered in cores by deep sea drilling (ODP Leg 146; Kastner et al., 1998) and hydrates were directly sampled from exposures at the sea floor during the RV SONNE cruises (Suess et al., 1999; Bohrmann et al., 2000). Water depth and temperature place these hydrates close to their stability limit, hence minor changes in these conditions may have a major effect on the destabilization of hydrates and in turn profound environmental consequences. Part of the methane from destabilization of hydrate is injected into the water column to form extensive plumes. The behavior of methane plumes appears critical in order to evaluate how much, if any, of this potent greenhouse gas escapes into the atmosphere or is utilized within the interior of the ocean. Another part of the methane provides an enormously rich carbon and energy reservoir for benthic life. Efficient methane turnover by highly specialized methane-oxidizing communities at the seafloor generate widespread authigenic carbonates

around the exposures of hydrates. Again, the question of partitioning the methane carbon pool into biological tissue, respired carbon dioxide, carbonate, and free methane gas remains to be addressed.

There is current consensus that research on the biogeochemical processes associated with gas hydrate dynamics and fluid venting in continental margins constitutes a first order scientific objective (Suess and Thiede, 1999). Therefore, understanding of hydrate dynamics and the effects on benthic fluxes and diagenetic pathways of carbon and trace gases in the specific tectonic setting of the Cascadia margin could ultimately shed light on several broader issues. Foremost among these are climate-forcing by gas hydrate eruptions on a global scale (MacDonald, 1994; Dickens et al., 1997; Kennett et al., 2000), the development of mega-slumps on continental margins by gas hydrate destabilization and the generation of tsunamis (Rothwell et al., 1998; Bralower et al., 1997), as well as perturbations on the global carbon cycle (Dickens, 1999), not to mention the need for better estimates of the magnitude of the fossil fuel-based energy resource which is believed to reside in marine and terrestrial gas hydrates (Kvenvolden, 1993).

1.3. Methane Hydrate Manifestations at Hydrate Ridge

A pavement of carbonate crusts, bacterial mats and hydrates was imaged on Hydrate Ridge by a video survey in 1996 and retrieved by a TV-guided grab sampler (Fig. 4). Massive hydrate was obtained at the southern summit from just beneath the thinly sediment-covered surface and at the northern summit from sediments accumulating in tensional fractures between blocks of the chemoherm carbonates (Suess et al., 1999; Bohrmann et al., 1998). In June of 1999 a new side-scan sonar survey of the area, supplementing earlier work (Zhou et al., 1999; Carson et al., 1994), showed in detail that the ridge flank, the saddle, and crestal region are covered by acoustically hard, highly reflective materials related to fluid venting. Several new targets were identified, either as "white spots", "scars", "pock marks", "pinnacles" or "mud diapirs", which indicate anomalous environments or manifestations of hydrates and fluid venting. Particularly on the southern summit such features at the sea floor as well as in the water column suggested a number of important targets for the TECFLUX'2000 campaign. Mapping and discovering new vent sites, chemoherms, and hydrate carbonate occurrences by OFOS is one objective of the SONNE Cruise 148. Determination of composition, structure and plumbing of carbonate pinnacles/chimneys from carbonate lithologies and fabric is another major goal of the cruise SO148.

The sea floor at the summit resembles a chaotic landscape dotted with pockmarks and sediment drifts, where carbonate pinnacles, hydrate exposures, bacterial mats, and clam colonies vary on a meter-scale. Astounding is the chaotic appearance of the surface with dune-like sediment bodies, barren of any biota, alternating with depressions containing multi-colored patches of prolific vent biota. Video-observations revealed a vague zonation of the vent activity with clam colonies and carbonate pinnacles at the outer perimeter, and bacterial mats and mixed patches of biota towards the center. The chaotic landscape is most characteristically developed towards the northern end of the summit with a vigorously flowing methane vent roughly in its center. During cruise SO148 visual observations of methane bubble behavior in the water column using ROPOS, bubble & mirror cameras are first order objectives. The mechanisms of transport of gases and fluids through the methane stability zone is still not clearly

understood and remains to be solved during SO148. With ROPOS suction samplers and the VESP funnel "pristine" vent fluids from hydrate reservoirs should be sampled.

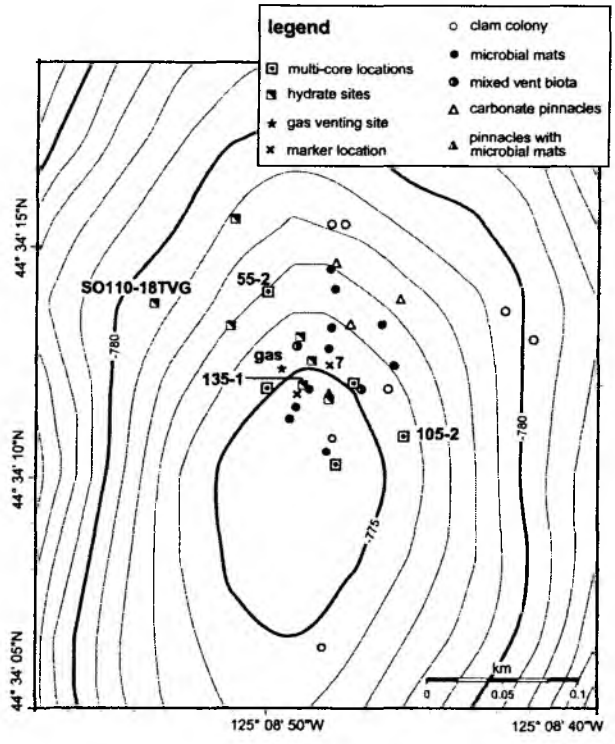

Fig. 4: Southern summit vent activities and core locations.

1.4. Chloride-Anomaly Pattern

Not until future samples can be taken *in situ* and transported to the laboratory for study with pressure and temperature maintained at *in situ* conditions, the retrieval of gas hydrates is fortuitous at present Indirect evidence for the presence of gas hydrates is provided by the well-known artifact of negative Cl-anomalies in pore fluids (Suess, von Huene et al., 1988; Paull et al., 1996). The anomalies result from the release of hydrate water during core retrieval with the dilution of the normal pore water salinity.

Using this approach, we have mapped the negative Cl-anomalies in pore fluids of near-surface sediments on the southern summit and estimated the hydrate content. Combined with the visual observations of methane ebullition and video-documentation of hydrate exposures intimately associated with biota and carbonates, these data provide convincing evidence for the highly dynamic and patchy distribution of seafloor hydrates.
Cl-depletion indicates the presence of gas hydrates in the sediments either as discrete layers between the surface and 25 cmbsf of the TV-guided multi-cores or as massive layer at depth. The TV-guided grab samples reached these more massive hydrate layers located between 30 and 50 cmbsf whereas the TV-guided multi-corer only reached the shallow layers. From the degree of Cl-dilution it can be estimated that between 10-30 vol.-% of the top 25 cm of sediment sampled at the southern summit consists of gas hydrates.
Evidence from hydrate water composition as well as from excess pore water chloride strongly suggests that the estimates of hydrate as described above are in need of revision. Equally, the general validity of "salt exclusion" and "water limitation" during

growth of porous hydrate needs to be ascertained. For these objectives a specific coring and sampling strategy was developed to be implemented during SO148 cruises.

1.5. Hydrate Floats: Evidence from Hydrate Fabric and Composition

Massive and catastrophic release of methane hydrates from the seafloor as the trigger for transient past warm climates or accelerated evolution of biota is one of the hottest research topics in current environmental research. Indirect evidence for this hypothesis accumulates rapidly (Kennett and Stott, 1991; Zachos et al., 1993; Katz et al., 1999; Kennett et al., 2000). A locality from which such release of methane hydrates preceding the Late Paleocene Thermal Maximum (LPTM) has been identified on the Blake Spur, based on chaotic and brecciated sediment fabric from disrupted strata left behind (Norris and Röhl, 1999). Except for the myth surrounding the hazards of the Bermuda triangle where catastrophic release of methane hydrate to the atmosphere is invoked, no direct evidence for such a mechanism has ever been presented. During SO143 we have documented that hydrate floats of up to a cubic meter in size rise to the sea surface and thus may constitute a mechanism for continuous or episodic rapid transport of methane from the seafloor directly to the atmosphere.

The basis for "hydrate floats" to develop is the highly porous fabric and related low bulk density as observed at the southern summit. This fabric develops from the accumulation of methane bubbles while becoming encased in a hydrate skin. At a depth of 770m bubbles were observed rising from below the seafloor, where they either escape into the water column or, when arrested beneath a crust of sediment or carbonate, become entangled in bacterial mats and solidify into hydrate. As a result a positively buoyant interlayered complex of hydrate-sediment-carbonate-biota-gas-water forms. Further ROPOS observations and investigations of physical and chemical properties of porous and massive hydrate fabric is essential in order to substantiate the "hydrate float" or "rafting hypothesis". Appropriate samples and sampling strategies during SO148 will provide the needed data.

Central to this hypothesis is the role of the bubble fabric and in that context the question of whether the pores *in situ* are filled with gaseous methane or with interstitial water. Because if they were filled with gas, the bulk density of hydrate layer would be very much lower than if they were filled with interstitial water. The lower density would give rise to a much more positive buoyancy needed to effectively float the hydrate pieces.

Whereas the initial hydrate find in 1996 appeared to show that then hydrate gas composition varied little and was dominated by methane and hydrogen sulfide with traces of ethane, propane, and carbon dioxide present, analyses by other workers show considerably more variation. This requires a more comprehensive set of gas analyses to explain this discrepancy. Similarly, the stable isotope composition of the hydrate gases varies as well. Although there is no doubt of the biogenic source of methane in the hydrate, a more comprehensive set of isotope analyses is also required here for a full interpretation.

A consistent feature of the hydrates recovered so far is the residual chloride and sea water ions found in the hydrate water. Initially, based on the Cl-, Na-, K-, and Mg-concentrations found in the residual hydrate water, we assumed that they came from contamination by about 10% sea water (Suess et al., 1999). But consistent and reproducible salt compositions found in all hydrate waters since indicate to us that these

may be an integral part of the natural gas hydrate fabric. In the context of the porous fabric and the possible water limitation during rapid hydrate growth, it seems possible that reactions take place between sea water ions in the hydrate interstices and the trapped pore water. Such reactions would explain the peculiar composition of the residual hydrate water; clearly specific subsampling and sampling protocols of TV-grabs containing gas hydrates during SO 148 would provide a major step towards understanding these peculiar compositional and textural features

1.6. Enhanced Benthic Turnover

One of the major implications from the injection of gas hydrate methane to the sediment-water interface concerns the benthic material turnover requiring oxygen. Stimulated by the injection of reduced chemical species, i.e. methane from gas hydrates and hydrogen sulfide and ammonia from vent fluids, an enormous microbe-supported habitat develops at vent sites as variously described (Suess et al., 1999; Boetius et al., 2000). The oxidation of the reduced species requires oxygen that far exceeds the consumption normally recorded at the deep seafloor. The rate of turnover at the hydrate vent was evaluated previously from VEnt-SamPler-deployments at Hydrate Ridge (Linke et al., 1994). These deployments yielded time-dependent changes of dissolved fluxes of reduced species and their reaction with bottom water oxygen. The overall stoichiometry, within a sampling-related uncertainty, was found to closely agree between the oxidation equivalents presented by the flux of methane, hydrogen sulfide, and ammonia and the measured oxygen demand. It is clear from these data that hydrate vents support biological oases in the deep sea comparable to those known from hydrothermal vents at oceanic spreading centers. Clearly though, the estimates of material fluxes and ensuing sediment oxygen demand are only first order since no long time-series measurements have been available. The data collected during TECFLUX'99 showed that the largest uncertainty is related to the non-steady flow from vents (Linke et al., 1999). Flux measurements were conducted lasting from hours to weeks at active vents. The results indicate, not unexpectedly, that fluid flux rates vary by many orders of magnitude spatially, due to the heterogeneity in fluid expulsion and underlying plumbing network and temporally, due to tidal forcing and other superimposed frequencies. *In situ* measurements reveal that orders of magnitude in variability occur at the strongest aqueous flux rate sites, with episodes of reduced flow and even flow reversals (Tryon et al., 1999). A short-period variability appears to correlate with tidally induced flow oscillations. Long-term oscillations were superimposed on these fluctuations. These temporal changes in flux behavior gave a unique insight into the complex dynamics behind hydrates and gas venting. These must be better understood and need detailed investigations during the SO148 cruises.

2 CRUISE NARRATIVE

2.1 Leg SO148-1

P. Linke

After 2.5 days of bustling activity on board RV SONNE to unload containers and establish the chartered ROV-system ROPOS, the vessel departed on 22 July at 1600 hrs from Esquimalt Graving Dock, Victoria. Since ROPOS had been installed already on cruises SO109/110 on board of this vessel, the installation of the system caused no major problems. After a short manoever in the Straits of Juan de Fuca to test the handling of the complex system, SONNE started the transit to the study area. Upon arrival, in the evening of 23 July, ROPOS was launched at the southern peak of Hydrate Ridge to make the deck and scientific crew familiar with the use of the ROV. From then on, CTD-surveys at low tide and OFOS-profiles were the night program of the cruise whereas every morning ROPOS was launched after rigging scientific tools and pre-dive checks. After retrieval of the ROV, sediment sampling by the TV-guided multicorer and lander deployments were conducted.

The next 2 ROPOS dives were performed again at the southern peak and were dedicated to the sampling of bacterial mats with the ROV's suction sampler and the dropping of markers for orientation and navigation purposes. The dives revealed the peculiar morphology of dune-like elevations (Beaver Mounds) as well as flat and nearly circular depressions as characteristic features not visible with conventional TV-guided methods. On these dives the autoclave piston corer lost during last year's cruise SO143-3 was found which was supposed to be recovered during the next leg. Against our expectation the giant autoclav laid almost horizontally on the sediment. Traces of fishing activities led to the conclusion that this might be the reason for the movement which has to be considered for the recovery of the corer and future long-term deployments. Additionally, a small crater with active gas bubble discharge was discovered and sampled on these dives.

On 26 July, ROPOS dived at the northern peak of Hydrate Ridge and found at once the benthic barrel lost during TECFLUX-98. This barrel proved to be a valuable marker for orientation between the huge carbonate blocks. The search for the gusher, a site with pronouced gaseous discharge which was intensively sampled during last year's dive program with DSV ALVIN revealed the necessity of good navigation which was slowly improved during the dive. Before finding the Gusher Site, a new site with active bubble discharge was found and signed with marker #2. Two additional markers were deployed between the barrel and the Gusher Site to improve orientation for the deployment of 2 digital camera systems. These self-contained systems were designed to document the variability and magnitude of gaseous discharge and were deployed for 2 days each intermittently at the Gusher Site. The observations revealed a tidal rhythm in gas discharge and indications of a gas reservoir effect overlaying this regular frequency. To investigate this effect, one of the camera systems was deployed for 10 days and recovered on the second leg. CTD-surveys conducted at low tide completed the investigation on the areal extent of the plume. Additionally, bubble chasing experiments were conducted to track the isotopic signature of methane downstream of the discharge sites and to follow the fate of the bubbles in the water column. A first experiment at the Gusher Site revealed that the rising bubble plume could be traced for 200 m in the open water column with the cameras and the sonar of the ROV before the bubble dispersed and probably dissolved. Since this depth was the stability limit of gas hydrate and the

maximum in methane concentration derived from various CTD casts, this exiting result was investigated more closely on the second leg.

On the next day, the first TV-guided VESP-Lander was deployed for 4 days on a bacterial mat within the Beaver Mounds. A subsequent ROPOS dive (563) revealed that the lander stood on a small rim between two depressions not visible during the usual TV-guided deployment. The sealing of the lander's chamber was corrected with the ROV and was used as an *in situ* experiment to investigate the effect of the bottom current (chimney effect) measured by ADCP on an unsealed versus a sealed chamber.

During the second week of this leg, new territory was investigated by OFOS and ROPOS besides the intense sampling program at known sites of near-surface gas hydrate and of gas and fluid discharge. SE Knoll, a structure discovered during last year's program proved to be a carbonate cliff elevating more than 90 m above seafloor. In the upper part of the cliff, active gas and fluid discharge sites with bacterial mats, clams fields and single vestimentiferans were observed and sampled by ROPOS. Further OFOS surveys east of Hydrate Ridge documented large clam fields and bacteria mats at reflectors seen in the side scan sonar maps. Furthermore, a detailled survey with ROPOS at the southern part of the northern peak not covered by past surveys revealed large clams fields where the second VESP-Lander was deployed and controlled by ROPOS. The first lander was re-deployed at this site for a long-term study of more than 2 months.

Another major objective was the detailed sampling of sediments in respect to the horizontal and vertical gradient pattern induced by venting activity and reservoir effects of gas hydrate. Different scenarios were intensively sampled with the TV-guided multicorer and investigated with geochemical and microbiological approaches. Furthermore, a camera system was mounted on the multicorer and one deployment documented for the first time the „Schliereneffekt" of fluids discharged from a bacterial mat.

On the last working day in the area, increasing wind and swell caused a change of the work program. ROPOS could not be used to deploy the digital camera at the southern peak and to check the deployment position of the long-term lander. This had to be accomplished during the second leg. After the successfull recovery of VESP-Lander II, the TV-grab was used to retrieve big chunks of gas hydrate instead. They were used immediately for detailed analyses of their structure and physical and chemical properties.

After conducting a last CTD cast on 2 August, RV SONNE returned to Victoria and was tied up at Odgen Point at 0700 hours on 3 August.

2.2 LEG SO148-2

E. Suess

After exchange members of the crew, the scientists, and the ROPOS team, RV SONNE departed from Ogden Point, Victoria on 4 August at 1000 h under sunny skies. A day later the vessel arrived in the area of investigation while the weather had changed to overcast but calm seas. These favorable conditions prevailed generally throughout the cruise and permitted regular ROPOS deployments with only one exception. On 5 August we dove on the summit of an elongated accretionary feature, known as R1 structure and observed strong venting activity and the associated fauna and authigenic carbonates. During the night methane determinations were continued using CTD casts. The casts were part of several NE-SW sections located obliquely to Hydrate Ridge venting sites in order to obtain a detailed pattern of methane plumes over the area. Sampling took place during low tides in order to encounter the same bottom currents which are thought to be largely responsible for the methane distribution.

On Southern Hydrate Ridge we investigated on 6 August a large outcrop which either constituted a fissure which had developed on the summit or which might have been initiated by TV-grab sampling during past deployments. On the hanging wall of the fissure ROPOS excavated a 15-25 cm thick massive horizontally oriented hydrate layer. Above that another thinner layer was exposed containing hydrate nodules and narrow hydrate-filled fissures which cut through the bedding and cemented the entire sediment package. The thick deeper layer consisted of massive, hard and bluish/white opalescing hydrate, the upper layer additionally contained white hydrate, probably due to bubble fabric. ROPOS broke off a massive piece from the upper layer and we observed the reaction of hydrate under changing temperature and pressure as the ROV ascended through the water column. After leaving the hydrate stability zone, bubbles and dissolution features formed on the outside as well as the inside of the piece of hydrate. Upon descend back into the stability zone the reaction stopped.

At the end of the dive the time-lapse camera system for recording the flow of bubble streams from vents was deployed. However, the position of the system could not be optimized because the bubble stream had ceased. During a later dive on 9 August the alignment of the camera towards the bubble escape site was improved.

During the night time as well as prior to and after the ROPOS dives, OFOS surveys were carried out. The area of acoustic anomalies from previous side-scan sonar mapping east of Hydrate Ridge was surveyed as well as the accretionary feature known as SE Knoll. The objective was to better define targets for subsequent ROPOS deployments. CTD-profiling was also continued and the *In Situ Schlierenoptic (ISSO)* deployed. This system yielded unexpectedly clear and unambiguous signals of venting which result from mixing of vent fluids with bottom water.

Recovery operations of the autoclave piston corer (AKL) began on 7 August after technical and navigational preparations by the ship's crew. This prototype instrument was conceived and built by the BGR-Hannover in cooperation with the TU-Berlin as a prerequisite for basic research on gas hydrates. It was lost during the first deployment a year ago but had been sighted on numerous occasions while deploying video-guided gear so that it could be readily located again. The recovery plan called for ROPOS to connect a heavy duty nylon rope between the instrument and a dummy weight tied to one end of a 1.2 km long rovery wire. The other end of the wire was connected to a float which allowed the wire to be taken on deck and attached to the deep-sea winch for

heaving in the instrument. Thus the AKL was recovered intact. During this operation as well as previously while excavating the hydrate layer and positioning the camera system, ROPOS fully used its great maneuverability, flexibility in tool handling, and its extraordinary video-camera system. All involved agreed that these and other operations would not have been possible with conventional means.

During 8 and 9 August we explored a 50 m high carbonate chimney structure, the Pinnacle, which is surrounded at the base by an extensive accumulation of large carbonate blocks. This feature was discoverd by DSV ALVIN and is characterized by several sets of large peculiar cracks. We sampled the carbonate lithologies with ROPOS up and down the edifice, collected vent fauna from the active cracks and determined strike and dip of these dominant venting channels.

When ROPOS was not diving, we collected hydrates, chemoherm carbonates, and bacterial mats using the TV-guided grab sampler and multicorer. The samples served detailed objectives such as determining the ratio between nitrate stored by bacterial mats and their biomass or experiments for the preservation of hydrates under *in situ* conditions.

On 8 August we began CTD casts for methane analyses along a transect from the shelf to Hydrate Ridge in order to elucidate the strong methane enrichment in the intermediate water which extends far to the west of the accretionary ridges.

Our TV-guided multicorer deployment and conventional gravity coring at the same location in the area of patchy acoustic anomalies surrounding the E-Basin, yielded surprisingly, an approximately 100 cm long section of completely hydrated sediment. Through OFOS observations we had detected for the first time colonies of vent organisms in these otherwise barren-looking patches. The hydrated sediment was composed of thin alternating layers of hydrate and sediment giving the impression of a marble texture. This find is of considerable importance for understanding the peculiar acoustic patches over the entire accretionary wedge and must be considered one of the cruise highlights.

On 10 August several problems developed which required a change in the science program. At first the deep sea winch with the conducting cable developed problems so that all TV-guided instrument deployments had to be cancelled. Then a strong westerly swell required the cancellation of the ROPOS dive for that day. With only the deep sea wire and the hydrowire available, we changed to gravity coring and CTD casts. A 200 cm long core with several distinct hydrate layers was recovered, one of which was massive and 6 cm thick. The sequence of layering, depth penetration, sediment fabric and lithology suggested a correlation with previously cored sites in the area. The additional methane data confirmed a very complex pattern of plumes throughout the waters bathing the margin.

Early on 11 August the deep sea cable and winch were replaced and tested so that the science program could be continued. The swell had also diminished considerably which allowed 2 separate dives during which both bubble camera recording systems were retrieved. The system on the northern summit had recorded up until and including 6 August after which power problems developed. We assume that continued autofocussing activated by floating particles exhausted the energy supply prematurely. The camera system placed on the southern summit recorded continuously until 2200

UTC on 11 August. A major success of the deployment is the clear documentation of what had been suspected, that tides modulate the bubble emission from vents at the seafloor. At rising tide and high tide, bubble activity on the Southern Hydrate Ridge diminished and even ceased completely whereas during low tide it increased by several orders of magnitude. Bubble activity on the northern site was generally stronger. It appears to be driven by tides as well but superimposed were higher frequency modulations not related to tides. It remains a challenge to determine the mechanism responsible for these modulations as well as the quantification of the bubble stream images. The success of the system is owed to the cooperation between GEOMAR and partners from the Japanese Geological Survey.

In the morning of 12 August we recovered another large load of hydrate. Several types of fabric and a large variety of shapes and sizes were thus made available for special investigations. The sampling followed an intricate protocol tailored to each type of analyses, thereby minimizing errors usually introduced by the rapid decomposition of hydrate. Bulk density was determined directly on board. The range of values from 0.3 – 0.8 g/cc appears in agreement with porosity variations and types of fabric observed. Controlled degassing allowed the collection and quantification of gas volumes emitted and the isolation of hydrate water per hydrate volume of known porosities. The variations agree with those expected from the different types of fabric. Samples for total gas content, for gas composition, and isotope ratios were prepared and conserved for laboratory analyses. Cl-anomalies of up to almost twice the sea water values were found in pore waters adjacent to hydrate layers. Salt exclusion through hydrate formation was discovered last year and was thus confirmed. The results expected from these very detailed and specialized procedures of hydrate characterization involve up to 100 samples and are statistically significant compared to most previous analyses.

During the night of 12 August a dense grid of OFOS lines was run over the Southern Hydrate Ridge and the adjacent Pinnacle. Markers had been laid out the previous day by ROPOS at certain grid points. The objective was to generate a coherent map of the distribution of bacterial mats, clams fields, hydrates, and carbonate formations and identify structural relationships between the Southern Hydrate Ridge and Pinnacle.

During the day of 12 August we investigated NW-Knoll with ROPOS. This lesser known accretionary feature is situated between the major accretionary ridges and showed quite a prolific vent fauna, primarily colonies of large clams. These were aligned along a narrow zone of glauconite sands which were partially cemented by carbonate and showed plumbing structures. No indication of hydrate was found nor did the *In Situ Schlierenoptic* indicate any venting activity, even though methane anomalies were found over the summit of NW-Knoll.

The deployment of a 10 m piston corer at the NW flank of Southern Hydrate Ridge was the last major operation during this leg. Core penetration, wire tension and all other technical parameters indicated long core recovery but the instrument yielded a core of only moderate length but of the most unusual overconsolidated lithology never seen before in the area and without any trace of hydrate or authigenic carbonates.

In general, the ROPOS dives were not only an exciting adventure for the scientists and investigator groups but also opened completely new perspectives for most of them. Among these the realization of how the capabilities of ROPOS could be combined and optimized by the excellent technical facilites of RV SONNE, such as the TV-guided

instrument deployments, navigation and survey capabilities, appeared most attractive. Last not least the extensive experience of the ship's crew and the ROPOS team and their mutual cooperation contributed significantly to the success of the cruise.

Early on 13 August RV SONNE set sail for Victoria BC with an estimated time of arrival at 0700 local time on 14 August.

3 MULTIBEAM SWATHMAPPING AND PARASOUND

M. Müller, G. Bohrmann

3.1 Multibeam Swathmapping

During SONNE Cruise SO148 the onboard HYDROSWEEP multibeam system from STN ATLAS-ELEKTRONIK was continuously used for bathymetric profiling. The system has a frequency of 15.5 kHz. By using 59 beams in a swath of 90° a seafloor stripe is covered of approximately the width twice of the water depth. The range of the central beam is up to 10,000 m with an error of 1%, for the outer beams up to 7,000 m with a precision of about 1%. The precision requires that the roll is less than 10° and pitch less than 5°. Corrections for roll, pitch, and heave are automatically applied during data acquisition. Due to the fixed angle between beams, resolution is dependent upon water depth, and varies from about 10 m in 200 m water depth to 200 m in depths of 5,000 m to 6,000 m.

For calculating depths from echo time delays the sound velocity in the different water layers is required. To determine an average water sound velocity profile HYDROSWEEP uses a second set of transducers and a calibration scheme with soundings along the track. However, in certain areas this algorithm fails. Thus, for better results, direct measurement of sound velocity at different depths using a CTD is required. During cruise SO148 several CTD stations were run (see Chapter 9). The comparison of the sound velocity data from these stations with the SO143 data shows no significant changes for a general water column model. In order to simply combine the data sets of both cruises we used the sound velocity model from SO143 (Bohrmann et al., 2000: page 22, Fig. 6).

HYDROSWEEP data were recorded on magnetic tapes and transmitted to the GEOMAR workstation (Hot black). Postprocessing of HYDROSWEEP data comprises the merging of navigation data, the calculation of water depth and positions of the footprints of the beams, removing artifacts and erroneous datapoints, and the generation of a digital terrain model (DGTM). The ATLAS HYDROMAP software, based on the CARIS software package, is available onboard for that purpose. However, for several reasons, the academic software MB-System (Caress and Chayes, 1996) from the Lamont-Doherty Earth Observatory was used onboard for HYDROSWEEP data processing.

Multibeam swathmapping was almost continuously recorded during RV SONNE cruise SO148. Hydrate Ridge as the main target area was intensely measured during former cruises (SO109, 110 and 143). Therefore, we focussed our measurements on gaps between the R1 structure (45°35'N) and Hydrate Ridge. Due to careful planning we could cover most of the area with 6 additional tracks (Figs. 5 and 6).

3.2 PARASOUND

During SO148 the parametric sediment-echosounder PARASOUND (PARAmetric sediment survey echoSOUNDer, Atlas Elektronik GmbH, Bremen) was used in order to define sites for sampling. Due to the lack of manpower during this cruise the system could not perform permanently. PARASOUND was mostly operated in the parametric mode using a frequency of 4 kHz. Raw analog data have been written to a black and white as well as a colour printer. We did not store the data on DAT tape using the program PARADIGMA (PARAsound DIGitalisierungs- und Mehrkanal Auswertesystem, Spieß, 1993).

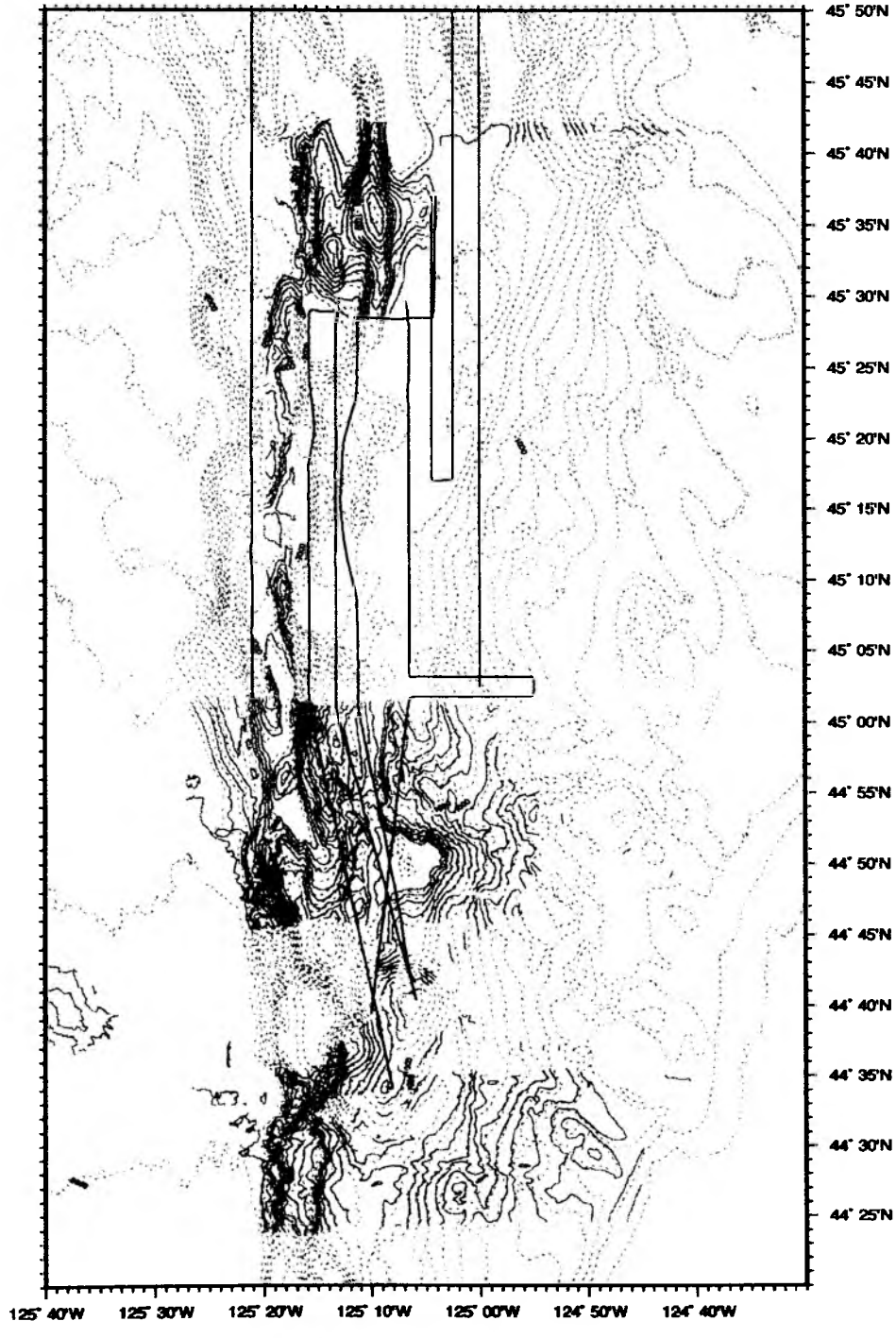

Fig. 5: Track lines of HYDROSWEEP profiles measured during SO148. Contour lines from HYDROSWEEP SO143 (solid lines) and the Chris Goldfinger data set (dashed lines) are also shown.

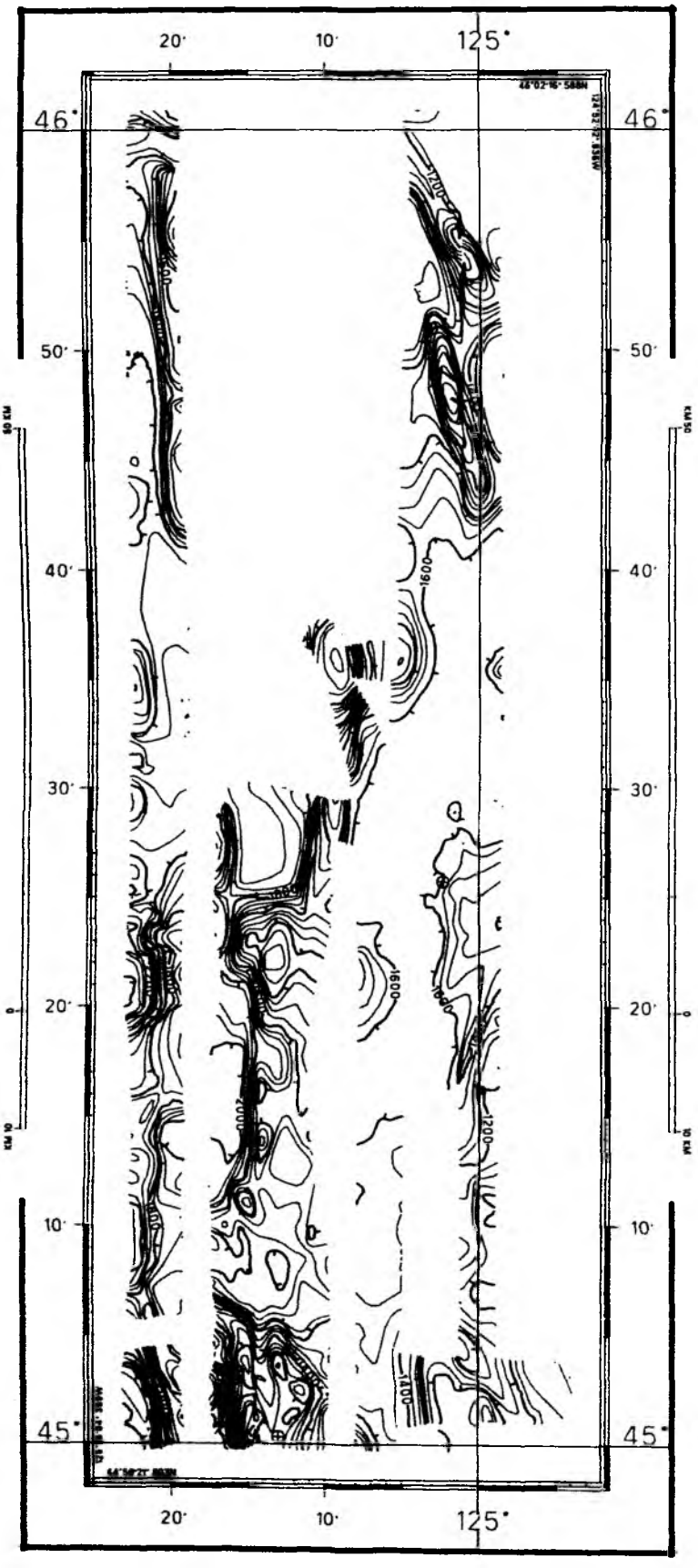

Fig. 6: Contour map north of Hydrate Ridge based on SO148 HYDROSWEEP surveys produced onboard with the HYDROMAP software.

PARASOUND works differently from traditional 3.5 kHz echosounders and uses a sound beam resulting from the interference of two high frequency narrow waves of similar frequency (18 - 23 kHz) forming a low frequency part of the signal. The depth of penetration of the parametric 2.5 to 5.5 kHz echo is as great as that of 3.5 kHz systems, but due to the narrower beam width, a clearer and more differentiated image of multi-layer structures is obtained. The opening angle of the sound wave is about 4° acoustically illuminating a spot with a diameter of 7% of the water depth. Therefore, information quality depends to a great extent on the morphology of the ocean bottom. In case of steep slopes, the image is often lost due to configuration reasons. Slopes steeper than 4° cannot be imaged, areas with a slope of more than 2° are normally only poorly imaged.

4 OCEAN FLOOR OBSERVATION SYSTEM (OFOS)

C. Jung, B. Teichert, H. Sahling

Introduction

The objective of the ocean floor observation program was to map geological, morphological and biological features of the Cascadia subduction zone. The detailed investigation focussed especially on chemoherm carbonate outcrops, gas hydrate occurrences and biological vent communities in the Hydrate Ridge working area. OFOS profiles were used to to look for previously unknown active vent areas as well as to verify earlier results. Based on last year's investigations (SONNE Cruises 143 TECFLUX I), we were able to concentrate our surveys on special target areas and deploy the sled in a very specified and unerring way. OFOS profiles proved to be a powerful survey tool for the deployment of other deep-sea tools, e.g. gravity cores, TV-grabs, multicores and ROPOS. We were able to discover a carbonate chemoherm structure of about 60 m height (OFOS 5 and 6) situated at the SE Knoll, where we later on performed an additional ROPOS dive (565). The chemoherm structure, a steep slope extending over several 100 meters, is about 100 m in height with a platform stretching to the south. Other successfull OFOS profiles (9 and 10) included the investigation of the round high reflectivity patches observed by side scan sonar at the E-Basin (map of C. Goldfinger). MUC and KOL stations (SO148-75/76) proved the vent relation of that site by recovering dispersed gas hydrate layers, clams, bacterial mats and carbonate fragments.

Equipment and Handling

The OFOS sled on board RV SONNE is a video-controlled deep-towed device recording video and data signals simultaneously. During the survey, data signals were sent every second and saved by the WERUM software on board. The fiber optic cable controls the data transfer and the coaxial cable provides the electric power supply. The optical observations were recorded continuously on video tapes and slides with a stereo photo system. Additionally, the operator is responsible for entering the visual online observations into a logbook (WERUM software, but in need of improvement).

The OFOS sled is equipped with two video cameras; a color one (DEEP SEA POWER & LIGHT, CCD Multi-Sea-Cam 2050) and a black and white one (KONGSBERG, OSPREY/SIMRAD, CCD OE 1390/1391). Two xenon spotlights and two halogene spotlights (DEEP SEA POWER & LIGHT, 2 x 200 W, 2 x 250 W) provide optimal brightness. Two still cameras (KONGSBERG, OSPREY/ SIMRAD, 2x PhotoSea 5000) are installed to take slides, they are coupled with two strobelights (BENTHOS, 383 M383-002 double-strobe with two flash-heads) for additional light during slide shots. The still cameras were loaded with 30.5 m slide film (KODAK Ektachrome, 200, ASA), providing a capacity of 800 images. Slides can be taken manually on request from board or in fixed time intervals (lasting 7 to 60 seconds). Three laser (DEEP SEA POWER & LIGHT Micro-Sea-Laser) point downward in a distance of 20 cm as a scale for the bottom observation and for exact bottom distance measurements.

The OFOS is provided with a sensor to correct pitch and roll (MARK II), and a compass (RTB, Vector 2XG) providing the heading of the sled and the orientation of the top of the video image. An altimeter (BENTHOS, Model 2110) provides the depth of the sled, a temperature sensor in the bottom-contact weight (RTB) is also installed. Depending on the distance to the bottom surface (between 120 cm to 300 cm) a sector of approximately 12 m^2 is visible. One slide shows an area of 2,20 m^2 (1,80 m x 1,20 m) automatically printing the date and time of exposure. A weight on a rope of 150 cm length served as a bottom-contact alert, determining the distance between the sled and

the seafloor. The winch operator used the weight as a visible marker (by video camera) to manually adjust the distance to the seafloor. OFOS is best operated at a ship speed over ground between 0.4 kn and 1.0 kn (mean 0.7 kn) and at a distance to the seafloor of 150 cm with a camera aperture between 4 - 5,6 for clear slides and video sequences. The slides were developed during the cruise by E6 processing (KODAK) using the equipment of RV SONNE.
The attached CTD (SEABIRD, SBE 9/11) allows simultaneous online data aquisition of conductivity, temperature and depth. For further investigations it would be more useful to have salinity data instead of conductivity data. Unfortunately, the hexadecimal raw data from the CTD cannot be stored in the ship's database, thus making further investigations (e.g. sound velocity and average calculations) more complicated. Therefore, we used the memory-unit of the SEABIRD 9/11 software to save the data directly after the OFOS was back on deck. The CTD has to be switched off, but the power supply must be still working. Then the data can be retrieved with the 'term 19' application of the SEABIRD software.
The bottom position of the OFOS was calculated by using the SSBL (Super Short Base Line) system (SIMRAD, Responder DHT 163) with a responder for online navigation. All measured data and navigation data of the SSBL and the ship's DGPS were saved and synchronised by time (UTC).

Results

During this cruise we performed 14 OFOS surveys (Tab. 1, Fig. 7) in the Hydrate Ridge area. We developed almost 9000 slides and saved 128 hours ocean floor observations on video tapes. A brief overview about the most interesting points is given below.

Daisy Bank

The first deployment (OFOS 1, Fig. 8) was at the Daisy Bank fault structure in the vicinity of the continental shelf region. Water depth was between 120 m and 300 m. The goal was to recover some indications of fluid venting at the fault structure of the Daisy Bank area. Therefore, the track was planned crossing several times a steeper slope related to the fault structure. The seafloor is covered by soft sediment, mainly the lower parts of the slope. In the upper parts of the slope we observed more boulder fields. These boulders are black because of a Mn/Fe oxidation coating, suggesting longer exposure on the seafloor. A variety of sponges is dispersed on the upper parts of the slope and usually they attach themselves to hard substrates, mostly exposed boulders. Many fishes and crinoides were also identified at this prominent area.

Southern Hydrate Ridge and Pinnacle

Three surveys were performed in this working area. The OFOS 3 (Fig. 9) at the Southwest Ridge of Hydrate Ridge was expected to discover new active vent sites and gas hydrate exposures. But it was not successful, even though water depth (top at 920 m) and structure are similar to Hydrate Ridge. The Southwest Ridge is characterized by an equally soft sediment accumulation without any geological, biological and morphological expressions indicating fluid activities and venting.

OFOS 2 (Fig. 10) was conducted across the active vent field of Southern Hydrate Ridge and the Pinnacle, a chemoherm carbonate formation. The top of Southern Hydrate Ridge is recognized by now as a well-known active vent field. Impressive bacterial mats and extensive clam fields, as well as gas hydrate outcrops are dispersed over the crest.

Tab. 1: Short overview of all OFOS deployments at cruise SO148.

Stat. No.	Direc-tion	Working area	Target	Observation	Technical Remarks	Tapes *	Slides No.
148							
3 OFOS 1	NW to SE	Daisy Bank Fault	looking for vent indications cause of the fault structure	no active vent indication	CTD upload incorrect	2c' / 2b'/w'	427
5 OFOS 2	E to W	HRS, Pinnacle	chemoherm carbonate and dimension of the Pinnacle	chemoherm carbonates and fracture structures	one spotlight defect	1c' / 1b'/w'	444
9 OFOS 3	NE to SW	HRS, southwes t ridge	looking for vent indications cause of the similar feature as HR	no active vent indication	slide counter incorrect	1c' / 1b'/w'	about 380
16 OFOS 4	W to E	HRN, Gusher site and western flank	Gusher Site, looking for active venting and bubbling	typical vent fauna and carbonate boulders and outcrop	slide counter incorrect, difference of 100 slides	1c' / 1b'/w'	about 226
21 OFOS 5	W to E	SE Knoll	looking for active venting and bubbling cause of plume registration from A. Trehu`s cruise	no active vent indication, but some clams and chemoherm carbonate features		1c' / 1b'/w'	107
26 OFOS 6	W to E, NNE to SSW	SE Knoll	again like OFOS 5, but from another direction	50 m meters high flank of chemoherm carbonate complex, platform of carbonates to the south (ROPOS Dive 565) active vent site	crash, sampling	1c' / 1b'/w'	201
39 OFOS 7	E to W	Southern Knoll of SE Knoll	looking for active venting and chemoherm carbonate structure cause of a last year OFOS track	some carbonate outcrop but nothing else (time problem occured)		1c' / 1b'/w'	74
46 OFOS 8	W to E	HRN, southern flank	side scan sonar reflectivity patches	carbonate fragments and boulders characterized the reflection patches		1c' / 1b'/w'	210
53 OFOS 9	W to E, E to W	Eastern Basin	side scan sonar reflectivity patches	patches were covered with many clam fields and bacterial mats		1c' / 1b'/w'	282
62 OFOS 10	all dir.	Eastern Basin	side scan sonar reflectivity patches, mapping the structure for further deployments	patches were covered with many clam fields and bacterial mats		1c' / 1b'/w'	361
70 OFOS 11	W to E	HRN	bathymetrical features	diagenetic carbonates, no active vent indication	two spotlight defect	1c' / 1b'/w'	383
83 OFOS 12	all dir.	Southern Knoll of SE Knoll	looking for active venting and chemoherm carbonate structure, continued OFOS 7	little chemoherm with cracks filled with clams, clam fields, some bacterial mats	short circuit, second try	2c' / 2b'/w'	492
84 OFOS 13		SE Knoll		winch broken	winch broken by 35 m rope length	0	0
100 OFOS 14	area grid	HRS and Pinnacle	high-resolution mapping of vent fields and Pinnacle mapping, looking for marker placed by ROPOS	avtive vent fields and chemoherm carbonates; no marker found but a lot of weights and marker 7 (ALVIN), TVG hole		2c' / 2b'/w'	716

*Color = c'; Black & white = b'/w'

At the Pinnacle some chemoherm carbonate fragments falling down on the still flat ocean bottom indicated the steep slope that was coming up soon. But former tracks across the Ridge and careful winch operators ensured a successful crossing.
In order to follow a grid section the main objective of OFOS 14 (Fig. 10) was to map the vent area of Southern Hydrate Ridge and the section between the Pinnacle and Southern Hydrate Ridge. The observation proved once more that the extensive active vent field is restricted. South of this area exist no extensive field of bacterial mats and clam patches. We observed many weights of deep sea tools and TV-grab holes as well as marker 7 from last year's DSV ALVIN expedition (TECFLUX I). The approach to the Pinnacle is mostly rocky and cemented sediment covered with boulders and talus. The sudden steep rise is no more suprising, but the cross shows again the rugged and fractured feature of the chemoherm. Bacterial mats and clams following fissures are typical for chemoherm vent outcrops. Some bigger faults through the rocky carbonates indicate tectonic activity.

Northern Hydrate Ridge
Three OFOS tracks (4, 8, 11, Fig. 11) were deployed at Northern Hydrate Ridge. These lines were performed for reconnaissance and mapping vent field areas and bubbling sites. It was not possible to recognize gas bubbles with the sled during OFOS track 4, which was crossing the Gusher Site and observing ALVIN weights. Chemoherm carbonates and clam fields, as well as bacterial mats are dispersed over the crest of Northern Hydrate Ridge. They were also found at the eastern end of the profile at the small ridge. To get a better idea about the distribution of carbonate layers and vent indicators, we deployed OFOS 8 and OFOS 11 more southwards. More or less cemented sediment is usual. Bathymetrical features are indicated by more carbonate boulders and carbonate outcrops. Some dispersed clam fields and bacterial mats indicate less fluid activity compared to the Gusher Site at the crest of the Northern Hydrate Ridge (ALVIN weight found, Fig. 11). The southern part of the Northern Hydrate Ridge is characterized by more extensive boulder fields and carbonate slabs. Living clams and clam shells occurred locally on the saddle structure.

Southeast Knoll (SE Knoll)
We decided to perform OFOS 5 and OFOS 6 (Fig. 12) at this site because of observations made during a cruise 4 weeks ago by our American colleagues: The 12 khz seismic registration indicated a gas plume in the water column. Therefore, we deployed OFOS 5 from west to east across the SE Knoll. At the top of the knoll some clams and chemoherm carbonates were observed. Unfortunately, we ran out of time for this survey and had to interrupt this track. The following track, OFOS 6, finally discovered the extensive chemoherm slope. The structure is similar to the Pinnacle at Southern Hydrate Ridge but seems to be broader and higher. To the south, the jagged chemoherm changes to an extensive carbonate platform smoothly dropping off. The chemoherm is heavily furrowed and rugged with many fissures and cracks. Clams and clam fields as well as bacterial mats occur in cracks and around. After discovering this structure we decided to conduct a ROPOS dive (565) there.
The steep flank appeared surprisingly, so that we nearly lost the TV-sled by crashing into the rock. After coming up on board a beautiful carbonate sample was lying on the sled.
Another southern knoll of SE Knoll is also quite interesting. Former investigations (TECFLUX I) suggested a chemoherm structure. But only a small chemoherm structure with some clam patches was observed by OFOS 7 and OFOS 12 (Fig. 13). No bacterial mats and no other active vent indicators were found.

E-Basin

The target areas for the survey were the round high reflectivity patches observed by side scan sonar and shown in the map of C. Goldfinger. OFOS 9 and OFOS 10 (Fig. 14) were performed to investigate characteristic features of these patches. The seafloor is covered by soft sediment. Extensive clam fields and bacterial mats occur exactly at the side scan patches (Fig. 14). The bacterial mats are less intensive than those we found at the Hydrate Ridge vent areas. They covered the rough sediment surface with a gray-blue color. The recovered sediment cores of this different venting area are characterized by gas hydrate flares dispersed in irregularly thin sections which is a new feature.

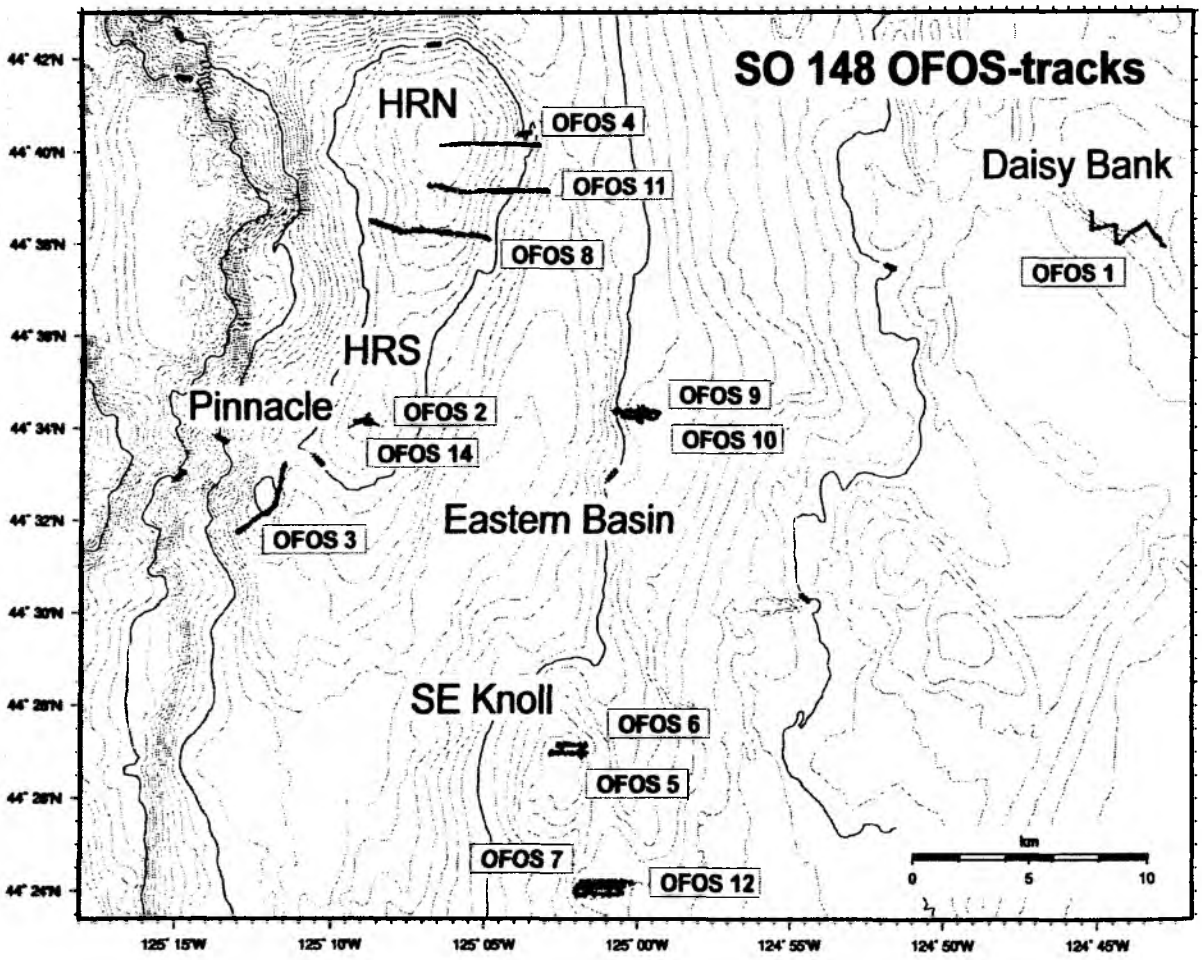

Fig. 7: Overview of the Hydrate Ridge working area.

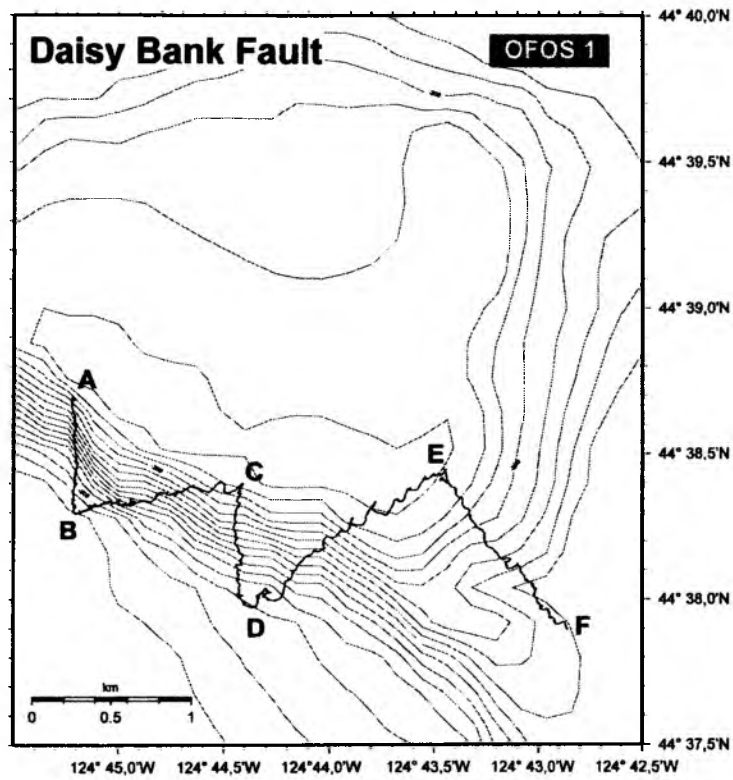

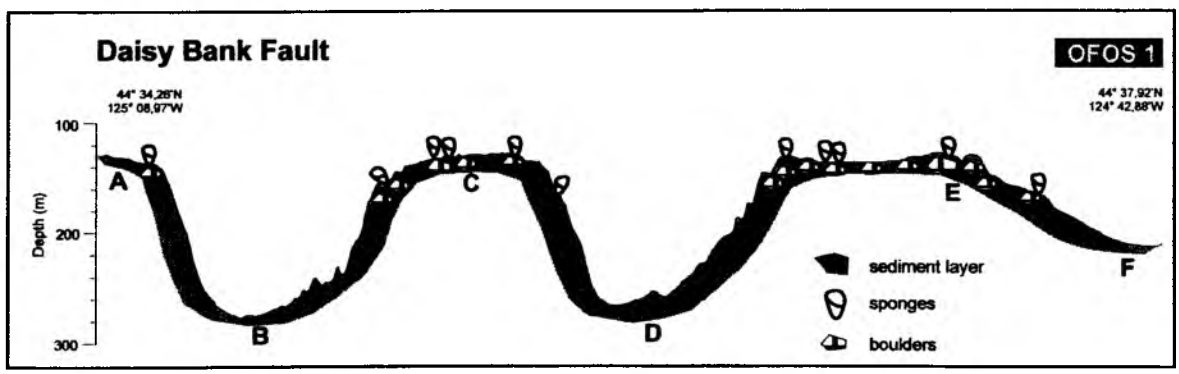

Fig. 8: OFOS profiles at the Daisy Bank fault.

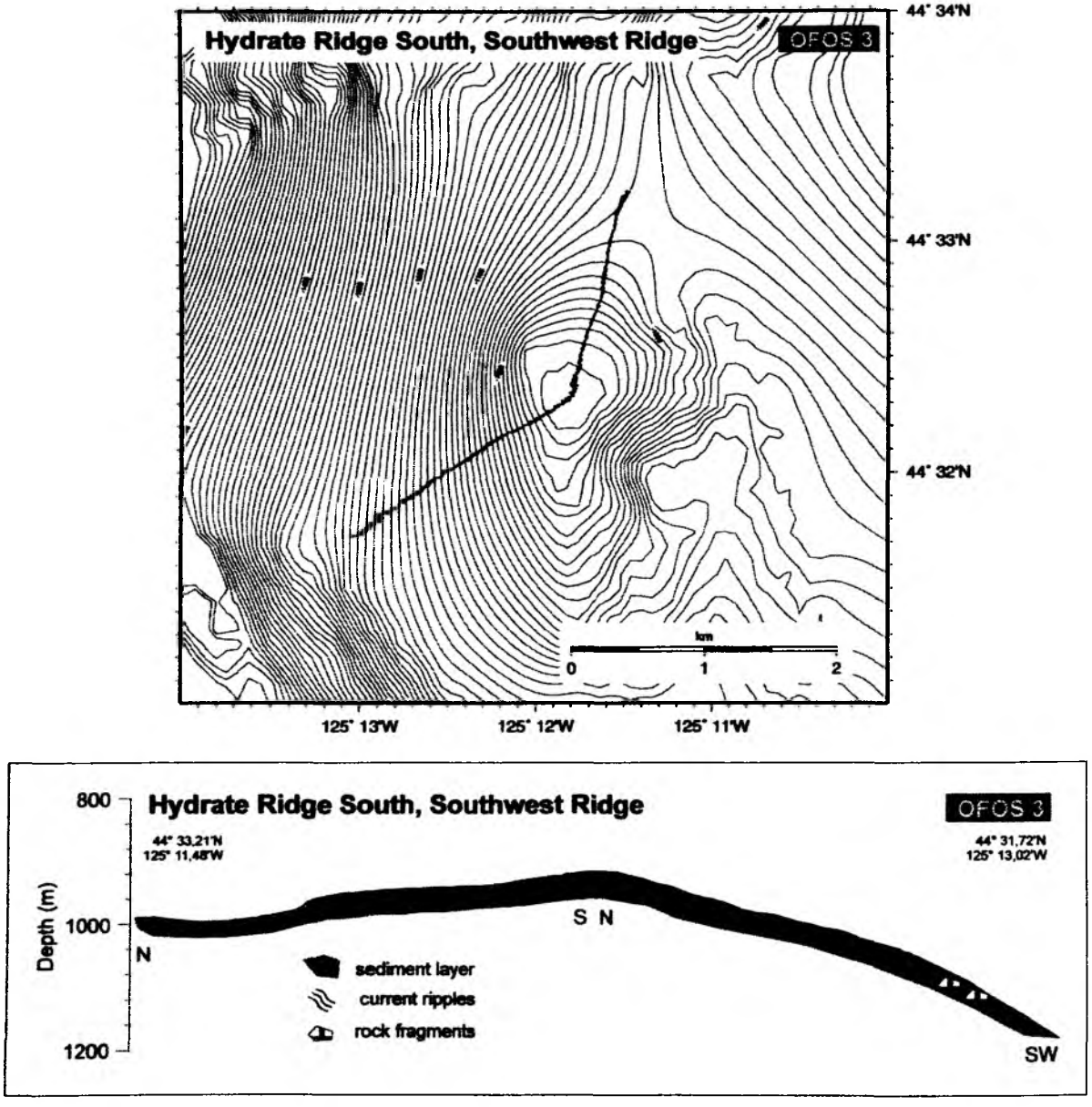

Fig. 9: OFOS profiles at the Southern Hydrate Ridge.

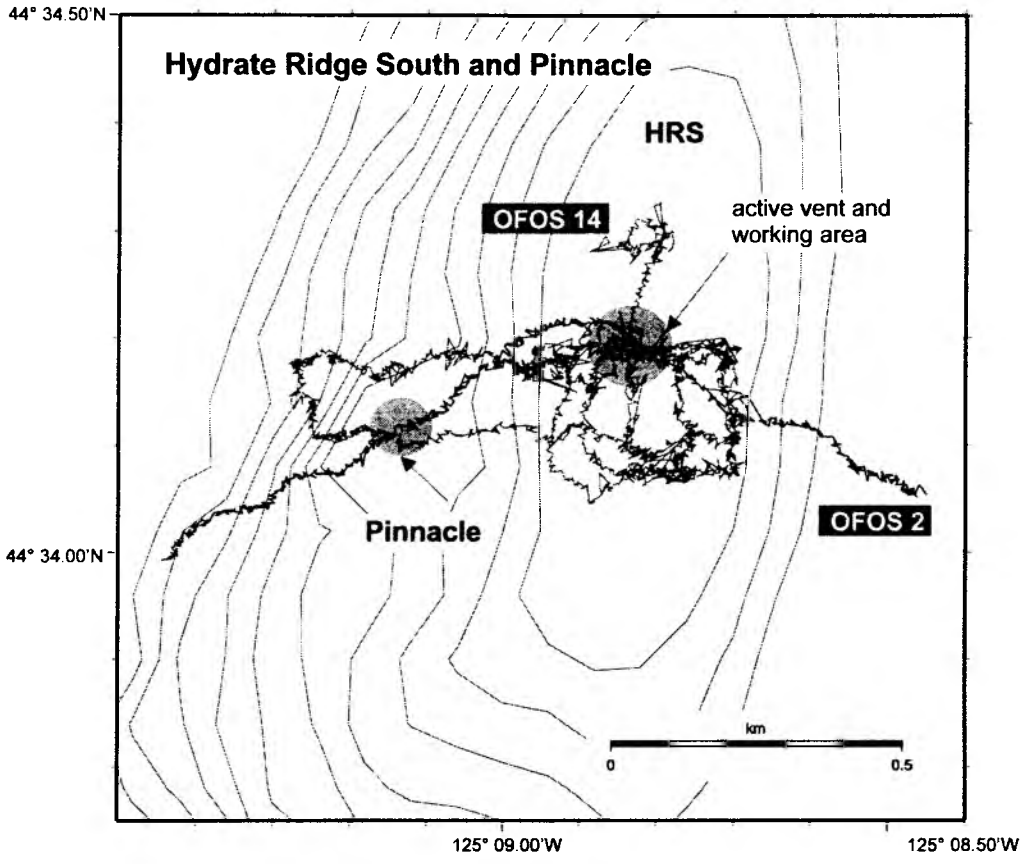

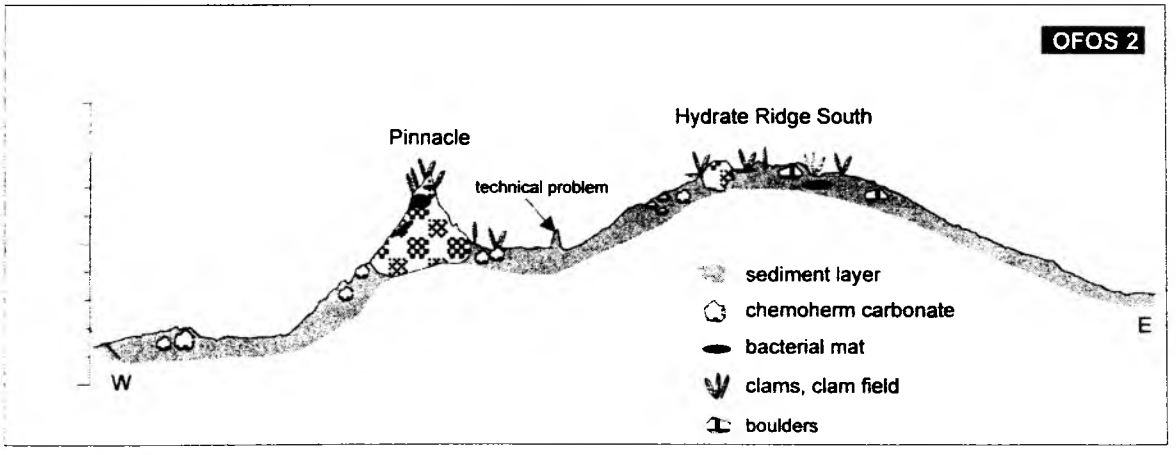

Fig. 10: OFOS profiles at the Southern Hydrate Ridge and the Pinnacle.

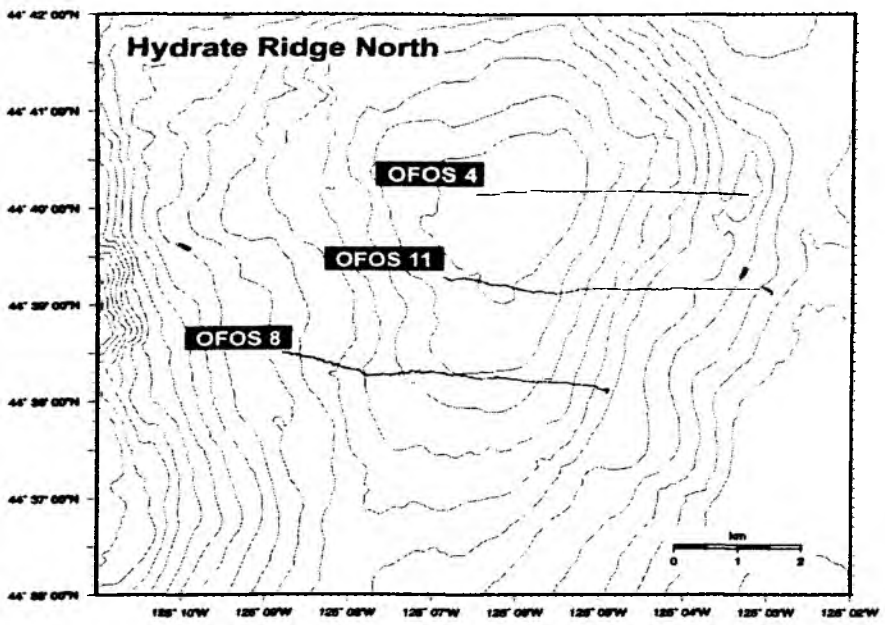

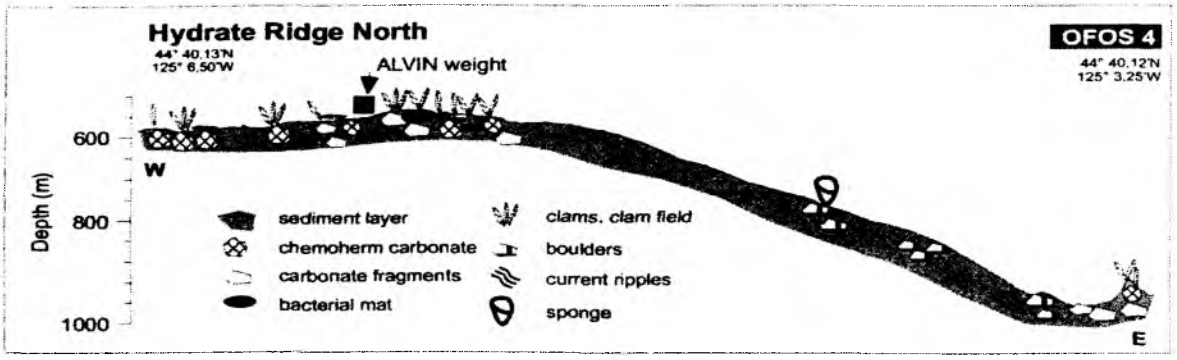

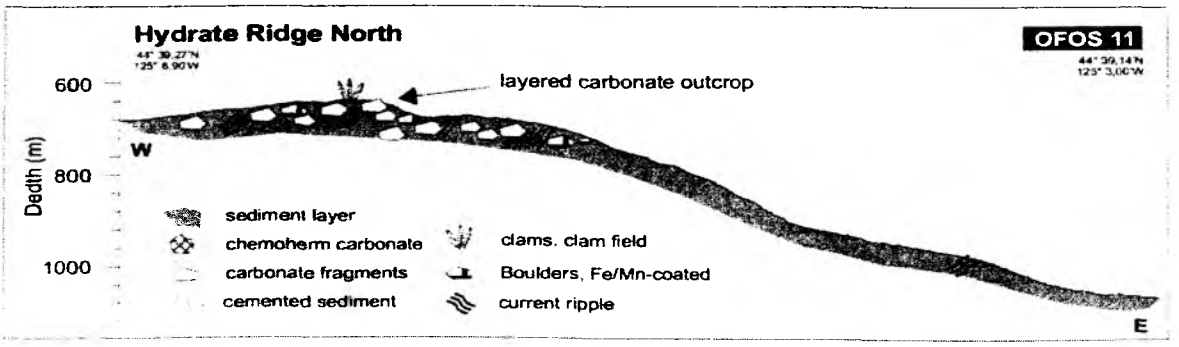

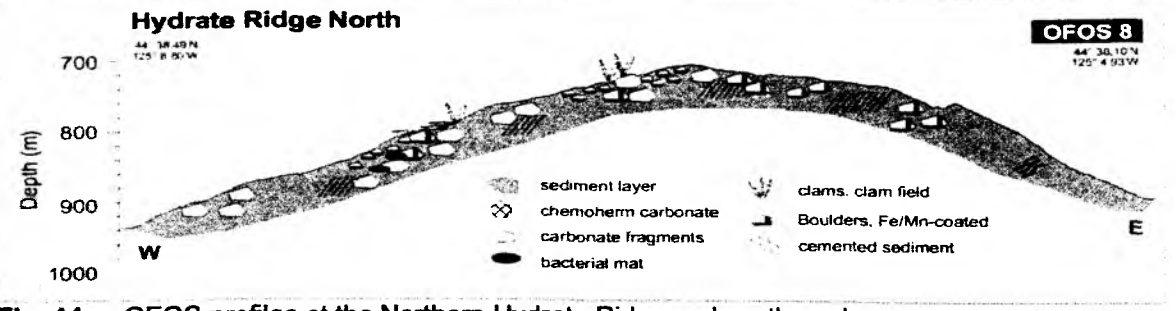

Fig. 11: OFOS profiles at the Northern Hydrate Ridge and southward.

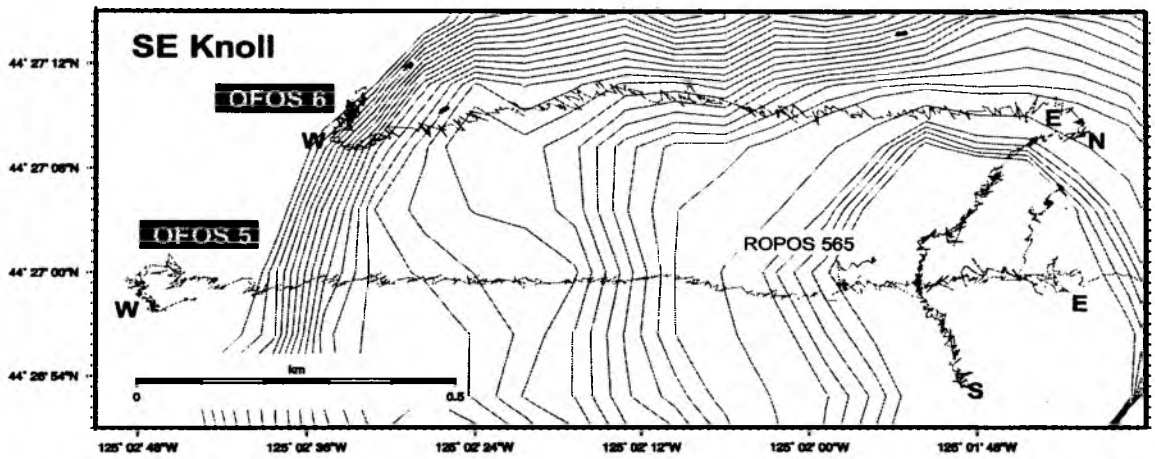

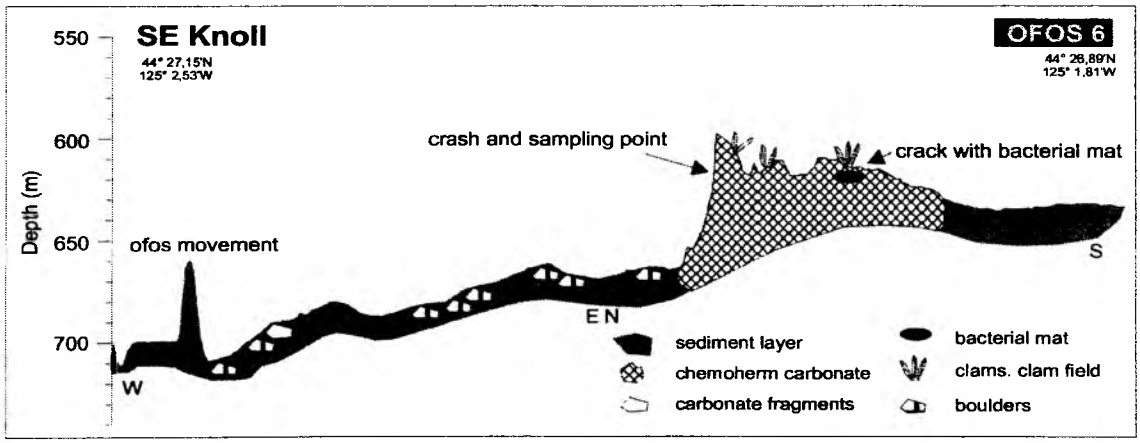

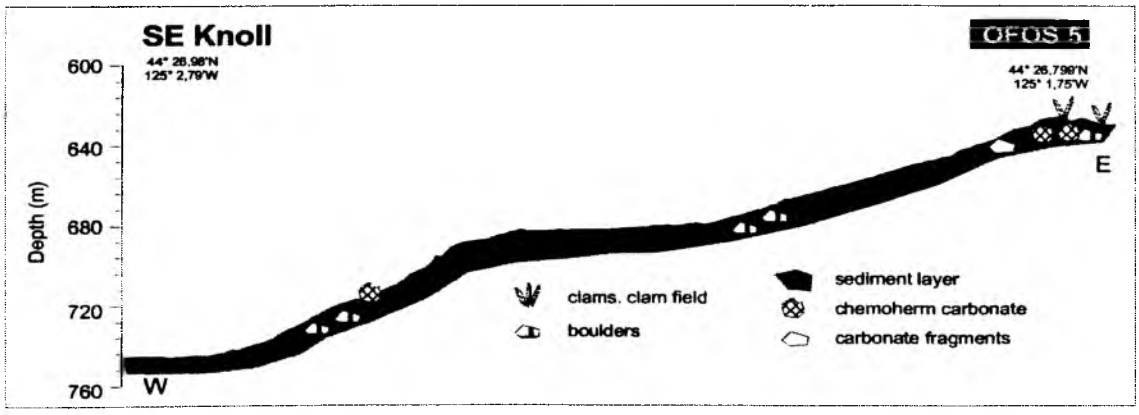

Fig. 12: OFOS profiles at the SE Knoll.

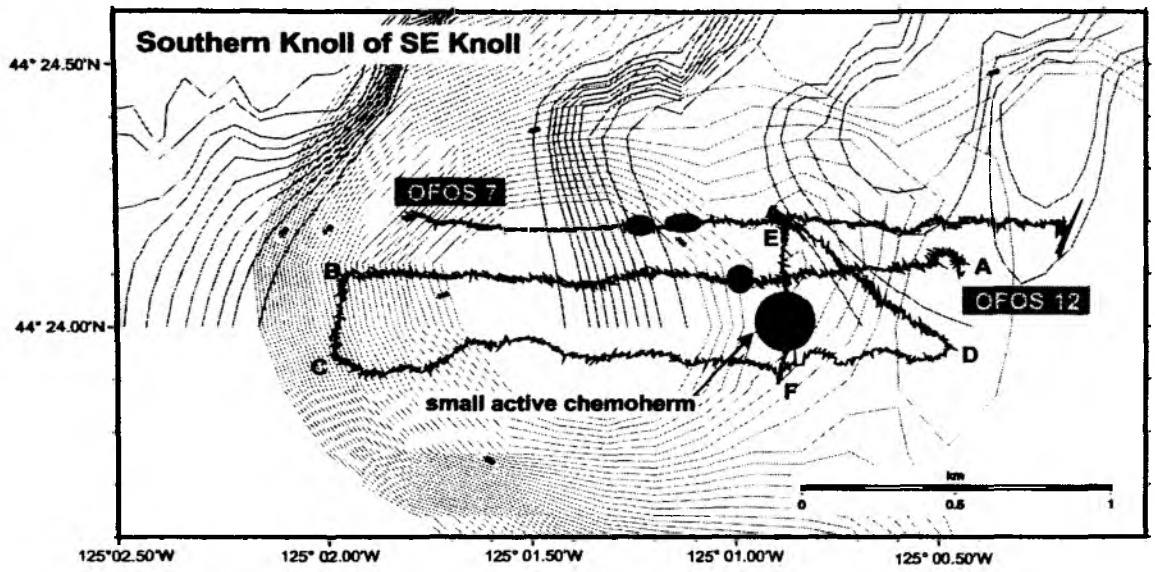

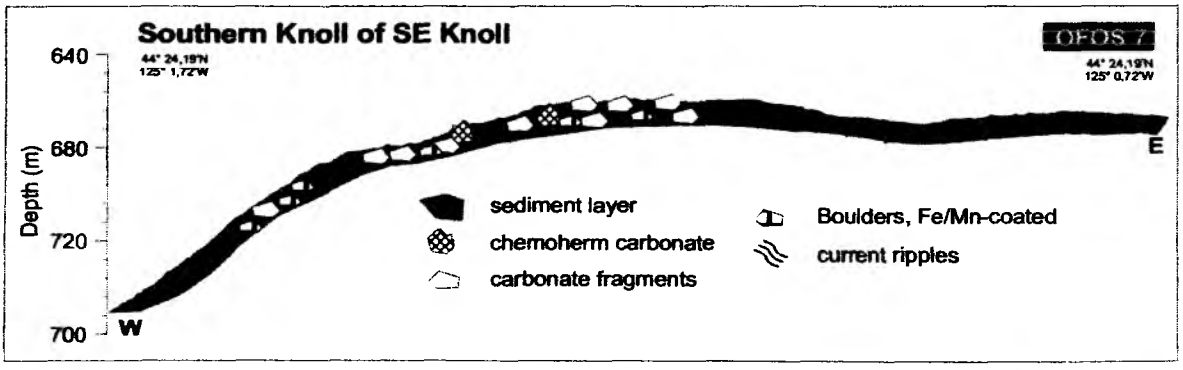

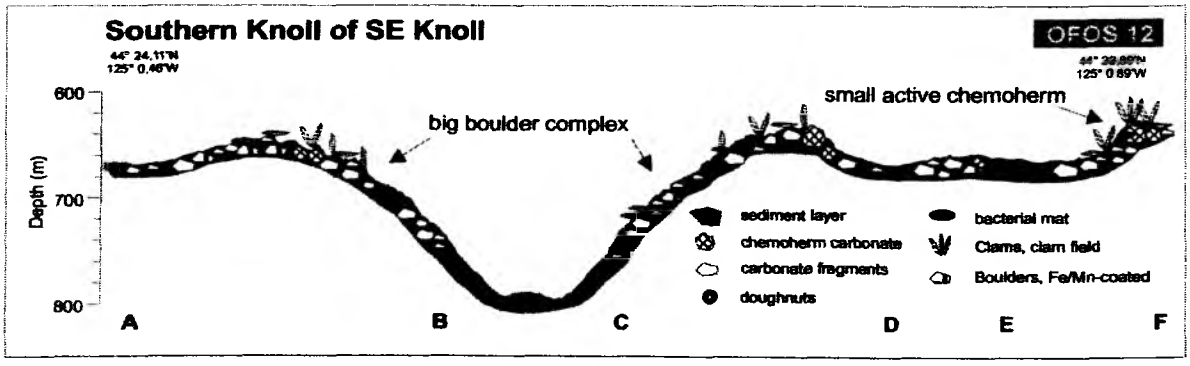

Fig. 13: OFOS profiles at the southern knoll of the SE Knoll.

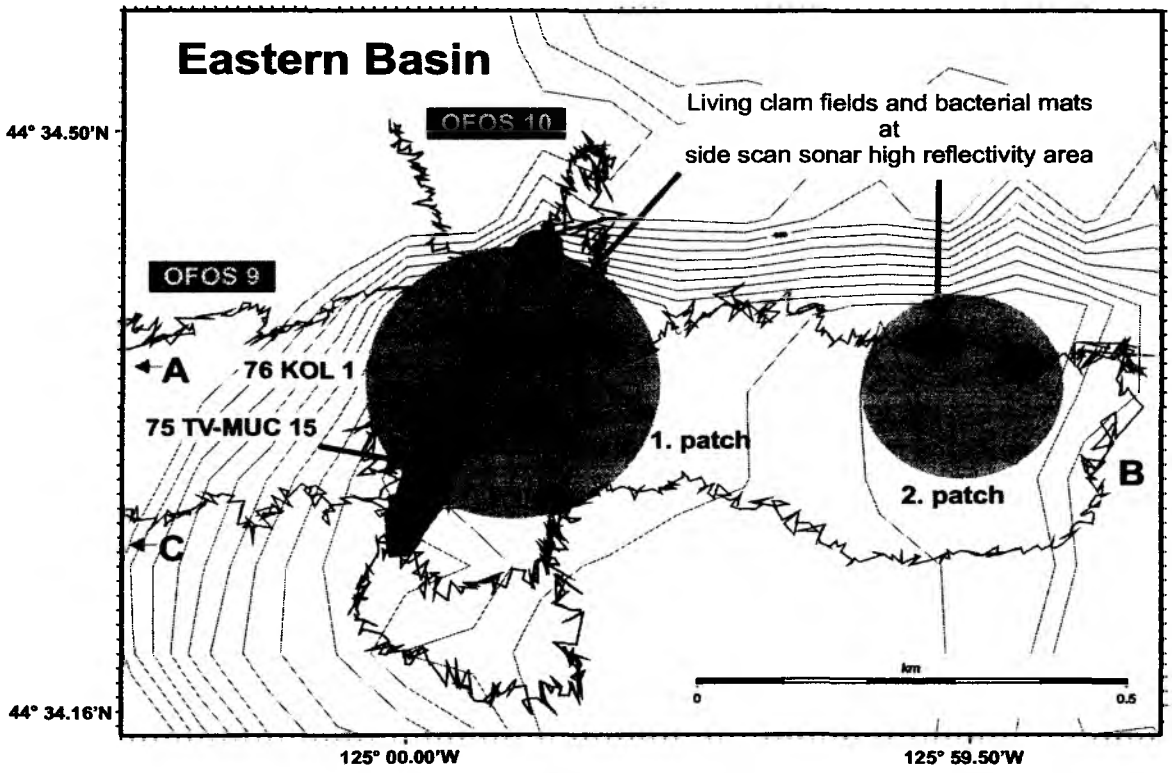

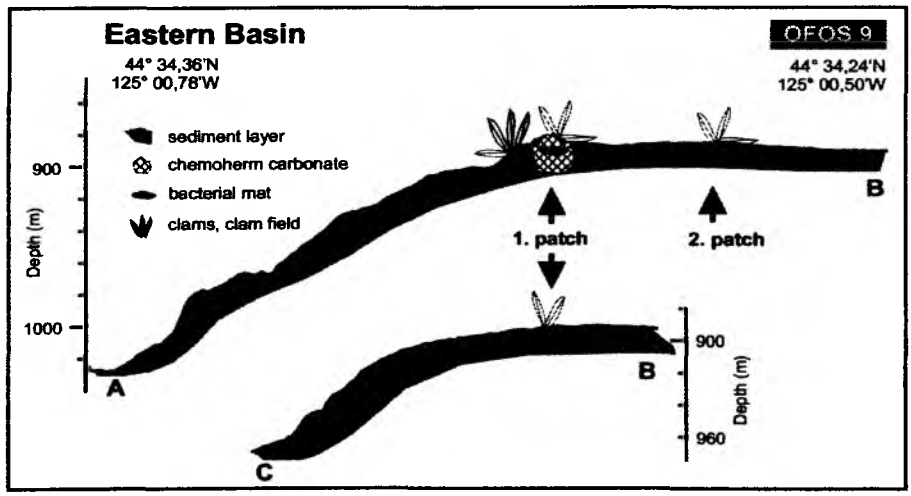

Fig. 14: OFOS profiles at the E-Basin.

5 THE ROPOS REMOTELY OPERATED VEHICLE (ROV) SYSTEM

5.1 General Specifications and Performance

K. Shepherd

The ROPOS Remotely Operated Vehicle (ROV) system, operated by the Canadian Scientific Submersible Facility (CSSF), was loaded on board the RV SONNE July 20, 2000. Mobilization was complete at July 22 and the vessel sailed for the TECFLUX working area. With four pilot/technicians on board, ROPOS was available for 12 hours per day operations. Operations typically were conducted from approximately 08:00 until 16:00 daily.

Tasks accomplished by the ROV included the following;

- Detailed bottom surveys,
- Precise deployment and recovery of time-lapse cameras,
- Triggering a bank of Niskin bottles mounted on the ROV in specific locations (Fig. 15),
- Re-positioning Landers to seal the chamber,
- *In situ* experiments with natural gas hydrates
- Recovery of instruments

Navigation was sometimes erratic, which caused some minor problems with sub positioning, but as all people became more familiar with the operations and area targets were easily relocated.

Fig. 15: Front view of ROPOS equipped with 4 Niskin bottles and biobox.

Fig. 16: View of the ROPOS system from the back with the vehicle in the cage.

General Specifications

ROPOS is a 30/40-horsepower electro-hydraulic vehicle (2.6m x 1.7m x 1.45m) with fore-aft, vertical, and lateral thrusters. A Mesotech colour imaging sonar, colour (3-CCD) and low-light silicon intensified target (SIT) video cameras, and seven- and five-function manipulators are mounted on the front of the vehicle. For deep-water operations (>500m; 30-horse-power) ROPOS is launched and recovered in a 4.2m x 2.7m x 2.1m cage containing a winch with a 250m tether (Fig. 16). The cage is linked to

the support vessel by a 5500m electrical-optical cable mounted on a large winch. This arrangement provides a decoupling of the vehicle from the ship's motion while operating at depth. The vehicle is well equipped with the following standard equipment:

Scientific Telemetry System
The Scientific Telemetry System (STS), completely independent of the vehicle telemetry system, is based on a PC/104 architecture, with a 486 CPU. It multiplexes up to seven bi-directional RS-232 channels together, permitting real time communication with, and control of many instruments. Further developments added to this versatile system include analog and digital input and output. An external junction box is provided for the user interface. It supplies 24, +\- 12 and 5 VDC from the telemetry system, as well as access to the RS-232 ports. Control and communications software for the STS was developed by Software Engineering Associates.

Laser Scales
Laser pointers are provided which project two parallel beams of light through the water. They provide scale in images for measuring object size or estimating organism density. The lasers appear in video frames as two points of red light on the surface of interest, 5cm apart, regardless of camera zoom and vehicle proximity to the target. More lasers are available, and can be fitted to meet specific user requirements.

3-CCD Video
A Sony DXC-950 broadcast quality video camera with a 16x zoom lens is provided by the University of Victoria. It transmits an RGB signal via the fiber optic link to the surface. A BetaCam recorder receives the signal and converts it to S-video for distribution to the onboard video archiving system that uses the S-VHS format. BetaCam recording is usually limited to high quality images of particular scientific interest or to material recorded for commercial production.

Integrated Real-time Logging system (IRL)
CSSF provides an HTML-based system for real-time text, data and video frame grab logging of dive operations. The primary hardware components are a PC with a video capture card, a text logging computer, removable hard drive media and CD-ROM burners. Sea floor features, sample collections and other interventions are recorded as captured video frames, in addition to being recorded in the continuous video tape archive. Real-time text logs are prepared in hypertext format and include hot links to corresponding video frames. Navigation data is tagged to each entry. At the end of a cruise, the entire dive log series is transferred to CD-ROM and copies supplied to users. ROPOS personnel provide technical assistance only, with users being responsible for all logging operations.

Suction Sampler
The suction sampler is an original design. The suction pump works at a variable speed. The suction inlet is attached to the end of a manipulator, usually the five function arm, in such a way that the manipulator can still perform other simple tasks. The samples are collected in eight, two litre jars that have a filter mesh on the outflow. The mesh can be changed on each jar, allowing for the collection of a wide array of specimens. We routinely use the suction sampler to collect water, bacterial mat, tube worms, clams, small fish and crabs, sediments and small rocks.

Pacman
The "Pacman" sampler is a clamshell shaped sampler that replaces the jaw end effector of the manipulator. It can bolt directly onto either the seven or five function arm. It excels at sampling soft or fragile items. It can also take a quantitative sample from a specific area ($0.045m^2$).

Sample Tray and Biobox
A large rotary sample tray has proved to be a robust, well-used addition to the system. It incorporates four to eight compartments for collecting geological and biological samples. It extends into, and retracts from the work envelope for easy sample stowage. A hydraulically-actuated Lexan "biobox" can be substituted for the sample tray in the same mount. The thick Lexan walls of the biobox provide thermal insulation for temperature-sensitive organisms sampled in deep water, at its greater dimensions permit the collection of specimens that would be damaged by forcing them into the sample tray. Removal of the biobox center divider provides a storage area of 80cm (long) x 30cm x 20cm.

Hydraulic Functions for Science
The hydraulic power packs on the vehicle provide eight separate hydraulic functions for scientific tools. The modification was undertaken in response to the increasing number of hydraulically-actuated scientific tools being used on ROPOS and frequent requirements to use several tools during a single dive.

Digital Still Camera
The Canadian Scientific Submersible Facility is purchasing a Digital Still Camera. This is expected to be on the vehicle for 2001.

System Performance
ROPOS was operational 100% of this period with no time lost to breakdowns or maintenance. Routine maintenance, usually allowed at the rate of 2 hours per 12 hours of operations, was conducted outside of the scheduled dive time. During the project, some minor problems were encountered with the sonar transmission path as well as with the compass. Both were repaired before the next scheduled dive operations. Overall, the system completed 18 dives, including one test/training dive, for a total of 109 hours of wet time (Tab. 2).

The IRL system was provided as part of the ROPOS system. At the end of the mission, it provides a CD set containing video frame grabs, comments, sample details and navigation details. Since CSSF did not provide navigation services, it proved to be quite difficult to import navigation data into the IRL system. This was finally completed, with coding by a software engineer on shore, by the third day of the project.

Tab. 2: Overview on ROPOS dives conducted during SO148 (Leg 1: Dives 558-566; Leg 2: Dives 567-574).

Dive No.	Stat No.	No.	Date	Begin	End	Area	Chief scientist	CD No.	Remarks
558	1	1	23-Jul	01:28	03:29	HR South	Linke	1	survey, no navigation
559	4	2	24-Jul	15:55	22:29	HR South	Linke	1	survey, no navigation
560	10	3	25-Jul	15:25	22:22	HR South	Linke	3	survey
561	17	4	26-Jul	15:26	23:09	HR North	Linke	3	survey, sampling
562	23	5	27-Jul	15:55	22:29	HR North	Linke	3	camera deployment
563	30	6	28-Jul	17:55	22:10	HR South	Linke	4	survey, lander
564	33	7	29-Jul	15:20	22:34	HR North	Linke	4	camera exchange
565	41	8	30-Jul	16:29	23:15	SE Knoll	Linke	2	Survey, sampling
566	48	9	31-Jul	15:10	22:30	HR North	Linke	2	camera exchange, lander
567	60	10	05-Aug	15:12	23:17	R1 Ridge	Bohrmann	5	survey
568	64	11	06-Aug	15:25	01:08	HR South	Suess	5	*in situ* gas hydrate exper.
569	69	12	07-Aug	16:08	22:27	HR South	Kudrass	5	AKL recovery
570	74	13	08-Aug	15:59	00:41	Pinnacle	Bohrmann	5	survey
571	81	14	09-Aug	15:31	23:12	Pinnacle	Bohrmann	6	survey, camera change
572	97	15	11-Aug	15:01	17:56	HR North	Suess	5	lander, camera retrieved
573	98	16	11-Aug	20:05	00:06	HR South	Suess	5	camera retrieved, marker
574	103	17	12-Aug	17:24	22:22	NW Knoll	Suess	6	survey

5.2 ROPOS Dive Protocols

P. Linke, G. Bohrmann, E. Suess, H. Kudrass

Dive number: **558**
Date: 23 July
Area: Southern Hydrate Ridge
Launch site: 48°18.078'N; 125°53.067'W
Scientist: Peter Linke
Logging: CD#1
Objectives: Look for active bubble sites, sample bacterial mats, obtain an overview about the areal extent, look for last year's sample and lander deployment sites.

Summary: First short scientific dive of the cruise to familiarize with the ROPOS system and its features. Problems with the navigation made the orientation very difficult; all other systems were operational.

Dive number: **559**
Date: 24 July
Area: Southern Hydrate Ridge
Launch site: 44°34.261'N; 125°08.978'W
Scientist: Peter Linke
Logging: Tina Treude, CD#1
Objectives: Drop markers, sampling of *Beggiatoa* mats with frame and suction sampler, extend survey to the west towards the Pinnacle.

Summary: Sites with highest methane enrichment were indicated by the presence of white and orange mats of giant sulfur-oxidizing bacteria (*Beggiatoa)* covering the seafloor. These patches of bacterial mats sized from a few centimeters up to several tens of meters at the Southern Hydrate Ridge.

The thinnest mats consisted of single vertically oriented white *Beggiatoa* filaments which extended 2-3 cm into the sediment. The thickest mats (0.5-2 cm thickness) were bright orange with strongly tangled filaments which were easily resuspended from the sediment surface in large aggregates. The suction sampler of ROPOS was used to obtain quantitative samples of these surficial *Beggiatoa* mats. For this purpose, a 40x40 cm metal frame with scales on each side was set on a mat and photographed before and after sampling of a patch of about 10x10 cm within the frame. The sample was sucked into one of the jars of the ROPOS sampler and the bacterial filaments were retained on a 20 µm gauze.

Dive number: **560**
Date: 25 July
Area: Southern Hydrate Ridge
Launch site: 44°34.171'N; 125°08.720'W
Scientist: Peter Linke
Logging: Tina Treude, CD#3
Objectives: Obtain samples from bacterial mats, survey Beaver Mounds area and drop markers at defined structures.

Summary: During the dive the lost AKL was found sticking no longer upright in the sediment but lying on the sediment. Traces of fishing activity indicate that it has been knocked over by trawling. The AKL was inspected visually to prepare recovery. Lander weights from last year's cruise were found. Within a large depression rising gas bubbles were observed; when ROPOS dived into the depression to find the origin of the bubble stream a bluish, opalescent material was found within the wall of the depression which was scratched but could not be sampled by ROPOS (revisited on dive 568).

Dive number: **561**
Date: 26 July
Area: Northern Hydrate Ridge
Launch site: 44°40.161'N; 125°05.822'W
Scientist: Peter Linke
Logging: CD#3
Objectives: Look for active bubble sites, deploy markers to improve orientation and navigation, prepare deployment of camera system, obtain bacteria samples.

Summary: Deployment of ROPOS above old OSU-barrel lost during TECFLUX 98, still problems with navigation, new bubble site discovered and marked with marker #2, carbonate sample from bubble site. After a long search due to problems with the navigation, the Gusher Site at marker #6 was found and examined for the deployment of the camera system. Bacterial mats were sampled with the suction sampler, a carbonate sample was taken. Deployment of marker #3 and #4 between the Gusher Site and the barrel to obtain an improved orientation for the deployment and recovery of the camera system.

Dive number: **562**
Date: 27 July
Area: Northern Hydrate Ridge
Launch site: 44°40.194'N; 125°05.854'W
Scientist: Peter Linke
Logging: Volker Karpen
Objectives: Deployment of the digital camera system and survey to the west.

Summary: The camera system was carefully deployed to obtain the optimal view for the recording of the gas bubbling activity. The bubble site at marker #2 was revisited and found still active.

Dive number: **563**
Date: 28 July
Area: Southern Hydrate Ridge
Launch site: 44°34.195'N; 125°08.49'W
Scientist: Peter Linke
Logging: Volker Karpen
Objectives: Bubble site survey, collect water samples and bacterial mats, check deployment site of VESP-Lander I.

Summary: Lander deployment sites of last year's SONNE cruise were found. Crater discovered during dive #560 was revisited and bubble discharge was found active and followed for up to 100 m above the bottom. The plume was lost easily with single bubbles rising too fast for ROPOS to follow. Niskin water samples were obtained at distinct distances from the bubble source. The VESP-Lander was found sitting on a rim between two craters allowing no proper sealing of the fluid flux chamber. ROPOS moved the lander and optimized the sealing by pushing the chamber into the sediment. TV-grab hole was observed. Bubble site revisited; carbonate and bacterial mat samples were obtained.

Dive number: **564**
Date: 29 July
Area: Northern Hydrate Ridge
Launch site: 44°40.180'N; 125°05.918'W
Scientist: Peter Linke
Logging: Barbara Bock
Objectives: Exchange camera systems I and II, conduct a survey to the SONNE chemoherm in the west.

Summary: Camera system II was deployed next to camera I at the gusher site to obtain a recording overlap with 2 different views during the dive. The bubble site at marker #2 was revisited and found still active. After this, a survey to the west heading for the SONNE chemoherm was conducted to map the distribution of carbonates and vent fields (Fig. 17). A large field of snail egg cases was found which have been produced simultaneously. Recovery of camera system I after 2.5 days of recording.

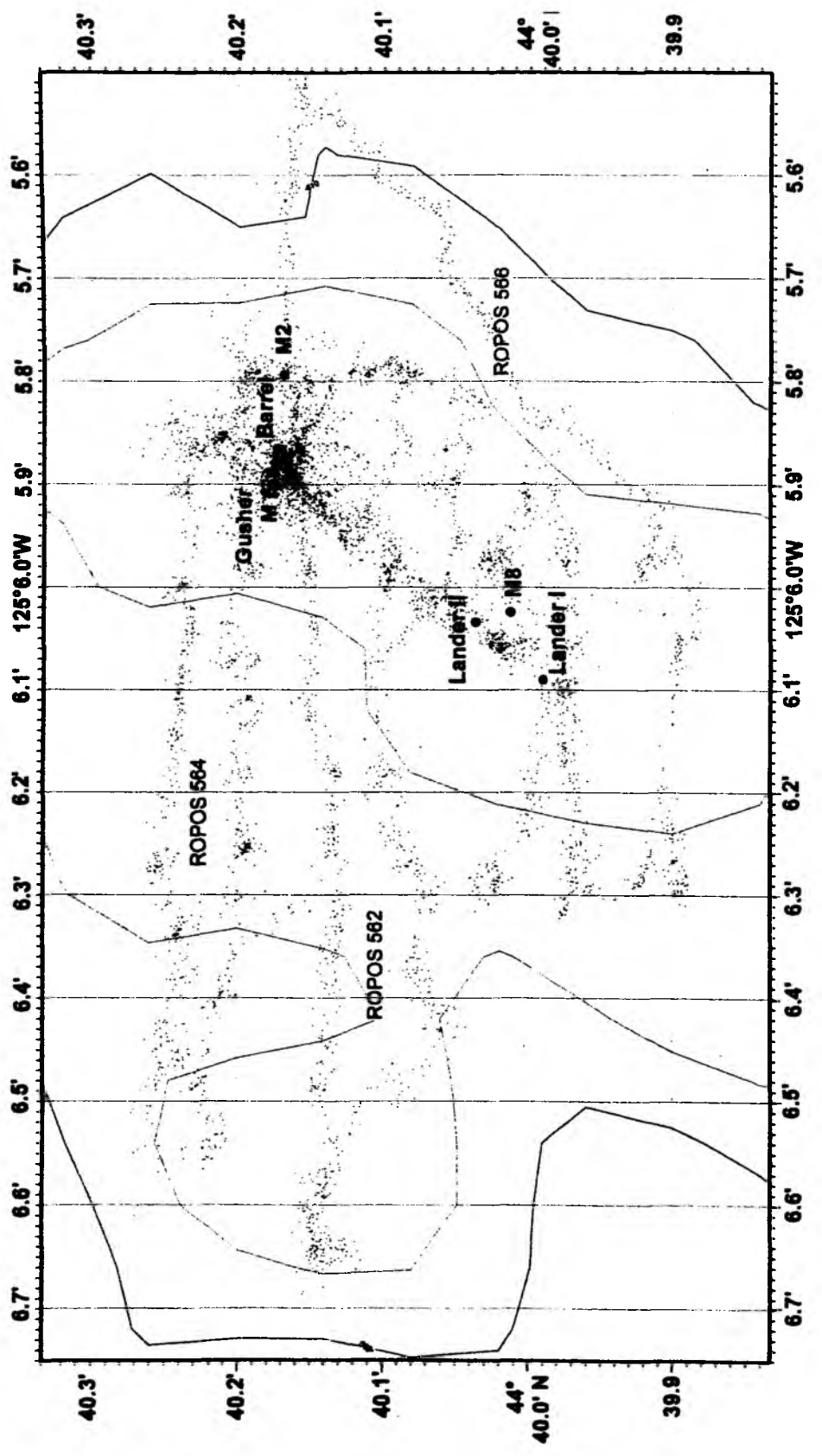

Fig. 17: Track lines of ROPOS dives 562, 564, and 566 at Northern Hydrate Ridge with marker and lander positions.

Dive number: **565**
Date: 30 July
Area: SE Knoll
Launch site: 44°27.061'N; 125°01.694'W
Scientist: Peter Linke
Logging: Barbara Bock
Objectives: Survey of unknown area, obtain samples from bacterial mats and carbonates, collect water samples.

Summary: A submarine carbonate cliff elevating about 90 m was surveyed. It had been discovered with OFOS during SO143. In the upper part of the cliff bacterial mats and clams aligned in small fractures and fissures of the carbonates, site of gas bubble discharge were dicovered and Niskin water samples were obtained at distinct distances from the source. Tube worm sampled from beneath carbonate overhang, carbonate and bacteria samples were obtained.

Dive number: **566**
Date: 31 July
Area: Northern Hydrate Ridge
Launch site: 44°40.136'N; 125°05.911'W
Scientist: Peter Linke
Logging: Volker Karpen, CD#2
Objectives: Exchange camera system, extend survey to the southern part of the northern summit, check deployment site of VESP-Lander II.

Summary: Second camera system was deployed next to the first device to obtain an overlap in recording. ROPOS was used to follow the gas bubbles rising from the seafloor through the water column. By using ROPOS' scanning sonar and video system for tracking the bubbles, the experiment showed a clear decrease in bubble concentration/size at a depth of about 450 m. Very low concentrations of visible bubbles could still be found as shallow as 387 m. Niskin water samples were obtained in 5 m steps above the gusher site at marker #6. The extension of the survey to the south revealed large clam fields with small bacteria mats. The visit of the deployment site of VESP-Lander II was used to inspect and check the proper sealing of the benthic chamber. Retrieval of the first camera system.

Dive number: **567**
Date: 5 August
Area: R1 Ridge
Launch site: 45°35.872'N; 125°°09.376'W
Scientist: Gerhard Bohrmann
Logging:
Objectives: Survey the R1 Ridge for gas and fluid vent sites, carbonates and gas hydrate exposures.

Summary: Survey followed from south to north along W/E or E/W profiles to explore the elongated ridge crest (Fig. 18); R1 has similar water depth

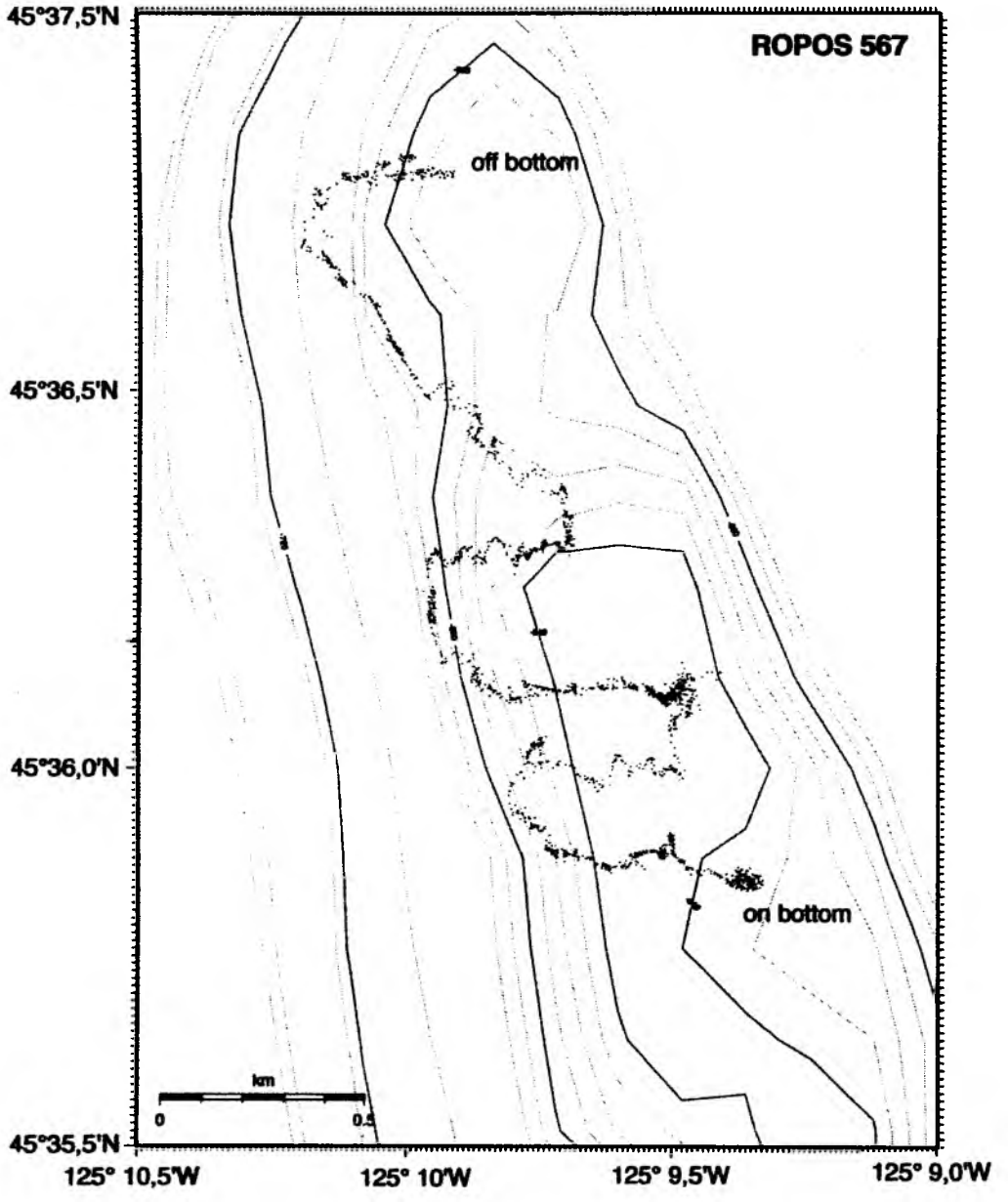

Fig. 18: Track line of ROPOS dive 567 at the R1 Ridge.

and morphology to Hydrate Ridge; small patches of clam fields with chemoherm-like carbonates were observed along the first W/E profile; large clams fields of *Calyptogena* partly covered by bacterial mats were discovered and sampled (suction sampler); four niskin bottle samples along a gradient from a center of the large clam field up to 45 m away; chemoherm carbonates on the western flank of the northern nose.

Dive number: **568**
Date: 6 August
Area: Southern Hydrate Ridge
Launch site: 44°34.19'N; 125°08.80'W
Scientist: Erwin Suess
Logging: B. Teichert/B. Bock; CD#5
Objectives: Ascertain surface exposures of hydrate; find and document vent sites (bubble streams) and sample hydrates and fluids.

Summary: Excavated 15-20 cm thick horizontally oriented hydrate layer partially exposed on the hanging wall of fissure (or impact crater of previous TV-G sampling); poorly bedded soft sediment below and above; several harder layers form overhang; sporadic bubble escape from cavity below hydrate layer; massive layer appears very similar to old glacier ice, but clean, with bluish/white opalescence; hard and scratchable surface; another thinner layer exposed above containing hydrate nodules and narrow hydrate-filled fissure which cut through the bedding and cement entire sediment package sampled massive piece from upper layer and conducted decomposition experiment under changing temperature and pressure while ascending and descending in the water column; observed bubbles and dissolution features forming above 380 ±20 m; reaction stopped below that depth. Deployed times-lapse camera for recording flow of bubble streams, but postion could not be optimized because bubble stream ceased.

Dive number: **569**
Date: 7 August
Area: Southern Hydrate Ridge
Launch site: 44°34.199'N; 125°08.855'W
Scientist: Herman Kudrass
Logging: B. Teichert/B. Bock; CD#5
Objectives: Recovery of autoclave piston cores (AKL).

Summary: Operation started at 16:08 UTC with basket containing 100 m spectra rope hanging below cage; stopped at 695 m to inspect basket; moved vessel 50 m N to position cage closer to AKL; at 18:20 lowered cage additional 50 m and located first AKL then dummy weight about 40 m apart; released basket and began several attempts to hook spectra rope to dummy weight; after completion moved to AKL which at 20:44 was hooked to steel wire; then attempted at 21:32 UTC to relocate bubble camera near marker 7 but failed due to poor visibility, returned to surface; on deck 22:27.

Dive number: **570**
Date: 8 August
Area: Southern Hydrate Ridge /Pinnacle
Launch site: 44°34.181'N; 125°08.849'W
Scientist: Gerhard Bohrmann
Logging: B. Teichert/B. Bock, CD#5
Objectives: Survey the Pinnacle area and collect carbonate rocks; check the position of the camera.

Summary: ROPOS reached seafloor close to bubble site at marker 6; no bubbles (high tide); bearing of the camera direction to the bubble stream was not possible; on the way to the Pinnacle a huge field of snail egg cases (*Buccinium*) was crossed; Pinnacle was crossed several times; vertical cracks were searched and followed by the ROV; cracks hosted clams and bacterial mats; water samples were taken by niskin bottles; marker 9 was deployed at the northwestern edge; white and orange bacteria were collected by suction sampler; several carbonate samples were taken by the ROV packman; setting marker 11 on top of the Pinnacle; carbonate sample close to the marker.

Dive number: **571**
Date: 9 August
Area: Southern Hydrate Ridge /Pinnacle
Launch site: 44°34.097'N; 125°°09.176'W
Scientist: Gerhard Bohrmann
Logging: B. Teichert/B. Bock, CD#6
Objectives: Change camera at bubble site (marker 7) and continue exploration of Pinnacle.

Summary: Landing on top of the Pinnacle close to marker 11; ROPOS dived the northern flank down and followed the western base of the chemoherm, reached the southern flank; a NNE trending crack with bacteria and clams was followed; water (niskin bottle) and rock sampling on top of the Pinnacle; steaming to marker 7 northeast of the Pinnacle; catching the time lapse camera from the pit site and deploying it at a new position closer to marker 7; camera is facing a small crack where bubbles are escaping; to the southeast marker 6 was exchanged by marker 12.

Dive number: **572**
Date: 11 August
Area: Northern Hydrate Ridge
Launch site: 44°39.841'N; 125°06.139'W
Scientist: Erwin Suess
Logging: B.Teichert/B.Bock; CD#5
Objectives: Recover bubble camera; inspect Lander deployed during Leg 1.

Summary: Lander found sitting on edge of clam field with weigths about 10 cm deep into the sediment; area under Lander about 40% covered by clams; edges of funnel appeared sealed (at least on 2 sides); attempted twice unsuccessfully to move Lander towards 100%-clam coverage by lifting and pulling; recovered camera system and return to surface;

recording stopped at 6 August after which power failed; assume auto-focussing activated by floating particles and/or wake-up exhausted energy supply; bubble stream generally more active than at southern summit; driven by tides but higher frequency modulations of unkown origin superimposed.

Dive number: **573**
Date: 11 August
Area: Southern Hydrate Ridge
Launch site: 44°34.199'N; 125°08.878'W
Scientist: Erwin Suess
Logging: B.Teichert/B. Bock; CD#5
Objectives: Recover bubble camera; deploy marker for OFOS survey.

Summary: 10 markers were deployed along 2 perpendicular transects centered at marker #7, markers long N-S transect placed 50 m apart, markers along E-W transect 30 m apart (see Fig. 19); recovered camera system and return to surface; system fully recorded up to 22:00 UTC on 11 August; at rising tide and high tide, strongly diminished bubble activity, during low tide activity increased by several orders of magnitude. No samples.

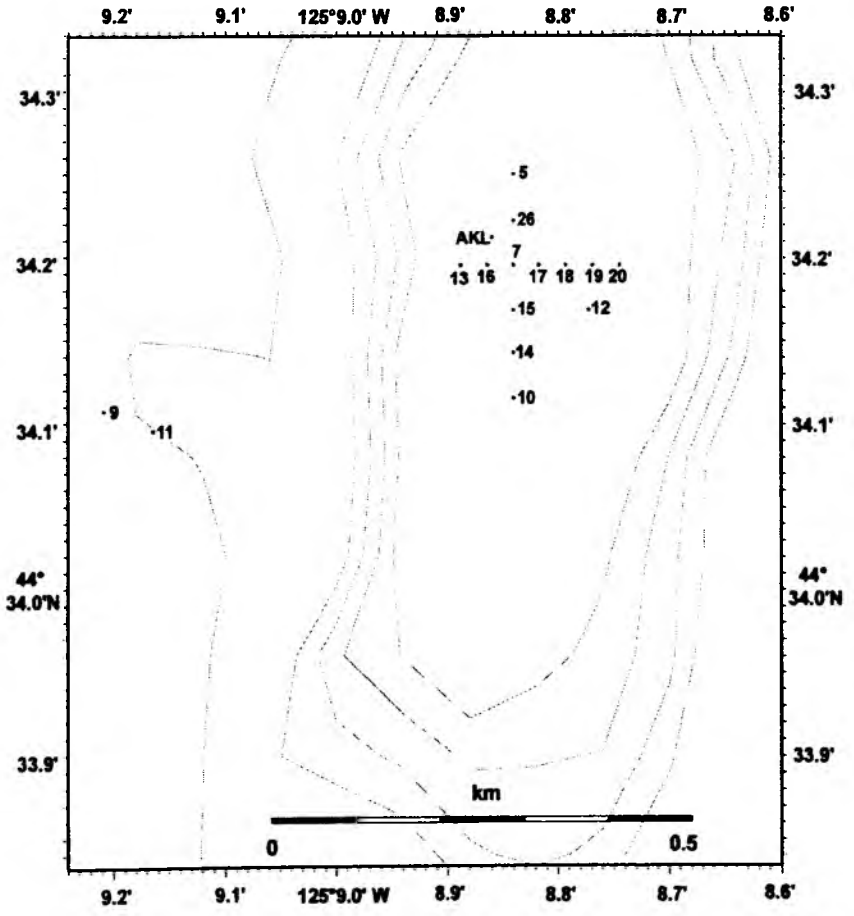

Fig. 19: Marker positions at Southern Hydrate Ridge.

Dive number: **574**
Date: 12 August
Area: NW-Knoll
Launch site: 44°43.782'N; 125°13.729'W
Scientist: Erwin Suess
Logging:
Objectives: Explore summit of knoll for venting activity to place *In Situ Schlierenoptic*; sample vent fauna and carbonates.

Summary: Flat to gently sloping surface; summit at 932 winnowed; on SW-facing slope; vent fauna, small colonies of large clams; about 3-6 individuals and few bacterial clumps; fauna aligned along depth contour 950-960 in narrow zone of partially carbonate cemented glauconite sand; numerous cemented ledges outcropping with fauna in overhang; cemented sands forming open pipes, channels, flanges and other features of fluid plumbing system exposed; well-developed string of mature colonies about 100m long (see detailed map); no indication of hydrate.

Tab. 3: Positions of markers dropped or found during SO148.

	Lat. °N	Long °W	Depl. Dive	SSBL pos./ROPOS SO148		Remarks
Northern Hydrate Ridge						
Marker 2			561	44:40.172	125:05.796	gas seep east of Gusher
Marker 3			561			between barrel and Gusher
Marker 4			561			between barrel and Gusher
Marker 6	44:40.165	125:05.897	1999	44:40.175	125:05.878	ALVIN marker, Gusher Site
Marker 8			564	44:40.057	125:06.033	clam field
Barrel	44:40.167	125:05.866	1998			Ron Brown cruise 1998
Southern Hydrate Ridge						
Marker 1			588			clam field, without navigation
Marker 5	44:34.250	125:08.840	573	44:34.195	125:08.840	grid field
Marker 7	44:34.195	125:08.840	1999			ALVIN marker, bubble site
Marker 10	44:34.115	125:08.840	573	44:34.142	125:08.779	grid field
Marker 12			567	44:34.166	125:08.773	exchanged at marker 6 position
Marker 13	44:34.195	125:08.888	573	44:34.189	125:08.869	grid field
Marker 14	44:34.142	125:08.840	573	44:34.148	125:08.818	grid field
Marker 15	44:34.168	125:08.840	573	44:34.168	125:08.810	grid field
Marker 16	44:34.195	125:08.864	573	44:34.202	125:08.841	grid field
Marker 17	44:34.195	125:08.817	573	44:34.202	125:08.797	grid field
Marker 18	44:34.195	125:08.793	573	44:34.196	125:08.765	grid field
Marker 19	44:34.195	125:08.769	573	44:34.194	125:08.723	grid field
Marker 20	44:34.195	125:08.745	573	44:34.192	125:08.705	grid field
Marker 26	44:34.222	125:08.840	573	44:34.231	125:08.813	grid field
AKL	44:34.212	125:08.860	1999	44:34.203	125:08.847	AKL lost during SO143-3
Southern Hydrate Ridge, Pinnacle						
Marker 9			570	44:34.108	125:09.209	NW flank of Pinnacle
Marker 11			570	44:34.097	125:09.165	Pinnacle top 773 m
NW-Knoll						
Marker 27			574	44:43.763	125:13.707	

6 VENT SAMPLING AND FLUX MEASUREMENTS

P. Linke, F. Appel, B. Bannert, K. Nakamura, A. Petersen, B. Vaessen

Introduction

Hydrogeologic processes can exert a fundamental control on the stress state, dynamics, and the thermal, and geochemical processes along continental margins. Hydrogeologic processes impact on (1) the physical and chemical evolution of sediments and the oceanic basement during subduction, (2) the state of stress and seismic properties of major plate boundary fault zones, (3) earthquake dynamics, and (4) global chemical cycles of greenhouse gases and other chemicals. It has also been recently recognized that in some regions ground water seepage may be volumetrically significant enough to effect the chemistry of the coastal ocean waters (Moore, 1996).

Although direct evidence for the chemistry and volume of fluids migrating towards the sediment surface is relatively sparse, especially in zones of diffusive flow, there is strong evidence for locally significant focused advection of fluids carrying reduced sulfur and/or reduced carbon compounds (e.g. methane) from the presence of dense chemoautotrophic clams (*Calyptogena*) and/or tube worm communities at cold seeps (Kulm et al., 1986; Boulegue et al., 1987; Suess et al., 1985). Other evidence for past and present fluid expulsion is the occurrence of carbonate pavements and chimneys (e.g. Kulm et al., 1986). Once seeps began to be identified based on this visible evidence, it was found that they were a common feature all along the continental margins in a variety of tectonic settings. Focused discharge rates can be large. Determinations made at seeps off Oregon suggest that, where seepage is marked by obvious biologic communities, H_20 and CH_4 flux rates can be as high as 100-1065 m/y (average Darcy flow) and 120 mmol m^{-2} day^{-1} respectively (Linke et al., 1994).

Focused discharge at these seeps may, however, be only part of a larger hydrogeologic puzzle. It quickly becomes apparent that fluid migration and discharge is strongly heterogeneous with regions of focused and diffuse flow (Moore and Vrolijk, 1992; Brown et al., 1995). The diffusive flow component could be of sufficient magnitude to promote the regional build up of significant gas hydrate bodies along continental margins (Hyndman and Davis, 1992). Structure, lithologic, and diagenetic patterns contribute to heterogeneity in flow and expulsion pattern through their effect on the permeability distribution at depth. Heterogeneity occurs at a variety of scales. Linke et al. (1994), for example, report they encountered at seeps off Oregon an „enormous variability in the rates of fluid expulsion within the same accretionary prism". Seeps, however, typically represent much less than 0.01% of the surface area of most active tectonic systems. There is also strong evidence for irregularly but widespread diagenetic hard grounds all around the Oregon seeps, suggesting that widespread elevated rates of diffusive flow may be occurring over a region of many 10's km^2 (Carson et al., 1994). Even though it occurs at generally lower rates, the diffuse component flow can be as important as focused flow in terms of the total mass balance of fluids because of the greater area involved. For a variety of reasons, however, direct quantification of this diffusive component has been difficult, with the exacerbating factor that it is also likely to be spatially heterogeneous.

These factors have fundamentally limited our past ability to constrain the complete hydrologic system in many environments. Ultimately, in large offshore hydrogeologic systems, the statistical relevance of mass flux and hydrogeologic determinations can only be proven through a large number of surface flux measurements that allow us to build accurate maps of heterogeneous fluid and chemical expulsion patterns. The basic problem associated with accurately quantifying heterogeneous fluxes applies to almost any type of studies our work relates to, whether we are interested in the relationship

between aqueous (and gaseous) discharge patterns and (1) structure/statigraphy, (2) gas hydrates, (3) other chemical fluxes, and (4) benthic biological seep communities and nutrient fluxes.

Material and Methods

Our basic concept to sample fluids and to measure the fluid and gas flow is the channeling of the effluent from the seafloor into a semi-enclosed benthic chamber with a large opening at the bottom and a small exhaust port at the top (Linke et al., 1994). After deployment of the chamber the internal volume is initially flooded with ambient sea water and is then slowly replaced by vented fluids. Sequentially timed water samples are collected inside the chamber. Changes in the concentration of dissolved components within these time series are used to calculate flux rates (Carson et al., 1994). Parallel to this, a thermistor flowmeter is mounted in the exhaust port of the chamber to record the *in situ* fluid flow rate.

During cruise SO148 two video-guided landers were used for the deployment of a benthic chamber from a conventional research vessel on a cold seep at the seafloor (VEnt SamPler - VESP). The ship's cable (either coaxial or a hybridic with fiber optic and coaxial fibres) is used for bidirectional transmission of the video images, commands, data, and power supply of the underwater units (ADITEC/SCHOLZ) and is connected with the launcher which carries the lander. The whole instrument is towed in view of the seafloor approx. 2 - 3m above the sediment. The lander is deployed and disconnected from the launcher when signs of seepage become visible (e.g. clam clusters, bacterial mats). The VESP-Landers are equipped with an improved chamber to obtain both direct water flow and samples expelled from active sites. They are designed as an instrument carrier for a variety of different measurements which could be integrated with this system. The landers are designed to stay on the seafloor for several days to weeks recording the different parameters (e.g. temperature, conductivity, methane, fluid flow, microseismicity etc.), and would take samples prior to the recovery of the instrument by acoustic release of the additional weight.

In the configuration used during cruise SO148 the launcher carried two video cameras, a color survey camera (DEEP-SEA POWER & LIGHT) on the front and a backward oriented b/w camera (OSPREY) showing the chamber during deployment. Both cameras and floodlights (DEEP-SEA POWER & LIGHT) can be switched with a PC-controlled telemetry surface unit (OKTOPUS). The attached lander can be disconnected from the launcher by a mechanic release (NICHIYU GIKEN KOGYO). It carries a floatation unit with up to 14 BENTHOS floats and 2 glass instrument housings for power supply and ARGOS transmitters which can be easily exchanged with a floatation unit containing syntactic foam instead. Pieces of train tracks are used as weights and are dropped by paired acoustic transponder releasers (MORS RT 661 B1S & RT 361 BS). For spotting and recovery, the lander is equipped with a radio beacon, strobe light (NOVATECH), ARGOS transmitter and flag.

Beneath the floatation unit the lander has a wide open space for carrying various instruments like i.e. benthic chambers. The chambers of the 2 landers used on the SO148 cruise are pyramidial stumps made of titanium or stainless steel with a height of 30 cm. The bottom covers 1 m^2 surface area and the exchangable top area (40 x 40 cm) was equipped with ports for the thermistor flowmeter and for different other sensors (CH_4, H_2S, pH). The chambers are suspended within the lander frame during deployment by strong rubber bands and lowered on the seafloor by its own weight. To faciliate water exchange during deployment and recovery valves are opened by rubber bands and kept close through spring action when the chamber is placed on the seafloor.

On VESP-Lander II a motor-driven syringe sampler with 8 x 50 ml glas syringes is attached to the chamber to take water samples in a time series during deployment. To obtain a larger sample at the end of the deployment both landers carry a single 1.7-l water bottle mounted within and another as a bottom water reference sample outside the chambers respectively. Both are tripped simultaneously at the end of the deployment when the acoustic releasers are activated and provide water samples for the analysis of dissolved seep fluid species. Furthermore, both landers carry a storage CTD probe to continuously record conductivity, temperature, and pressure. Lander I is equipped with a storage CTD (FSI) directely mounted on the top of the funnel. On Lander II, a Sealogger (SBE25) is mounted on the frame with silicon tubings connected to the pump (SBE5T) of the Sealogger to provide a better convection within the funnel.

Results

Three deployments were conducted during SO148-1 (Fig. 20); one with Lander I for 4 days on a bacterial mat at the southern peak (#18) and another one with Lander II for 2 days on a clam field at the northern peak of Hydrate Ridge (#35). Both lander sites were inspected and the orientation of the chamber was corrected by the ROV. This will provide valuable information about the effect of bottom currents on the efflux measurements by comparison of a sealed and an unsealed chamber. The effect of the ROV handling can be clearly seen in the conductivity data at site #18 (Fig. 22) where the lander had been deployed on a rim between 2 craters (Fig. 21). The bad sealing of the chamber due to the rough topography of the area was improved by ROPOS.
A precise pressure sensor (Digiquartz, Paroscientific,Inc.) with a data logger was installed on one of the legs of the VESP-Lander. The pressure sensor was located about 70 cm above the lander paw. It was deployed with the VESP-Lander in the evening of July 26 (Local time, St. 18) at the southern summit of the Hydrate Ridge and recovered in the evening of July 30 (Local time). The pressure sensor recorded the *in situ* pressure from GMT 1:04 of July 27 (Local time, 18:04, July 16) to GMT 23:58 of July 30 (Local time, 16:58, July 30) at the interval of one minute.
As in Fig. 23, the *in situ* pressure measurement has good correlation in phase with the calculated Newport tide data provided by Dr. Robert Collier. The magnitude of the tide in the Hydrate Ridge is slightly smaller than that at Newport Harbour.

At the end of Leg 1, Lander I was deployed for a long-term measurement at a clam field south of the northern peak of Hydrate Ridge (#49). The position of the lander was inspected with ROPOS during Leg 2. It was successfully recovered during SO150 on October 10 after 70 days of recording data.

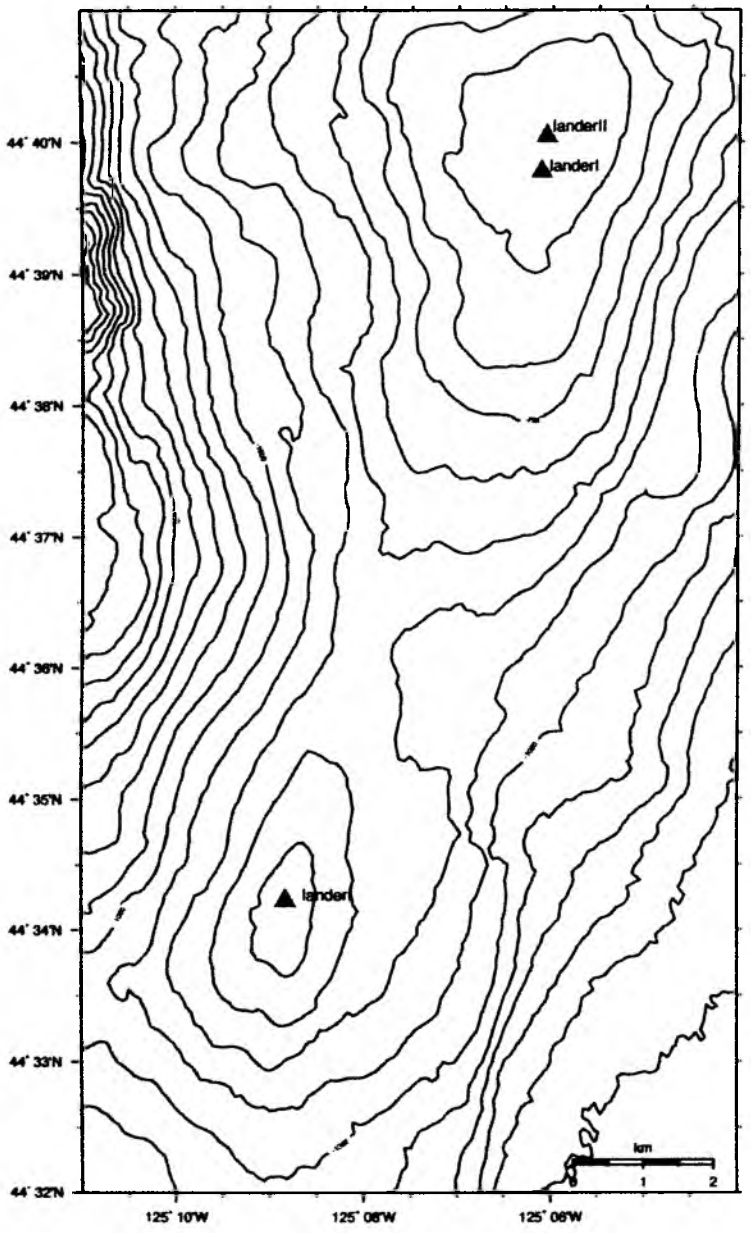

Fig. 20: Position of VESP-Lander deployments on Hydrate Ridge.

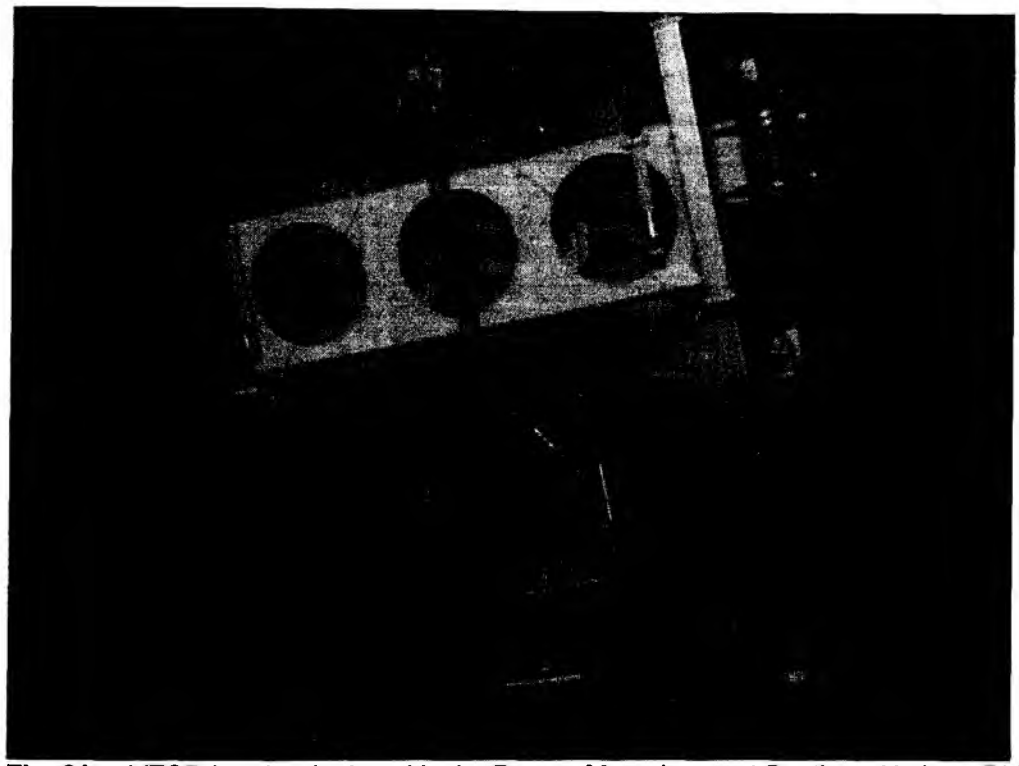

Fig. 21: VESP-Lander deployed in the Beaver Mound area at Southern Hydrate Ridge.

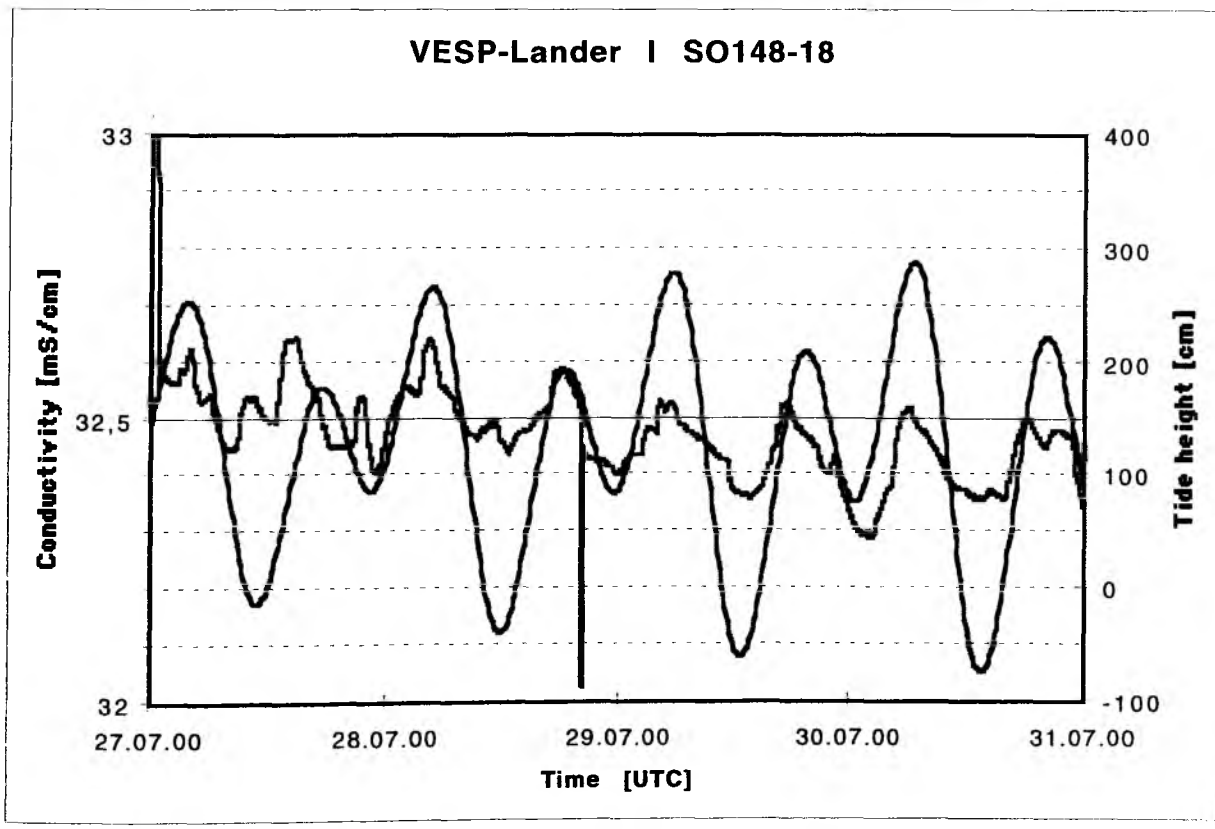

Fig. 22: *In situ* conductivity record in the enclosed water of the VESP chamber on the Southern Hydrate Ridge and the calculated Newport tide data provided by Dr. Collier. Note the impact of ROPOS on the sealing of the VESP chamber at ROPOS-Dive 562: Pushing on the chamber on 28.7.2000: 20:05 - 20:30.

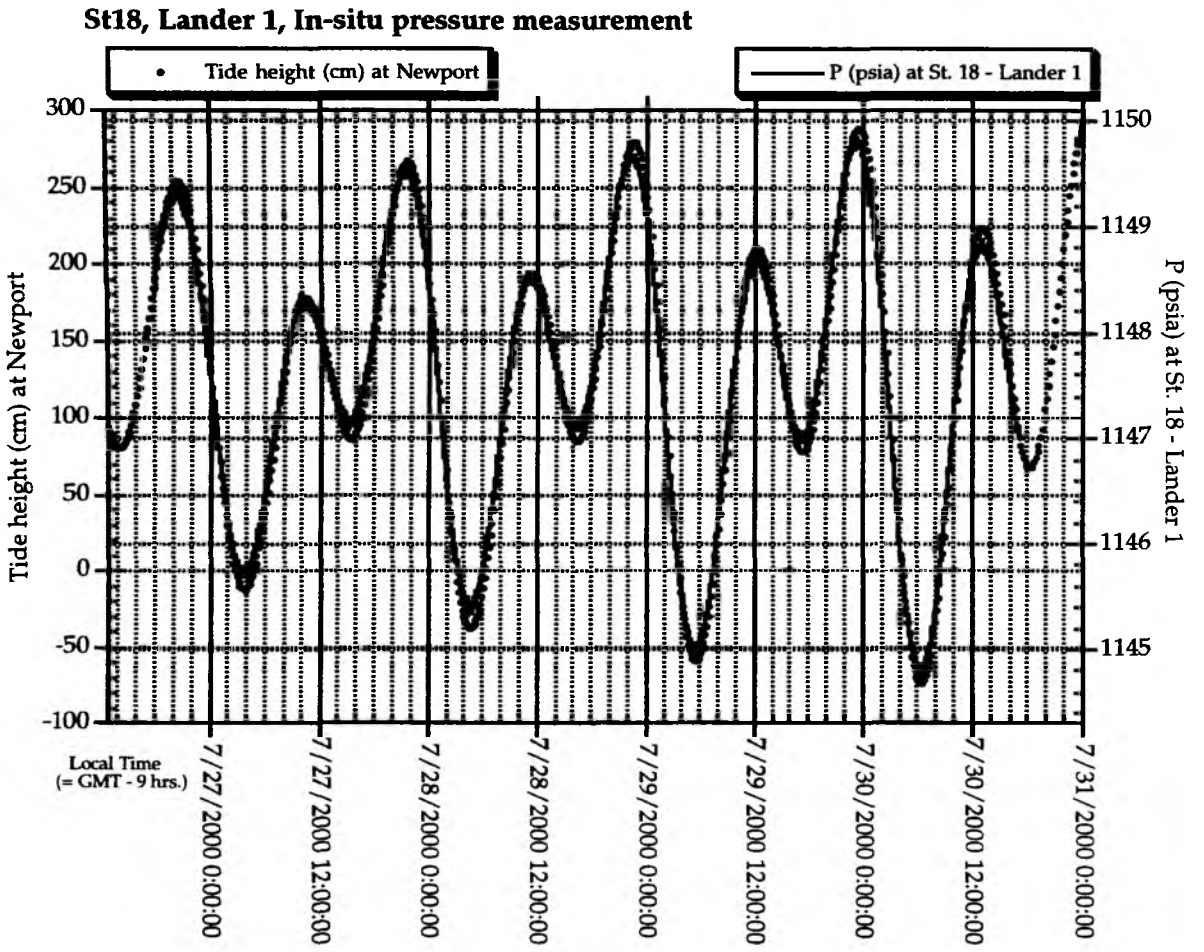

Fig. 23: *In situ* pressure record near the seafloor on the Southern Hydrate Ridge and the calculated Newport tide provided by Dr. Collier. Each pressure scale is adjusted such that 1 atmosphere equals 14.7 psi and a 10 m column of water.

7 OPTICAL FLUID FLUX MEASUREMENTS

V. Karpen

The fluid discharge at active subduction zones is an important parameter to understand the geochemical processes at cold seeps. The fluids contain methane and hydrogen sulfide which are used by symbionts of *Calyptogena* clams and *Beggiatoa* bacteria mats. Clam fields and bacteria mats are thus important indicators of active fluid discharge systems.

On this cruise we tested for the first time a new technology to detect the dewatering processes. The *In Situ Schlierenoptic (ISSO)* is able to detect heterogeneous water masses formed by fluids of different densities. The salinity and temperature of the discharged fluids at cold seeps are supposed to be different from the ambient bottom water. In the case of hydrogeologic processes heating occurs in deeper layers of the sediment. If methane hydrate occurs, another important aspect has to been taken into consideration. The dissociation of methane hydrate releases methane and fresh water. Thus, ascending fluids should have a lower salinity than the ambient bottom water. In both cases, the fluid expulsion is detectable by the *ISSO*.

The system was deployed several times. We used the frame of the TV-guided multicorer (MUC) as a carrier to deploy the camera system TV-guided as well.

The system was placed on bacteria mats as well as on clam fields. In two of the deployments a significant fluid discharge was detectable. A strong signal was recorded on a bacteria mat, a lower signal was recognized at a clam site.

It was quite obvious that mixing of interstitial and overlying water did not occur immediately. Fluids of different optical properties persist for a time. Thus, dewatering processes are detectable even if the camera system is not deployed directly on a source.

To quantify the fluid outflow the video records will be analyzed by image processing software at GEOMAR.

8 TIME-LAPSE VIDEO OBSERVATION OF GAS BUBBLE FLUXES

K. Nakamura, T. Yamazaki

Introduction

Methane gas bubbles were first observed on the Northern Hydrate Ridge in 1996 (Suess and Bohrmann, 1997, Suess et al., 1999). During the RV BROWN-ROPOS cruise in August 1998, an extensive gas bubble emission was observed at the edge of the northern summit of Hydrate Ridge, which was named "Gusher site" later. The gas discharge rate from a single vent at the intense bubbling period was estimated to be in the order of 5 liters/minute under the seafloor pressure based on the observation of the water replacing rate by gas in the gas sampler (Torres et al., 1998). Bubbling was observed at least at 5 discrete gas-discharging vents at this site during DSV ALVIN dives in 1999. A marker labeled "6" was deployed near one of the vents (hereafter, we call it "ALVIN Marker #6", Torres et al., 1999). First, methane gas bubbling on the southern summit of Hydrate Ridge was also detected by the ALVIN dive in 1999. The vent was located in the Beaver Mounds area and was marked by ALVIN Marker #7. Although the episodic nature of the bubbling was clear by the repeated observation, the mechanism generating the episodicity was not clear without continuous bubbling observation (Torres et al., 1999).

The aim of deploying the time-lapse deep-sea digital video camera (DSDVC) on this cruise was to record the bubbling episodicity and to estimate the change of discharging rate of methane gas to reveal the bubbling mechanism on Hydrate Ridge.

GSJ Time-Lapse Deep-Sea Digital Video Camera

Two sets of time-lapse DSDVC were used for this study. A commercial consumer-type digital video camera (SONY, DCR-TRV900) controlled by a PC board was installed in a 6,000 m-rated Ti-alloy pressure housing with two laser pointers, which create parallel laser beams to estimate the size of the objects in the video image. The camera and a Deep Multi-SeaLite, Model MC-12/50 (DeepSea Power & Light, Inc.) were connected to an external battery package by underwater cables in a rectangular Ti frame. A syntactic foam float block was also bound to the Ti frame to reduce the ROV manipulation load under water. Eh (Redox potential) electrodes and a temperature probe with the independent data loggers were also attached to the Ti frame to measure the bottom environment.
Although the total video recording time is limited to 120 minutes in the LP mode, the recording interval can be set in any minute between 2 minutes and 1,440 minutes (24 hours) independent from the pre-set recording length in any seconds between 1 sec and 60 sec. The progressive mode recording is also possible to get the maximum resolution of still picture image from the video record.

Camera Deployment

During the entire SO148 cruise the cameras were deployed by the ROV ROPOS. The cameras were held by the two ROPOS manipulators before the dive started, released at the bottom and deployed at the appropiate position in respect to the gas vent and optimal video recording. They were also recovered by the ROPOS manipulators.
Three deployment were performed at the Gusher Site near ALVIN Marker #6 on the northern summit of Hydrate Ridge and one in the Beaver Mounds on the southern summit of Hydrate Ridge. All of the camera settings were 28 sec recording length in progressive mode. The video images of the first two deployments at the Gusher Site were recorded at an interval of 15 minutes, whereas the other images by the latter two deployments were recorded at an interval of 1 hour.
DSDVC #1 (NTSC format camera) was deployed near the ALVIN Marker #6 (Fig. 24) at the beginning of ROPOS dive 562 on July 27. It was recovered at the end of the dive 564 on July 29. To succeed the first camera observation, DSDVC #2 (PAL format camera) was deployed at the beginning of the dive 564 facing DSDVC #1 so that the bubbling activity was recorded simultaneously by two different cameras for 5 hours and 30 minutes (Fig. 25). DSDVC #2 was recovered at the end of the dive 566 on July 31. DSDVC #1 was deployed again at the beginning of the dive 566 facing DSDVC #2. The overlap of the recording was 5 hours. DSDVC #1 was recovered at the end of the dive 572 on August 11, but the video recording had stopped already at GMT 13:00 (Local Time 3:00) on August 6.
DSDVC #2 was set on the seafloor again near ALVIN Marker #7 in the Beaver Mounds on the southern summit of Hydrate Ridge during dive 568 on August 6. It was removed to a small pit near the end of the dive and stayed there until the morning of August 9 (Local time). During dive 571 on August 9, the camera was moved to the vicinity of ALVIN Marker #7 to observe gas emission. It was recovered during dive 573 on August 11. Unfortunately, the gas bubbles at the ALVIN Marker #7 were recorded at the left edge of the video image.

Fig. 24: Deployed DSDVC #1 at Northern Hydrate Ridge near ALVIN Marker #6. Note the flare of rising bubbles on the left-hand side of the picture.

Fig. 25: Photograph of the gas oulet at Northern Hydrate Ridge near ALVIN Marker #6 taken by ROPOS. The light is coming from DSDVC #1 (on the right-hand side). Red laser spots can be seen from both digital video cameras (DSDVC #2 on the top).

Observation Results at Gusher Site (Northern Hydrate Ridge) and Discussion

From the repeated check of the video image, we classified the bubbling in 5 major levels and 2 sub-levels as they are described in the figure caption of Fig. 26. This classification is somewhat the logarithmic scale of the real discharged gas volume. Further data processing of the digital still images produced from the video records is still going on to get the quantitative estimation of the bubbling gas volume change. From Fig. 26, it is clear that the bubbling was controlled by the ocean tide. During high tide, bubbling was diminished or completely stopped. During low tide, the bubbling was activated. The reverse correlation between the tide height and the relative gas volume is also suggested either in high tide intervals and low tide intervals. The semi-diurnal temperature change about 40 cm above the seafloor in the camera flame and the semi-diurnal redox potential change in the flame correlated with the semi-diurnal bottom current direction change recorded in the video image. However, the Newport tide data and the relative bubble volume change agree much better than the Newport tide and other environmental parameters, such as temperature, redox potential and bottom current direction.

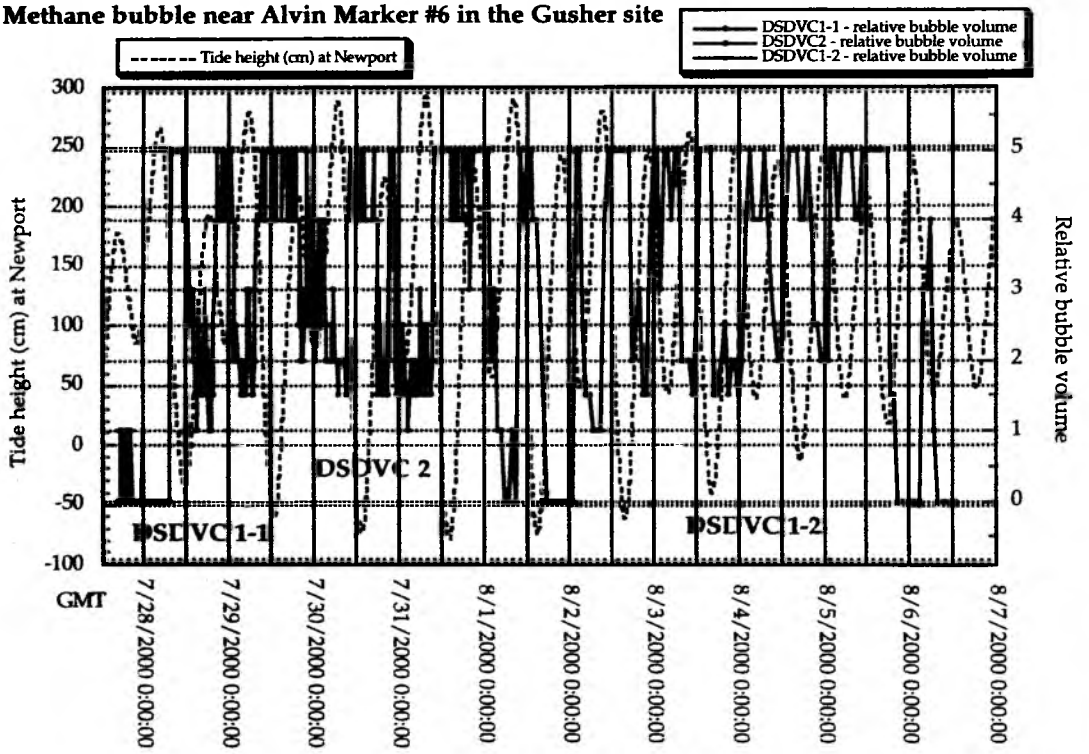

Fig. 26: Relative methane gas volume at a vent near ALVIN Marker #6 at the Gusher Site on the Northern Hydrate Ridge along with the calculated Newport tide. Relative bubble volumes were determined by repeated check of the video image. Level 0: No bubble during the 28 sec record. Level 1: Only one bubble in 28 sec. Level 1.5: More than one bubble in 28 sec. Bubbling interval is less than 5 sec. Level 2: Bubbling interval is 5 to 10 sec. Level 2.5: Bubbling interval is 10 to 13 sec. Still the bubbling interval is shorter than the intermittence in 28 sec record. Level 3: The bubbling interval is longer than the intermittence in 28 sec record. Level 4: Some intermittence of bubbling in 28 sec record. Level 5: Continuous bubbling.

Many lines of evidence, for example, bubble texture of the subseafloor gas hydrate, suggest that the shallow gas hydrate beneath the seafloor on the Hydrate Ridge is saturated by methane gas (Suess et al., 1999). A plausible mechanism to produce the ocean-tide generated gas-bubbling change is that the methane gas reservoir connected to the vent and semi-constantly fueled from the deeper part beneath the seafloor changes the capacity in relation to the water load. From the quantitatively estimated bubbling gas volume data through the image processing, we expect that we can estimate the gas reservoir volume connected to a single vent and the methane gas supply rate from the deep as well as the gas discharge rate and its change from a single vent.

9 WATER COLUMN WORK

K. Heeschen, A. Voorhees, N. Grant, B. Bock

Introduction

The active continental margin of the Oregon coast is characterized by processes driven by the subduction of the Juan de Fuca plate under the North American Plate (see Chapter 1). Fluids vent at the seafloor due to the tectonic compression within the accretionary wedge. At Hydrate Ridge, the second accretionary complex, intense fluid venting and gas expulsion occur as a result of this compression and are highly modulated by the occurrence of gas hydrates within the upper sediment close to their stability limits (Suess et al.,1999). In addition, free methane gas is abundant in the sediment underneath the area of stability - seen in geophysical records as a BSR - and can be expelled from the sediment where subsurface faults reach the surface.

The continental margin is an area with high sedimentation rates and large amounts of organic matter, which are fermented under anaerobic conditions and within forms the high concentrations of methane abundant in this system. Methane at Hydrate Ridge has a light stabile carbon isotopic signature demonstrating the biogenic origin. However, sources of methane with a heavy isotopic signature suggesting thermogenic origin have been found nearby on the shelf and upper slope. The methane concentration of pore water in equilibrium with sediments containing gas hydrates at a water depth of 700 m is 70 mmol/L (Egeberg and Dickens, 1999). The gas escaping the sediment contains about 98 % CH_4 (Torres et al., 1999). Compared to those amounts the background concentration of CH_4 in sea water of 0.3 – 2.4 nmol/L CH_4 is comparatively low.

What is the fate and significance of these large methane fluxes? Oxidation in and close to the sediment is a large sink for methane, which is converted into CO_2. Another quantity of methane, however, escapes into the water column, where it can be transported out of the area. This methane is oxidized within a yet unknown time scale and the balance is released into the atmosphere. Since CH_4 is a greenhouse gas, which - on a molecular basis - has an even stronger impact than CO_2, it is important to know how much methane reaches the atmosphere.

The hydrocast surveys conducted during last year's TECFLUX 99 program concentrated mainly on the summits of Hydrate Ridge (HR) as well as related features on the margin. Characterizing concentrations at the source area and changes in concentrations and distribution over time were the main goals of these earlier experiments. An intense survey of methane distribution in surface waters was also completed.

During SONNE cruise SO148, our work focused on the quantification of CH_4 transported away from the source area and on the characterization of mixed sources coming from HR and those coming from the shelf. Therefore, the hydrographic work included 4 hydrographic transects (see Fig. 27 for positions). Three of these transects (T1 – T3) were laid out normal to the expected current direction at a distance of 1.5 to 3.5 nm from the summits of Hydrate Ridge. The forth transect (T4) was carried out between the shelf and the southern summit of Hydrate Ridge. A background station was taken in the Western Basin at a depth of 2800 m. At all CTD stations in the working area, surface water concentrations of CH_4 were determined to establish changes in methane emission from this part of the ocean. In addition, two CTDs were taken at nearby knolls with known active vent sites (SE Knoll, CTD 05 and NW-Knoll, CTD 25) as well as at Southern Hydrate Ridge (CTD 01). See Fig. 27 for the CTD cast positions.

The amount of methane released from the seafloor and the flux out of the area of Hydrate Ridge is modified by the amount of CH_4 used by methane-oxidizing bacteria. However, methane oxidation does not only change the concentration but also the stable

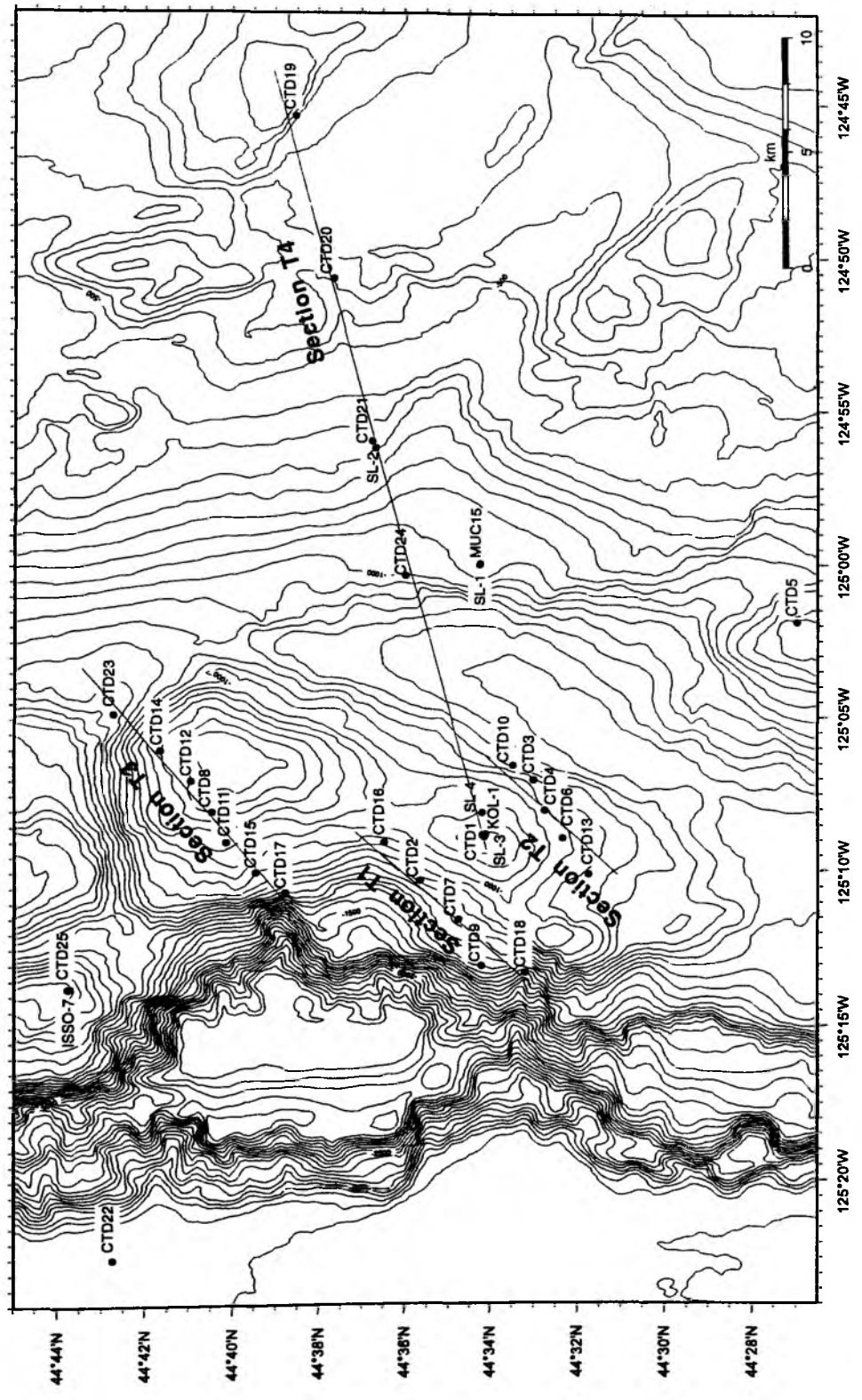

Fig. 27: Positions of CTD casts during SO148.

isotopic signature $\partial^{13}C$ of methane, providing a second tool for the determination of methane oxidation rates next to ^{14}C incubation done by the Humboldt University during TECFLUX 99. Samples were collected for $\partial^{13}C$ measurements to address the oxidation rates and the sources. They included ROPOS samples and were spaced downstream from the source and within rising bubble plumes.

CTD Deployment and ROPOS Samples

Water column sampling was performed using the ship's CTD/rosette system equipped with sensors for temperature, conductivity, pressure, and oxygen (Seabird 911 plus, SBE 13 oxygen sensor, SBE 32 carrousel with 24*10L Niskin bottles). Also attached were a membrane/chemical CH_4 sensor (METS sensor), a transmissiometer (Seatech, 25 cm path length) and an altimeter. Although calibration is not generally possible, the METS sensor was helpful for qualitative observations and for taking water samples within areas of elevated methane. The oxygen sensor showed good recordings when compared to the results of Winckler titration.

On all stations, the water column was characterized by a strong thermocline at about 10m water depth with a warm (12.8 – 17.5 °C), low salinity (30.6 - 32.2) water lens at the surface reflecting the influence of freshwater input, with high salinity waters generally being colder. This general trend is due to coastal upwelling and mixing with Columbia River plume waters, although no simple pattern can be seen. Deviations from simple end member mixing might be due to solar warming over the 4 weeks of measurements. Temperature and salinity properties in the deeper water column were relatively similar at all stations. For a typical profile see Fig. 29a.

During SONNE Cruise 148 a total of 25 CTD casts was collected (Fig. 27). To avoid changes in the methane signal due to tide-related current changes and benthic fluxes all casts around Hydrate Ridge were undertaken at low tide. Altogether, 490 samples from the CTDs were degassed and the methane concentrations determined. Gas samples were collected for shore-based stable isotope measurements. Samples taken on 5 different ROPOS dives (Tab. 4) with a row of 4 Niskin bottles mounted in front of the vehicle were handled similarly. Due to high gas contents of these samples a phase separation resulting in replacement of water by expanding gas within the Niskin bottles made sampling difficult.

Tab. 4: Samples taken with ROPOS for CH_4 measurements

ROPOS Dive	Location	Experiment	Niskin bottels/ jars
563	Gusher Site at SHR	closing Niskins while following the bubble plume. Depth: 765 m. Sampling depth:765m, 756 m , 749 m and 736 m depth	4 Niskin bottles closed - Niskin 1 empty and Niskin 4 too little sample
565	Gusher Site at SE Knoll	closing Niskins going downcurrent with 10 m spacing starting at the gusher site	4 Niskin bottles closed
566	Gusher Site at Northern Hydrate Ridge	closing Niskins going upward with 5 m spacing between sampling starting 3 m from the gusher	4 Niskin bottles closed
567	R1 structure	closing Niskins going NNE from a central clam field with 15 m spacing and taking fluid samples from a clam site and bacterial mat site where a hole was digged	4 Niskins closed 2 Jars filled
572	Gusher Site at NHR	closing Niskins going downcurrent with 15 m spacing starting at the gusher site	3 Niskins closed – Niskin 1 empty

Methane Sensor

Determining the concentration of methane dissolved in water is a pivotal analytical effort in the study of cold seeps and methane dynamics from a variety of environments, as methane determination by gas chromatography can only provide a limited data set from a highly variable environment. Without *in situ* detectors, conventional CTD-rosette sampling is essentially blind.

The methane sensor, METS, was developed at GKSS-Forschungszentrum (Geesthacht, Germany) for long-term monitoring of dissolved methane in water. Methane diffuses from the water across a membrane into the sensor through a support frit. It is detected in the gas phase at the heated surface of an internal semiconductor, which changes its conductivity as a function of hydrocarbon adsorption. The current depth limitation is 1000m, which is limited by the support frit. The METS sensor was interfaced with the CTD using three analog voltage channels.

Because of the long, diffusive path to the sensor, the response time is slow (several minutes) and the signal may never reach equilibrium in a heterogeneous environment. When deployed in a low concentration background, the system can easily detect changes of +10 nM. Once high concentrations of methane diffuse into the sensor cell, it takes a long time to return to low values. This slow response time currently limits quantitative on-line applications (e.g. on CTDs). Throughout the cruise, however, the sensor was a helpful prospecting tool to identify areas of higher methane concentrations and by this guiding the collection of discrete water samples.

Methane Measurements

Water column methane was measured from discrete samples collected directly from the ship's CTD/rosette and from 4*2L Niskin bottles mounted on ROPOS. For CH_4 analysis of these samples, a modified vacuum degassing method as described by Lammers and Suess (1994) was used. The procedure involved a sample volume of 400 ml (for background stations 1500 ml) of sea water obtained directly from the Niskin bottles by using a 200 ml glass syringe (high volumes were taken without a syringe). The water sample was immediately injected and sealed into pre-evacuated 600 glass bottles (2000 ml for background). Shaking for at least 30 min equilibrated the head space and water phases in the sample bottles. The gas phase was subsequently recompressed to atmospheric pressure in a preparation line. The CH_4 mole fraction of the total extracted gas was determined by gas chromatography using flame ionization detection. The FID was calibrated with bottled mixtures of 10.0 ppm ± 2% and 1002 ± 5% methane in synthetic air. The total gas concentration of the sample was calculated by adding up the measured dissolved oxygen concentration, and the calculated N_2 and Ar concentrations. The latter were assumed to be 100% saturated relative to their atmospheric partial pressures, temperature and salinity (Weiss, 1970). The dissolved methane concentration was calculated as the product of the mole fraction in the extracted gas phase and the amount of total gas (STP) in the sample. The oversaturation of CH_4 in the surface waters was estimated by using formulas from Wiesenburg et al. (1979) with an atmospheric CH_4 concentration of 1.79. The measurements from samples taken with ROPOS are not calculated from ppm volume into nmol/L so far.

Preliminary Results for CTD Samples

To know about the different source signals in the working area, CTD casts were undertaken at 3 known fluid venting locations including two with observed gas expulsion (Fig. 28). Whereas Southern Hydrate Ridge shows a distinct signal of gas ebullition about 140 m above the bottom and a very small signal of fluid venting in the bottom most samples, SE Knoll has a distinct signal for fluids but a much smaller signal of gas escaping the seafloor. NW-Knoll, where last year we found a distinct enhancement in methane close to the bottom, did not show any significant venting signal this year. Several very small signals, most probably from sources upcurrent, are found between 50 m above the bottom up to a water depth of 500 m. The most distinct and broad maximum at NW-Knoll was found at 400 m.

SHR, SE Knoll and NW Knoll - sites of fluid venting and gas ebullition

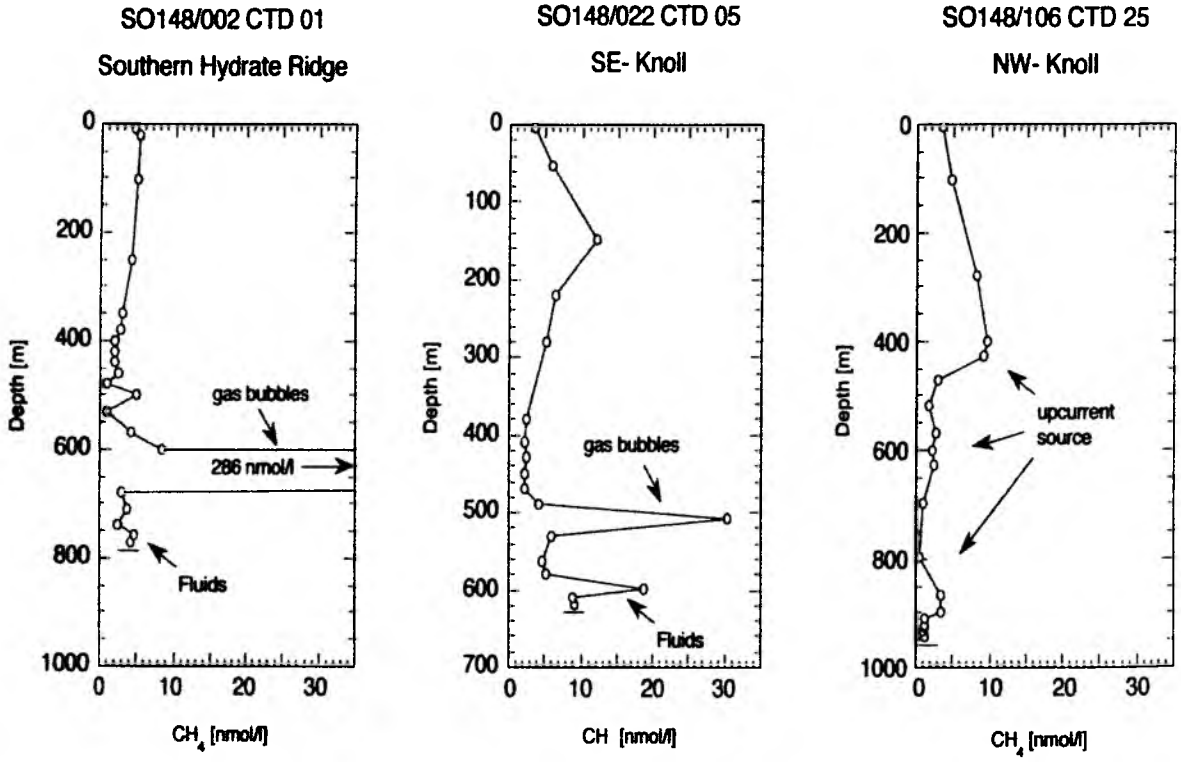

Fig. 28: Methane profiles in the water column at vent sites with maximum concentrations in altered depth due to different mechanisms.

This maximum was also found frequently during previous cruises. Even in the profile carried out to obtain background values (CTD 22) about 9 nmol/L were found at 400 m water depth. It is not all clear whether this methane is coming from sources of Hydrate Ridge, from the shelf/slope or an additional source. One of the CTDs with the most intense methane signal at 400 m was CTD 03 (Fig. 29b). The CH_4 correlated very well with a decrease in transmission and a change in the temperature gradient between 300 – 480 m (Fig. 29a). This slightly colder, well-mixed, particle-rich water could be derived from the slope contact (intermediate nepheloid layer). Within the 4 CTD transects the appearance of the maximum at 400 m was variable, suggesting changes in source strength, current strength or directions and the upwelling system during the 4 weeks of

sampling. Correlations with oceanographic and meterologic parameters, information about gas expulsion at Hydrate Ridge and the determination of the isotopic signature $\partial^{13}C$ CH_4 are still to come.

SO148/008 CTD 03

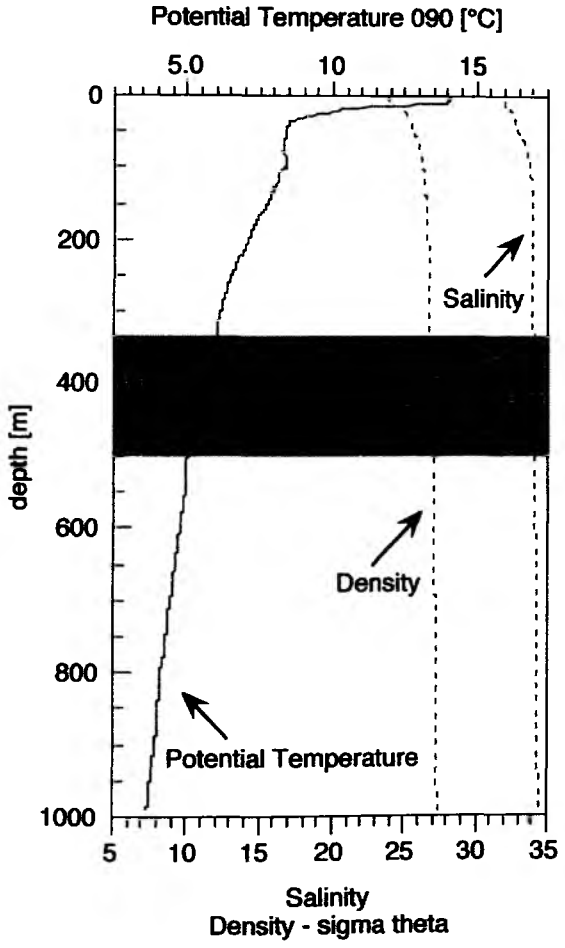

Fig. 29a: Distribution of the physical oceanographic properties: temperature, salinity and density of cast SO148/008CTD03.

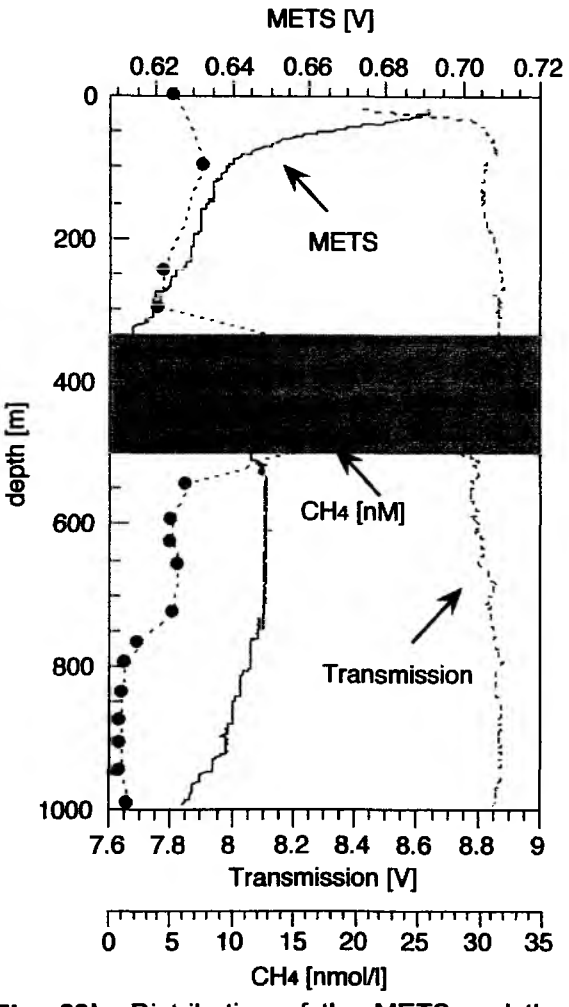

Fig. 29b: Distribution of the METS and the transmissiometer signals with significant changes at 350 – 500 m. Lower transmission and higher METS signal correlate with the elevated methane concentrations measured. The METS signal is uncorrected for temperature, humidity and slow response time.

CTD 3 was part of the transect T2 near Southern Hydrate Ridge (see Fig. 27 and for results Fig. 30a). Although transect T2 was projected upcurrent of Southern Hydrate Ridge (Fig. 27) the 3 CTDs in the center of T2 revealed elevated CH_4 values at depth between 850 – 600 m with concentrations as high as 24 nmol/L (CTD 6). Most probably those were due to venting at Southern Hydrate Ridge (see Fig. 28) and thus revealed more complicated and variable current systems. In addition, the high variety of

characteristics at different depth in the CH_4 profiles supported differences due to a variety of sources as well as current and mixed layer changes with time. To specify current directions direct observation were made with the ADCP mounted on the VESP-Lander system (see Chapter 6). Tidal related source and current changes were minimized by CTD deployment at low tide only.

Section T2 - located SE of Southern Hydrate Ridge

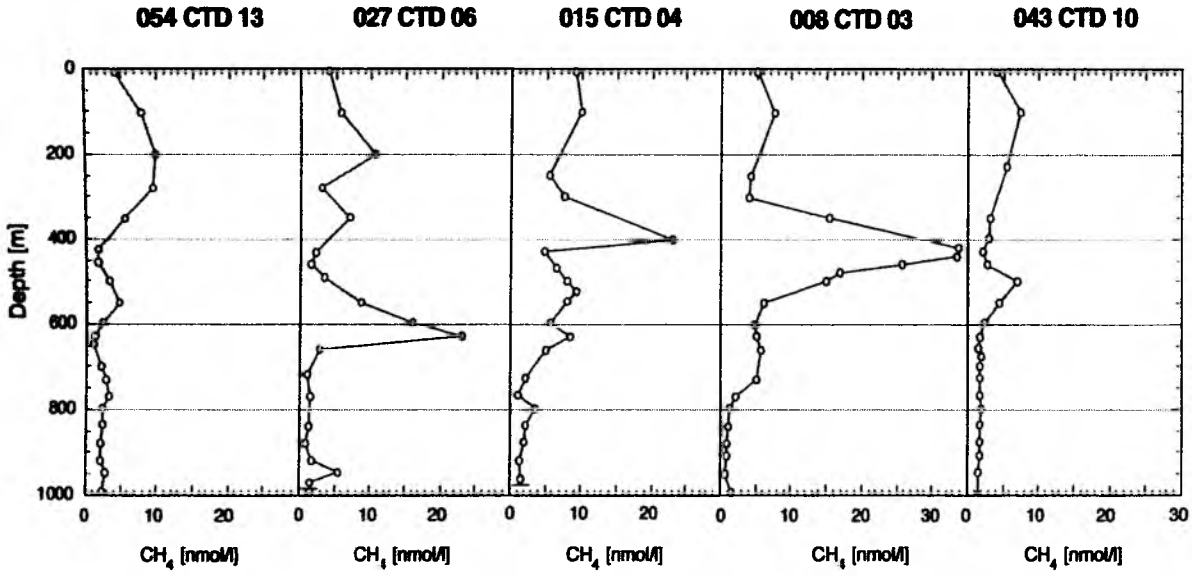

Fig. 30a: Methane concentrations of section T2, which was located SE of Southern Hydrate Ridge.

Transect T1, located to the NW of Southern Hydrate Ridge (for location see Fig. 27, for results see Fig. 30b), also showed the high variety of methane profiles in the water column with several peak values in the upper 900 m of the water column. The CH_4 concentrations at depth between 900-600 m are similar to those found in transect T2 (maximum: 16 nmol/L, 600 m CTD 07), supporting the interpretation made above about the current regimes changing. T1 was projected to be downcurrent of Southern Hydrate Ridge and should reveal higher concentrations in the depth-range discussed. The ambient casts show slightly elevated values although they are to the very west and to the NEN of the source.

Compared to T1 & T2 transect T3, located to the NW of Northern Hydrate Ridge (for location see Fig. 27), showed distinctly higher CH_4 concentrations at the depth range where maxima derived from Northern Hydrate Ridge were expected. Up to 47 nmol/L were found between 600 – 480 m. Next to the higher concentrations found in the center profiles the ambient cast to the NNE also showed highly elevated methane concentrations. Within transect T3, the CTDs to the north showed peak values at 480 m, whereas to the south of the transect the maxima were found between 620 – 570 m. The water depth of the maxima derived from gas bubbles at the source is 480 m, the one induced by fluid venting at Northern Hydrate Ridge is close to the bottom of Northern Hydrate Ridge at around 590 m. However, the concentrations of up to 47 nmol/L at a distance of 3 miles from the source are rather high for being induced by fluids only. The

upper water column showed highest concentrations in the southern end of T3, which are getting smaller towards the north. Unfortunately, there was no time to complete a transect to the SE of Northern Hydrate Ridge. But the one carried out last year also revealed clear maxima between 600 – 480 m.

Section T1 - located NW of Southern Hydrate Ridge

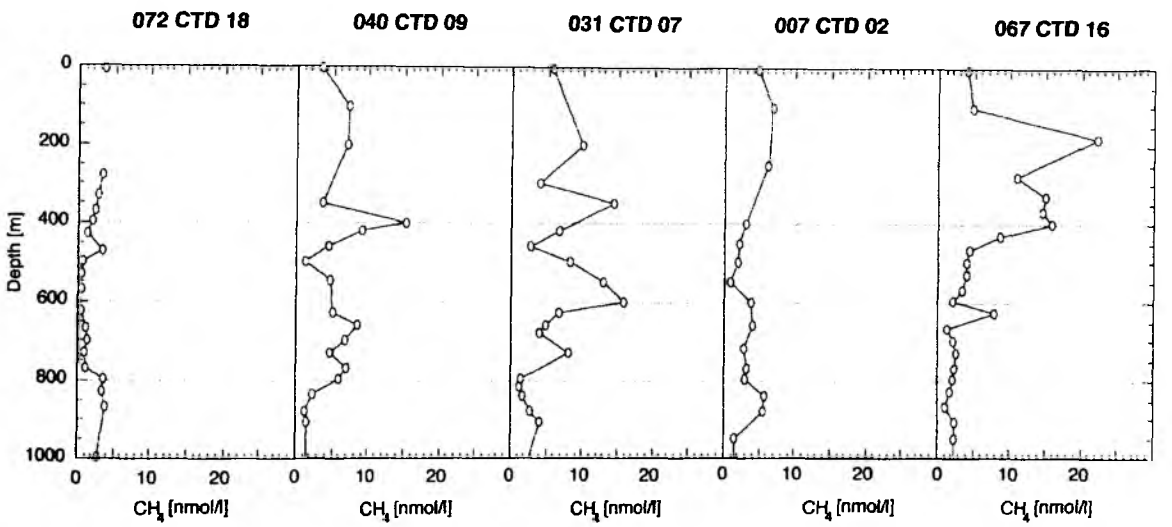

Fig. 30b: Methane concentrations of section T1, which was located SE of Southern Hydrate Ridge.

Transect T4 led from close to the shelf (Daisy Bank: 250 m) across the E-Basin towards Southern Hydrate Ridge (for location see Fig. 27). Maximum concentrations (20 - 30 nmol/L) on the shelf and the upper slope were found near the bottom at 250 - 400 m depth with methane concentrations dropping slightly below 300 m at the slope. CTD 21 in the E-Basin (700 m) showed a profile different from the shelf profiles. It only revealed a small maximum at 330 m, but showed distinct maxima at 450 m (15 –30 nmol/L) and at 650 m (22 nmol/L), whereas CTD 24 (1000m) had no significantly elevated concentrations at 200 - 400 m at all. However, concentrations are high (10 nmol/L) in all samples between 430 – 600 m. Slightly higher CH_4 values (6 nmol/L) from the bottom up to 800 m suggest local fluid sources near the site.

All CTD profiles whether or not they were taken at locations with known CH_4 sources revealed elevated CH_4 concentrations in the upper water column between 300 m and the upper thermocline (e.g. CTD 16, T1, 23 nmol/L, 180 m). They can be attributed to *in situ* production in anoxic microhabitats such as particles and guts of microorganisms (Tilbrook and Karl, 1994) or due to an intermediate nepheloid layer (INL) resulting from currents alongside the continental slope. Within bubble chasing experiments visible bubbles where found as high as 380m (see ROPOS Dive 566), but it is unlikely that this source causes maximum at 300 or shallower.

Surface values were 2.2 - 5.7 nmol/L on average. Except from the background station (-6 %) all surface samples are oversaturated in methane with an average of 80 % when including casts CTD 04 and CTD 12 and 65 % excluding CTD 04 and CTD 12. The latter showed exceptional high oversaturations with 257 and 357 % respectively. As sediment

work was done at some time before those CTD stations (clean ship during the CTD station) those values are suspect. In any case the working area is quite a strong source for methane.

Preliminary Results for ROPOS Samples

The two samples received from the bubble "chasing" experiment on ROPOS dive 563 showed high but not extremely high values of about 1300 ppm. However, those values could be artifacts, as there was a phase separation within the Niskin bottles when ROPOS was recovered. Samples taken on ROPOS dive 566 revealed concentrations of 43950 ppm CH_4 5 m above the ground, which was an order of magnitude higher than the concentration of the sample right next to the Gusher Site. This could be due to the solubility and diffusion processes of the fast rising gas bubbles. The samples 10 and 15 m above the ground show a linear decrease in CH_4 concentration to 9800 ppm, what is still double of the first sample taken.

Concentrations measured at and downcurrent of the gusher site at SE Knoll in ROPOS dive 565 are shown in Fig. 31. They revealed mixing and a high dilution starting about 10 m away from the source with a linear decrease in concentration 10 – 30 m away from the source. This can be due to a furious fluid venting (see Chapter 8) with uneven mixing patterns or to other vent sites occurring downcurrent. ROPOS dive 572 at Northern Hydrate Rdige showed extraordinary low methane concentrations, however methane also increased between 15 m to 30 m distance from the source form 10 ppm to 33 ppm. Due to a failure of the first Niskin bottle there is no information about the values at the source. The current direction could have been mistaken.

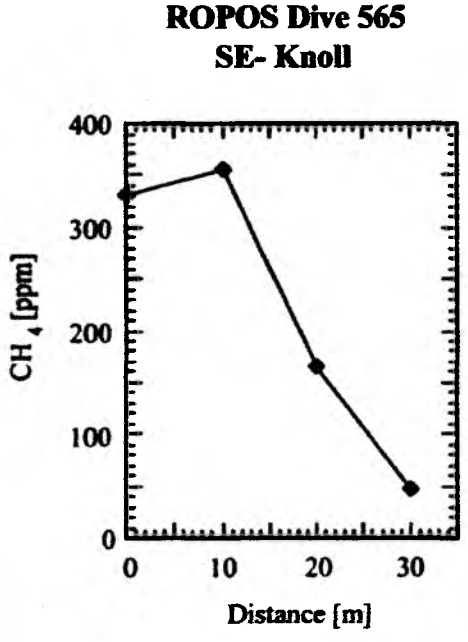

Fig. 31: Methane concentrations of samples spaced downstream from the source at SE-Knoll.

The samples taken with the Niskin bottles on ROPOS dive 576 above a clam field at the R1 structure showed values of 4.8 nmol/L down to 2 nmol/L. Compared to gusher sites the fluid flux at this clam field into the bottom water is rather small. For determination of the methane concentration of those fluids, a sample was taken with the hose of ROPOS sucking in the fluid right above the ground into a jar. Unlike the Niskin bottles, which were mounted to the vehicle in a height of 2.5 m, samples with the hose could be taken right above the ground. The sample had 428 ppm methane, which was comparable to samples taken at clam fields on Hydrate Ridge. The jar sample taken within a dug hole at a bacterial mat site revealed 21002 ppm – half of what was found at the Gusher Site of Northern Hydrate Ridge but within the range of values found for bacterial mat sites at Hydrate Ridge.

10 SEDIMENT SAMPLING AND SEDIMENTOLOGY

G. Bohrmann, C. Jung, A. Cremer, B. Bock, B. Domeyer, R. Joergens, R. Steinemann, B. Teichert

10.1 Performance of Equipment and Sampling

During SONNE Cruise 148 sediment sampling was concentrated on Southern Hydrate Ridge in an area close to the summit. Besides ROPOS, gravity and piston corer, TV-multicorer and the TV-grab were used to recover sediment, rock and gas hydrate samples.

Gravity and Piston Corer

Sediment cores were sampled at 5 stations (Tab. 5). At four sites we used the BGR coring system (ø = 10 cm) either as gravity corer or as piston corer. The gravity corer with a 10 m (at Site 77) or 5 m long core barrel (Sites 85 and 86) used a weight of 3.000 kg. A 10 m long piston corer was performed at Site 105. At Site 80 we used a GEOMAR gravity corer. The core barrel segment of approximately 5 m length and 10 cm in diameter was used with a weight of 1,200 kg. Both penetration and recovery varied considerably, which was mainly a result of sediment induration and the presence of gas hydrate layers of variable porosity. Penetration varied between 1 mbsf (meters below seafloor) and 5 mbsf. Consequently, core recovery ranged from 0.50 to 477 meters.

Tab. 5: Sample list of gravity and piston cores recovered during SO148 (Abbrevations: pw = pore water; pp = physical properties; SL = gravity core, KOL = piston core).

Station SO148-	Date	Tool	Lat. ° N	Long° W	Depth m	Recovery m	Samples
76	09-Aug	SL-1	44°34.288	124°59.983	887	477 cm	5 hydrate
80	09-Aug	SL-2	44°36.782	124°55.951	776	50 cm	No sample
85	10-Aug	SL-3	44°34.212	125°08.872	777	189 cm	9 pw and pp; 4 hydrate
86	10-Aug	SL-4	44°34.216	125°08.816	777	248 cm	20 pw and pp; 5 hydrate
105	13-Aug	KOL-1	44°34.217	125°08.797	777	234 cm	24 pw and pp

TV-guided grab

Tab. 6: Sample list of TV-grab stations during SO148.

Station SO148-	Date	Tool	Lat. ° N	Long° W	Depth m	Samples
36	30-Jul	TV-G-1	44°34.190	125°08.847	786	gas hydrates, carbonates
56	01-Aug	TV-G-2	44°34.160	125°08.810	779	not deployed
57	01-Aug	TV-G-3	44°34.154	125°08.807	777	gas hydrates
58	01-Aug	TV-G-4	44°34.172	125°08.831	776	gas hydrates
65	07-Aug	TV-G-5	44°34.197	125°08.830	777	carbonates
66	07-Aug	TV-G-6	44°34.207	125°08.845	776	gas hydrates, carbonates
73	08-Aug	TV-G-7	44°34.188	125°08.825	777	gas hydrates, carbonates
82	09-Aug	TV-G-8	44°34.220	125°08.790	777	gas hydrates, carbonates
99	12-Aug	TV-G-9	44°34.187	125°08.824	772	gas hydrates, carbonates

The TV-grab onboard RV SONNE is extremely valuable in order to sample gas hydrates in shallowly buried sediments close to the seafloor. The system is equipped with two lights (150 W each) and the telemetry unit and two cameras. Power for lighting and the

hydraulic unit is supplied by two deep-sea batteries. The sample size is roughly 100 x 170 cm.

The TV-grab was deployed from RV SONNE at 9 sites on the southern summit of Hydrate Ridge and gas hydrates as well as carbonate rocks have been recovered quite successfully (Tab. 6).

TV-Multicorer/Multicorer

Tab. 7: List of MUC stations. Abbreviations see text below.

St.No. SO148	Date 2000	Instrument	Area	Latitude N°	Longitude W°	Depth (m)	Recovery	Samples Comments
6	24.7	TV-MUC-1					not deployed	
11	24.7	TV-MUC-2	SHR	44°34.225	125°08.135	776	4 cores	
12	25.7	TV-MUC-3	SHR	44°34.235	125°08.844	775	3 cores, 10-18 cm	no SSBL
14	25.7	TV-MUC-4	SHR	44°34.218	125°08.804	777	4 cores, 12-16 cm	pw, pp, bims, ox, Ch_4
19-1	26.7	TV-MUC-5	SHR	44°34.228	125°08.791	776	3 cores, 10-14 cm	agg
19-2	26.7	TV-MUC-6	SHR	44°34.104	125°08.807	777	6 cores, 20-26 cm	pw, pp, ox, Ch_4, bims
28	27.7	TV-MUC-7	SHR	44°34.196	125°08.816	777	4 cores, 11-17cm	bac, agg
29	27.7	TV-MUC-8	E-Fl. SHR	44°34.222	125°08.834	777	7 cores, 20-26 cm	pw, pp, ox, bac, bims, Ch_4-ox, Ch_4-iso
37	29.7	TV-MUC-9	SHR	44°34.195	125°08.838	788	2 cores, 12-16 cm	no SSBL
38	29.7	TV-MUC-10	SHR	44°34.186	125°08.847	787	4 cores, 15-19 cm	
44	30.7	TV-MUC-11	SHR	44°34.185	125°08.834	776	5 cores, 15-19 cm	pw, pp, ox, Ch_4, bims
51	31.7	TV-MUC-12	SHR	44°34.198	125°08.858	775	6 cores, 12-16 cm	pw, ox, bims
52	31.7	TV-MUC-13	SHR	44°34.201	125°08.808	777	4 cores, 13-18 cm	bac, ox
63	5.8	TV-MUC-14	SHR	44°34.197	125°08.812	776	3 cores, 15-28 cm	pw, agg, bac
75	8.8	TV-MUC-15	E-Basin	44°34.311	124°59.976	797	3 cores, 23-24 cm	pw, pp, ox, Ch_4, mac
88	9.8	TV-MUC-16	SHR				not released	problem with MUC
89	10.8	TV-MUC-17	SHR				aborted	problem with winch
90	10.8	TV-MUC-18	SHR	44°34.200	125°08.830	777	4 cores	LT, bac, mac, agg
91	10.8	TV-MUC-19	SHR	44°34.200	125°08.820	778	3 cores, 23-24 cm	LT, bac, mac, agg
92	10.8	TV-MUC-20	SHR	44°34.208	125°08.809	777	8 cores	LT, agg
93	10.8	TV-MUC-21	SHR	44°34.182	125°08.822	776	5 cores	LT, agg
94	10.8	TV-MUC-22	SHR	44°34.202	125°08.805	776	7 cores	LT, agg
95	10.8	TV-MUC-23	SHR	44°34.145	125°08.855	777	5 cores	pw, ox, bims

A conventional multicorer was equipped with a deep-sea telemetry, a B&W and sometimes with a color video camera. Main investigation area was the southern summit of Hydrate Ridge. Since the main area of interest was only a few square meters in extension, the TV-control during the MUC-sampling was indispensable.

The TV-MUC was used to collect sediments and bacteria (bac) for investigations described in the chapter microbial ecology. Cores were collected for the studies of aggregates (agg) conducted by V. Karpen in collaboration with L. Thomsen. Whole cores were collected for investigations in a fume conducted by L. Thomsen (LT). Cores were used to collect macrofaunal specimens (mac). Cores were analyzed for porewater (pw), physical properties (pp), methane (Ch_4), methane oxidation rates (Ch_4-ox), methane isotopes (Ch_4-iso) or the oxygen concentration (ox) in the overlying bottom water. Cores were taken for biomarker (bims) investigations conducted by M. Elvert, MPI.

10.2 Preliminary Sedimentological Results

During cruise SO148 sediments were recovered by mainly TV-MUC and TV-grab. Longer sediment cores were taken by gravity and piston corer. TV-grab does not allow recovery of intact surface, which TV-MUC does excellently. In total, 5 longer cores (Fig. 32) were recovered in two areas.

With the exception of hydrates and some authigenic carbonates, sediments sampled are almost entirely visually monotonous sequences of mud, silty mud and partly clayed mud. Colors are dominantly olive gray (5Y 5/2), dark olive gray (5Y 3/2) and very dark gray (2,5Y N3). The muds are composed of clay minerals with varying amounts of detrital fine to coarse silt grains. The uppermost 15-25 cmbsf are mostly homogeneous and show no specific structures. Occasionally, *Acharax* or *Calyptogena* clam shells are found. Below this soft uppermost interval, muds and mudstones are indurated to semi-consolidated.

Gravity core SO-148-76 was taken close to 75 TV-MUC within a patch of high backscatter reflectivity shown on the side scan sonar-map of Chris Goldfinger in the eastern basin. During OFOS tracks 9 and 10 two circular patches were investigated and showed extensive clam fields and bacterial mats on the seafloor (see Fig. 14, Chapter 4). In order to define the site location we used the Parasound and we could observe that the patches are clearly associated with blank zones in the echosounder records just below the observed vent fields. Such zones show distinct areas where fluid and/or gases are ascending. The core retrieved (recovery = 477 cm) was intercalated by numerous thin horizons of gas hydrates intimately distributed in much of the recovered sediments (Fig. 32). Thicker layers are often broken in several pieces (see Fig. 33c). The core represents the first gas hydrate recovery within the Cascadia hydrate province outside of Hydrate Ridge. The seafloor in 887 m water depth lies in the stabilty field of gas hydrates. Other sediment components are occasionally authigenic carbonates and shells of chemosynthetic clams.

All other cores were taken around the summit of Southern Hydrate Ridge. Cores 80, 85 and 86 contained various amounts of gas hydrates. Thicker layers up to 5-8 cm could be found in several horizons (Figs. 32 and 33). Depending on their water content, the lithologies either showed a broken, scaly texture with angular shards and fragments, or

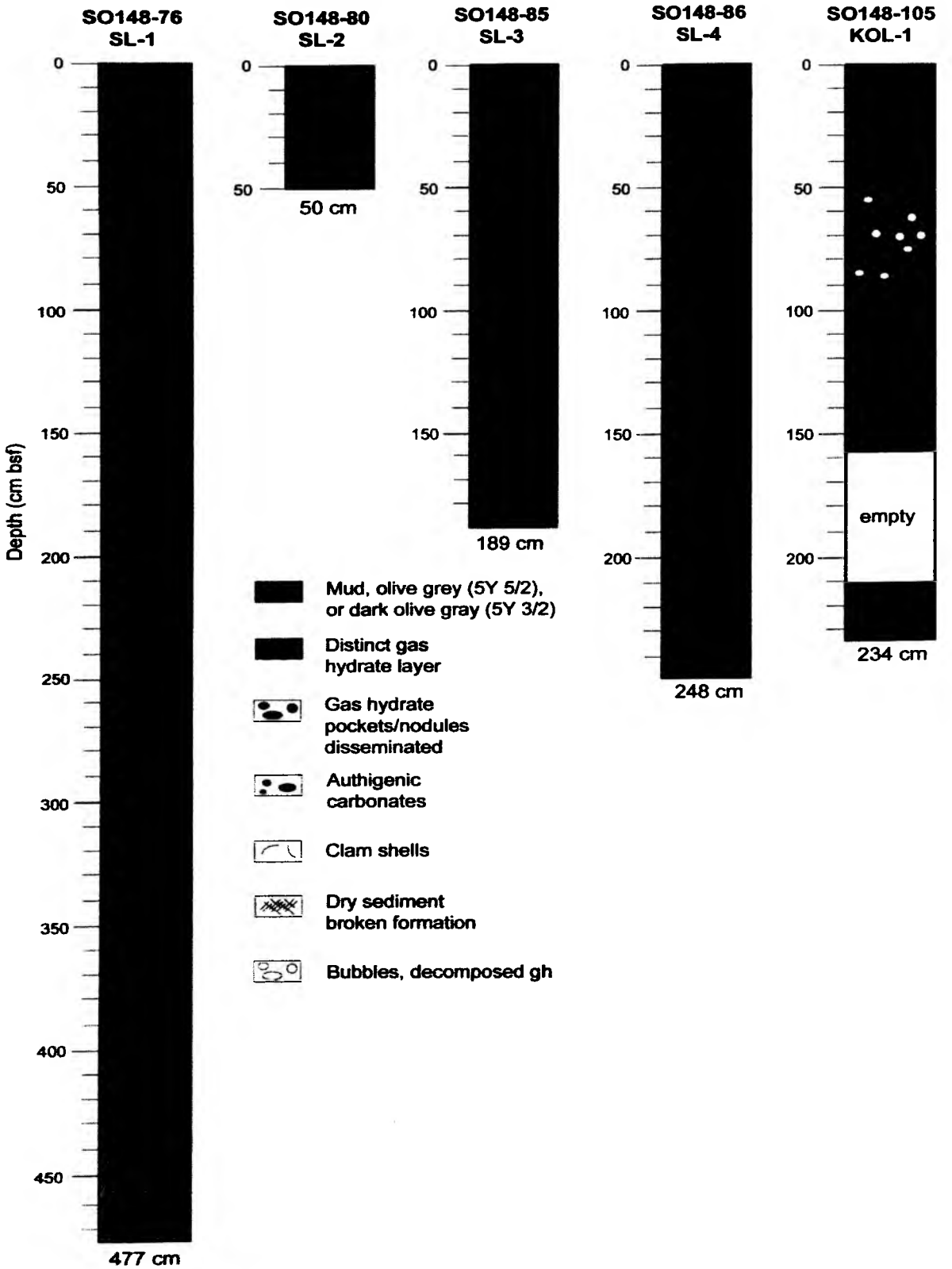

Fig. 32: Graphic representation of the sediment cores taken during SO148.

appear mousse-like with gaseous pockets and highly soupy intervals. The latter is interpreted to be a result of gas hydrate dissociation and the dry and fragmented intervals seem to originate from water loss in the vicinity of distinct gas hydrate layers. This was clearly observed in core SO148-85 (Fig. 32) and proved by pore water signatures (see Chapter 13). Most sediments have been accompanied by a strong smell of hydrogen sulfide.

An unusually fine-grained lithology of clayey mud was recovered within core SO148-105 (Fig. 32). The water content was distinctly lower than in the other cores and the composition was surprisingly homogenous. Some gaps have been recovered in the lower part of the piston core, which resulted from the pull of the piston and represent an artifact. The plained surface of the half core showed after ca. 40 minutes numerous knobs 2-6 mm in diameter. Such slow bubble emissions are related to disseminated, fine gas hydrates which started decomposing after a longer time of temperature increase.

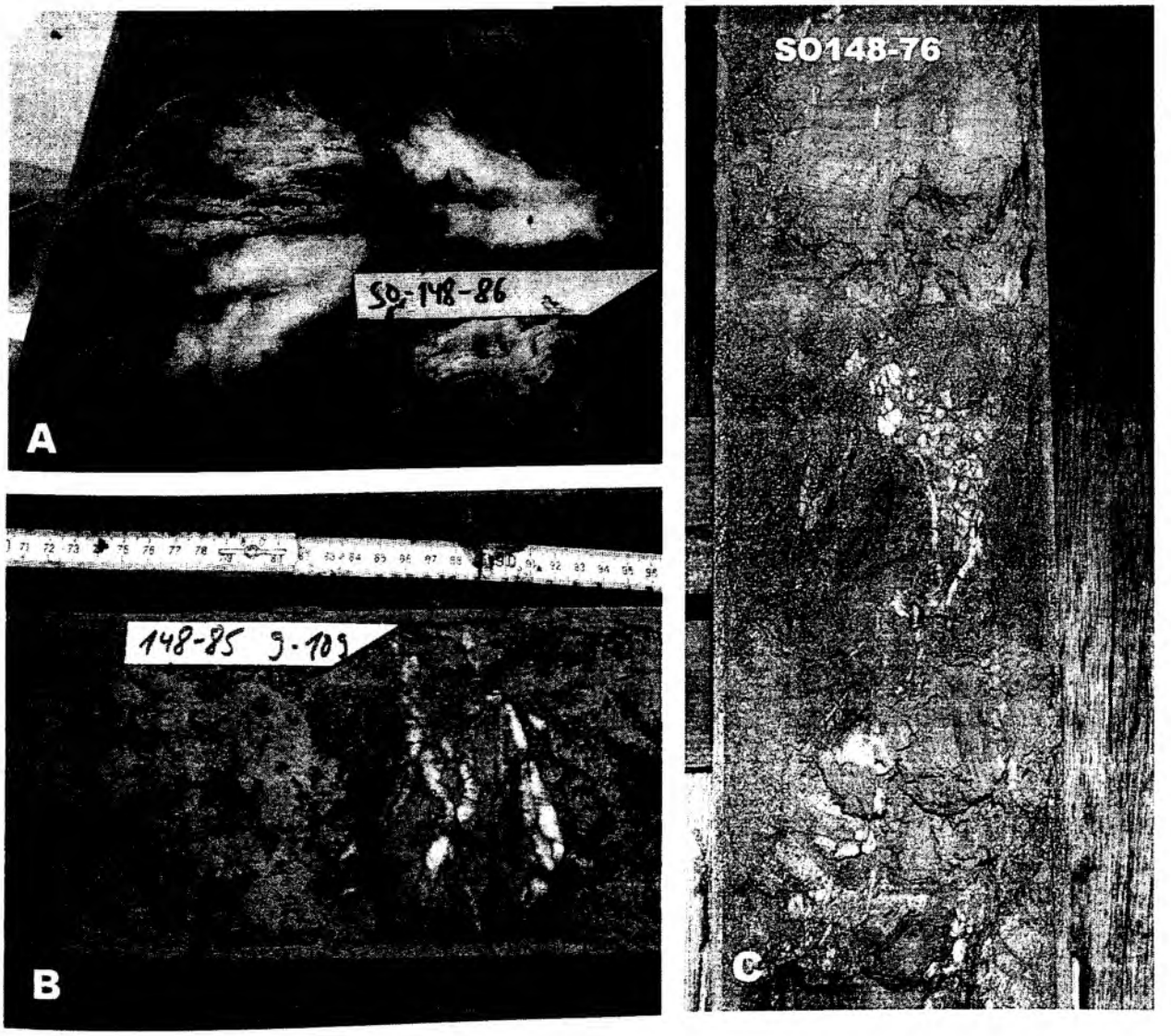

Fig. 33: Gas hydrates from sediment cores taken during SO148.

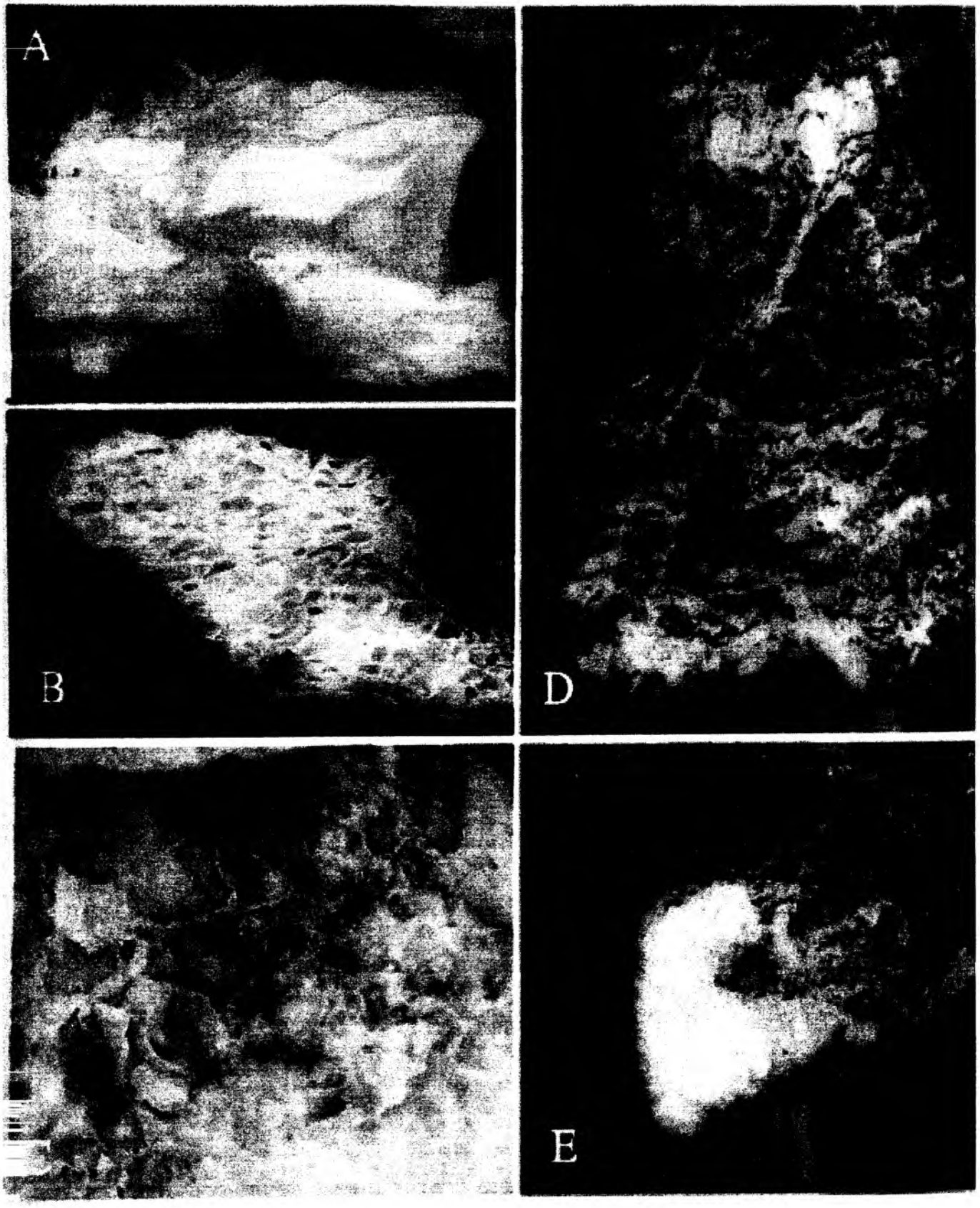

Fig. 34: Images of gas hydrates taken by TV-grab.

10.3 Structure of Gas Hydrates

Huge gas hydrate samples were repeatedly recovered by TV-guided grab sampling from the southern summit of Hydrate Ridge (Fig. 34). Pure gas hydrate occurred in layers or joints several millimeters (Fig. 34C) to decimeters (Fig. 34A) thick. The layers are generally oriented parallel to bedding planes obliquely. Gas hydrate often filled large pore space either as fractures or joints (Fig. 34D), or seemed to create its own space during growth by fracturing or pushing apart the sediment framework, most often along bedding planes.

The internal fabric of pure gas hydrate showed a peculiar structure with large pores (Fig. 34B and C) that remind of gas bubbles. Such pores occurred in variable sizes and indicated that free methane gas was closely related with the formation of these hydrates. These features strongly suggest that gas hydrate formation from the accumulation of methane bubbles is encased in a hydrate skin. On Southern Hydrate Ridge siding bubbles from below the seafloor were observed by ROPOS investigations at a depth of 780m. They either escaped into the water column or, when arrested within the sediments turned into hydrates. As the porous hydrate grows downward within the sediment towards rising methane bubbles, the buoyancy increased and it was interpreted by Suess et al. (in press) that large chunks detach and float directly to the sea surface. The crater-like seafloor on Southern Hydrate Ridge may indicate such patches of floating gas hydrates.

10.4 Physical and Chemical Properties of Natural Gas Hydrates

D. Rickert, A. Heuser, B. Domeyer, B. Bock, V. Karpen, C. Jung, A. Cremer, M. Mueller, B. Teichert, G. Bohrmann, E. Suess

Introduction

Natural gas hydrate samples have been recovered from a number of deep-sea sites by DSDP and ODP drilling (e.g., Shipley and Didyk, 1982; Kvenvolden and Barnard, 1983; von Huene et al., 1985; Westbrook et al., 1995). Shallow gas hydrate deposits were found in only few areas usually associated with active fluid or gas venting. They were sampled by gravity and piston cores in the Black Sea (Yefremova and Zhizchenko, 1974), the Caspian Sea (Ginsburg et al., 1992), the Gulf of Mexico (Brooks et al., 1991; MacDonald et al., 1994; Sassen and MacDonald, 1994; Sassen et al., 1998), the Sea of Okhotsk (Zonenshayn et al., 1987; Ginsburg et al., 1993), the Norwegian Sea (Vogt et al., 1997), in the eastern Mediterranean Sea (Woodside et al., 1998), in the Baltic Sea (Egorov and Rozhkov, 1997), and in the Barents Sea (Egorov et al., 1999). During SO110 cruise on Hydrate Ridge our working group recovered massive gas hydrates for the first time in large volumes (Suess and Bohrmann, 1997; Suess et al., 1999, Bohrmann et al., 2000).

However, our knowledge of fundamental properties of natural gas hydrate, including the composition of gas and water, molecular ratio of gas to water, structure, and crystallography is surprisingly limited because of the overall scarcity of well-preserved gas hydrate samples (e.g., Bohrmann et al., 1998; Kastner et al., 1998; Greinert, 1999; Matsumoto et al., 2000; Lorenson et al., 2000; Matsumoto and Borowski, 2000; Greinert et al., in press; Suess et al., in press). Matsumoto and coworkers (2000) reported the first extensive data set on gas hydrates sampled from ODP Leg 164 drilled on the Blake Ridge. They determined structure, molecular and isotopic composition, thermal conductivity, and equilibrium dissociation conditions. X-ray computed tomography (CT) imagery, X-ray diffraction, NMR, and Raman spectroscopy, have revealed that the

natural gas hydrates at the Blake Ridge are almost 100% methane hydrates with structure I.
During this expedition, we started a well-prepared extensive sampling program to investigate the physical and chemical as well as textural properties (see Chapter 10.3) of almost pure natural gas hydrate samples immediately on-board.

Material and Methods

Using conventional sampling techniques (gravity corer, multicorer) there is very limited chance to study original gas hydrates. Unless we are able to take gas hydrate-bearing sediments under *in situ* pressure and temperature conditions the use of the TV-grab is most capable to retrieve a large mass of sediment permitting the recovery and subsampling of larger volumes of gas hydrates. The TV-grab was deployed on the southern summit of Hydrate Ridge and sucessfully recovered large volumes of gas hydrates (TVG-148-36; TVG-148-57; TVG-148-58; TVG-148-66; TVG-148-82; TVG-148-99)
Upon recovery, a number of large pieces of massive gas hydrates were immediately sampled for geochemical and textural analysis. The samples were carefully cleaned from sediment, cut on the catwalk and subsampled with cylindric liners (Fig. 35) or using a drill (Fig. 36) in order to avoid breakage of hydrate pieces. Cylindric liners with three defined volumes (10 ml, 36.9 ml, 100 ml) or various boring devices were used depending on size and texture of the sample. Volume of subsamples obtained with the drill were calculated from measured height and diameter.
Samples were weighed for density and degassed for determination of water to gas volume ratios and chemical and isotopic water composition (both water and gas were quantitatively sampled), subsampled for determination of gas and isotopic composition of the gas phase or transferred to pore volume determination.

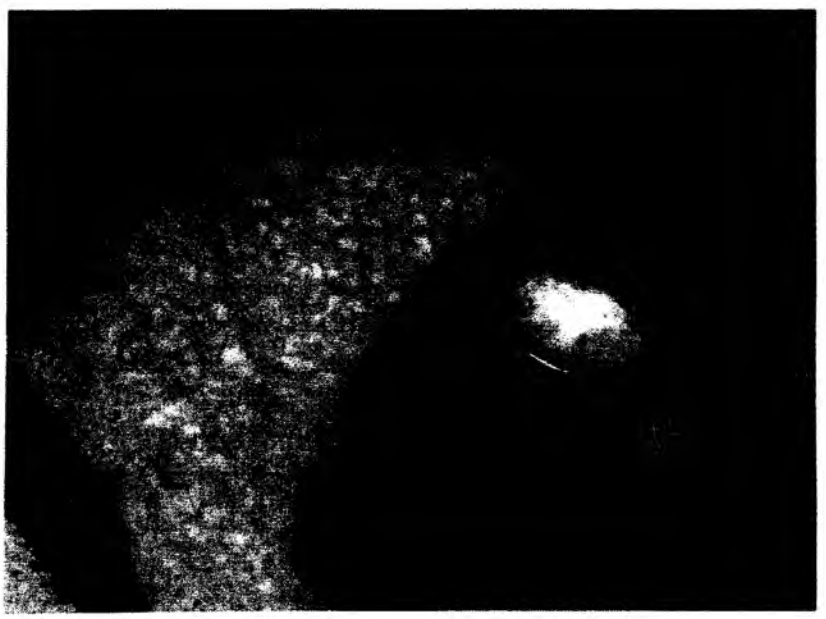

Fig. 35: Subsampling of highly porous gas hydrate pieces with a cylindric liner.

Fig. 36: Subsampling of gas hydrates using a drill machine with different drill devices.

Samples which were not processed immediately were stored in liquid nitrogen to avoid further decomposition. Water samples were directly analyzed for sulfide and chloride using standard photometric methods (see Chapter 13).
Gas hydrate samples which were not subsampled were stored in liquid nitrogen for shore-based measurements and experiments. The measurements of structural characteristics of these gas hydrates is aimed. Furthermore, the study of thermodynamics and kinetics of gas hydrate dissociation under natural conditions in laboratory experiments is planned as part of the OMEGA project funded by the Bundesministerium für Bildung und Forschung (BMBF).
Acidified subsamples (10 µl/ml sample) were prepared from hydrate water for ICP analyses (Na, K, Li, Mg, Ca, Sr and Mn) as well as subsamples for isotopic determinations. Subsets will be analyzed in the shore-based laboratory.
In the following a more detailed description of shipboard investigation and preliminary results are given.

Preliminary Results and Discussion

Fabrics of recovered hydrates are almost the same as on SONNE Cruises 143 (Bohrmann et al., 2000). They are either massive layers forming along bedding planes, highly porous bubble-like fabric forming in void space of near-surface sediments, but also massive and up to dm in diameter containing only few percent sediments. A more detailed description of recovered hydrates is given in Chapter 10.3.
Here we focus on results from massive hydrates where subsampling was possible and contamination through adjacent sediment was minimized.

Pore Volumes

With samples recovered during SO143 cruises we have made first order estimates of pore volume by image analyses of the volume of the macropores over 2-3 selected areas of the sample (Suess et al., in press). We observed that ~ 55 ± 5 % of the area is occupied by void space.

During this cruise pore volumes were quantified using an oleo-hydraulic pelletising press (Model TP/2d Herzog Maschinenfabrik GmbH + Co., Osnabrück) with max. 200 kN compression force per 12.3 cm^2 area, i.e ~ 160 bar. Gas hydrate subsamples were stored in liquid nitrogen prior to volume determination. The pelletising press was also cooled with liquid nitrogen to minimize melting artefacts during processing. The difference between sample volume before and after compression was used to calculate the pore volume. Results of 15 measurements including samples of 5 TV grab deployments are illustrated in Fig. 37.

Analogously to our visual observation of highly variable fabrics of naturally occuring gas hydrates, the pore volumes show a high variability ranging from ~ 10-70 Vol.%. This has enormous consequences for the stability of gas hydrate layers on the seafloor. In all our experience with sampling, processing and cleaning of numerous pieces of natural porous gas hydrates, not once did we observe water flowing out of the pores. If this pore volume is instead occupied by gaseous methane this would result in much lower bulk density numbers than the material density of 0.91 g/cm^3 (Sloan, 1998; Suess et al., in press). This would result in an enormous positive buoyancy force which could lift off gas hydrates from the sea-floor even if covered by thin layers of sediment (Suess et al., in press).

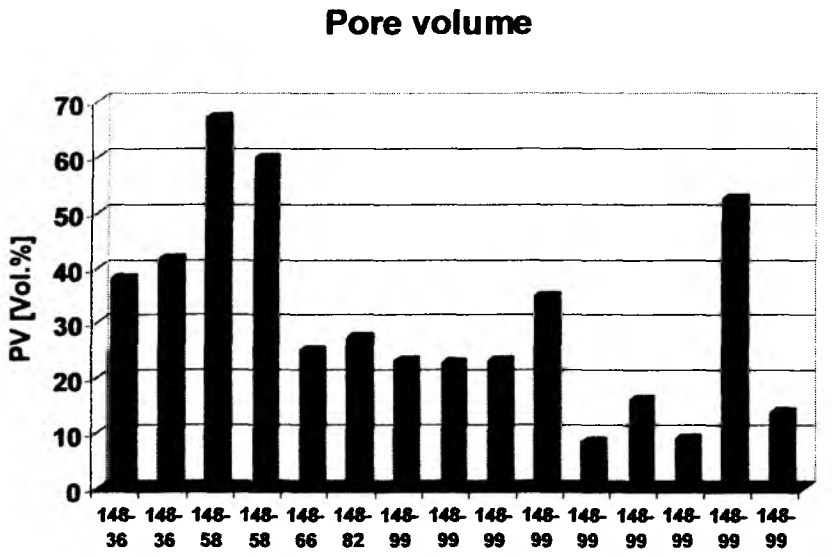

Fig. 37: Pore volumes determined on different samples of 5 TV-grab deployments. Pore volumes of natural gas hydrates are highly variable ranging from ~ 10-70 Vol.%.

Besides geochemical investigation (Kvenvolden and Kastner, 1990; Froelich et al., 1995; Kastner et al., 1995; Yuan et al., 1996; Paull et al., 1996; Matsumoto and Borowski, 2000) the assessment of gas hydrate amounts has been made using techniques such as seismic investigation or well logging. These methods, however, are largely dependent on material densities. Therefore, estimates of global gas hydrate inventory (e.g., Kvenvolden, 1988) require further refinements due to observed pore volume or density variations.

Density

Almost 80 gas hydrate subsamples with a well-known volume were weighed in order to determine the *wet bulk density* variations among naturally occurring gas hydrates on Hydrate Ridge.

Wet bulk densities show variations between 0.2 and 1.0 g/cm^3 with a mean value of 0.53 (±0.17) g/cm^3 (Fig. 38) This value is much lower than the material density of gas hydrate of 0.91 g/cm^3 (Sloan, 1998). In Fig. 39 we demonstrate that this observation is a direct consequence of the variations natural gas hydrates show in pore volumes. Pore volumes and wet bulk density are negatively correlated. A least-squares linear regression gives a correlation coefficient (R^2) of 0.751. Consequences due to pore volume increase or wet bulk density decrease among natural gas hydrates were discussed in 3.1.

An extrapolation to a pore volume of 0 % yields a density value of 0.81 g/cm^3 which is slightly lower than the theoretical material density and that determined during SO143 cruise (0.89 (±0.04) g/cm^3, Suess et al., submitted). To distinguish this experimentally determined from the theoretically defined value we define this value as *compressed material density*. Unlike wet bulk density, this value excludes pore volumes.

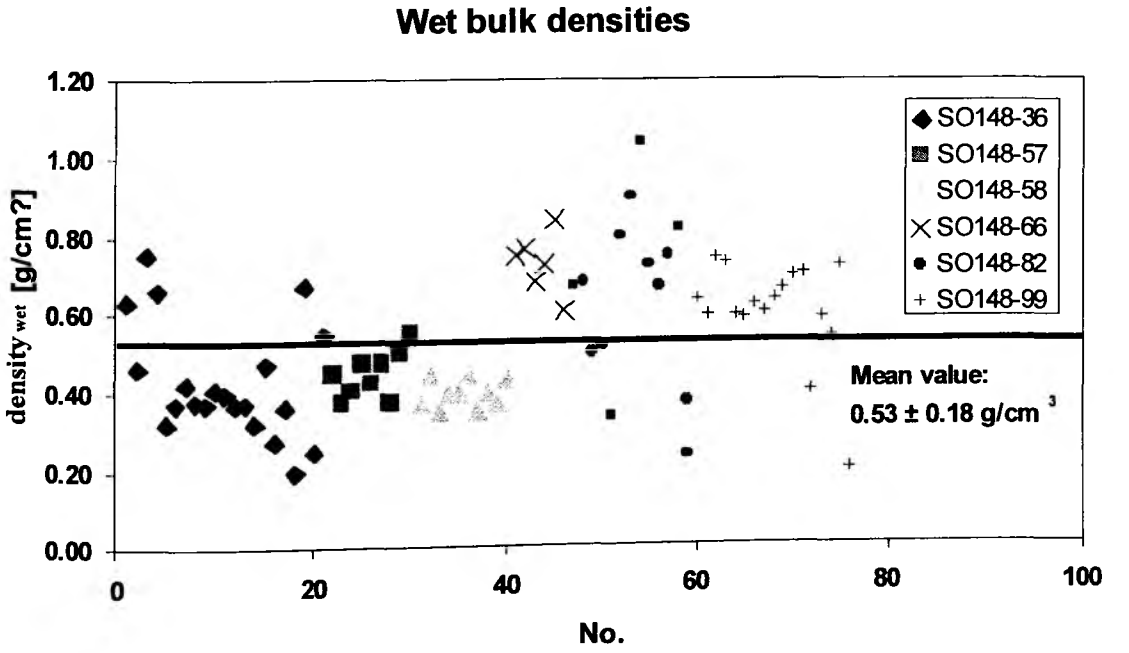

Fig. 38: *Wet bulk densities* of gas hydrates recovered from 6 TVG deployments on the southern summit of Hydrate Ridge. The mean value of 0.53 g/cm^3 is significantly lower than the material density of 0.91 g/cm^3 (Sloan, 1998).

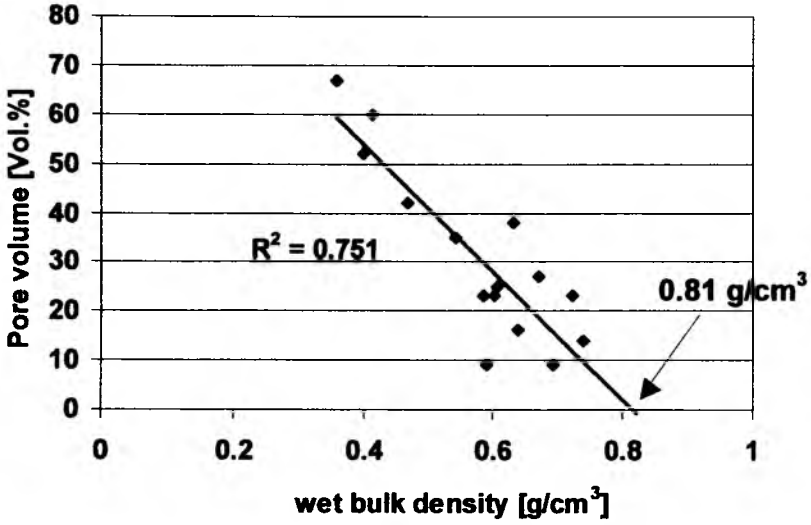

Fig. 39: Crossplot of pore volume vs. wet bulk density.

Hydrate Composition

Along with the structure of natural gas hydrates the molar ratio of water to gas is one of the more important parameters to estimate the amount of methane gas trapped in gas hydrates in marine sediment. Furthermore, the measurements of structure and composition of natural gas hydrates may also provide the knowledge of their formation conditions. Especially carbon and deuterium isotopes are useful to distinguish between thermogenic and biologically induced growth of hydrates (Rosenfield and Silverman, 1959; Schoell, 1980; Rice and Claypool, 1981; Whiticar et al., 1986).

To determine the molar water to gas ratio gas hydrate samples were placed in a dissociation chamber and allowed to decompose at room temperature (Fig. 40).

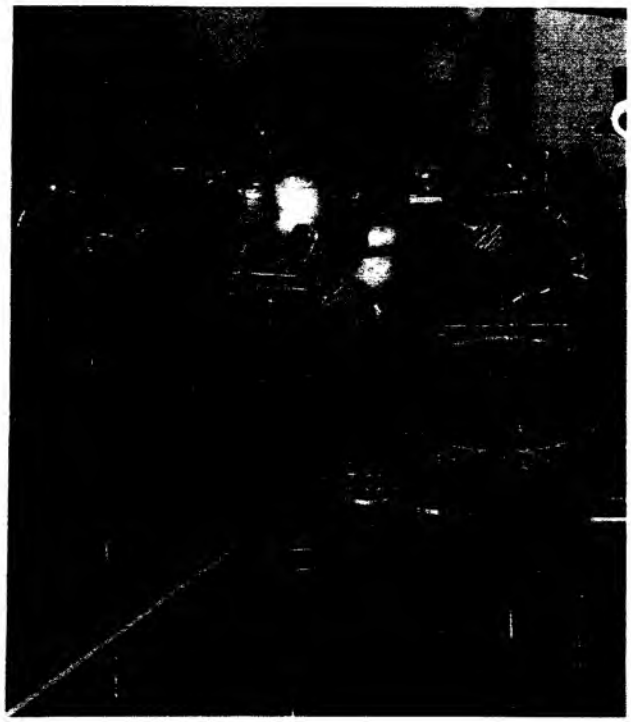

Fig. 40: Gas hydrate dissociation chambers.

The hydrate gas was transferred to 1 liter water-filled inverted graduated cylinders and the total gas volume was determined. The volume of water left in the dissociation chamber was measured, filtered through 0.2 µm membrane filters and stored in polypropylene flasks. In Fig. 41 the average hydrate to gas to water composition of 34 hydrate samples is given. These values are compared with theoretical values given in Sloan (1998) for structure I methane hydrate.

Hydrate Ridge gas hydrate gas to water volumetric ratios have a wide range of values from 10 to 200. The highest ratios can be compared with the theoretical maximum of 205 ml gas/ml water. An average value of 80 (± 40) ml gas/ml water clearly demonstrates that the ratios determined are minimum gas/water ratios for gas hydrate because of partial dissociation during sediment recovery and potential determination with pore waters.

The gas hydrate/gas or gashydrate/water ratio is conspicuously small because the pore volumes are not included yet. A more detailed evaluation of the large data set is necessary to give concluding comments on the composition of gas hydrates from Hydrate Ridge.

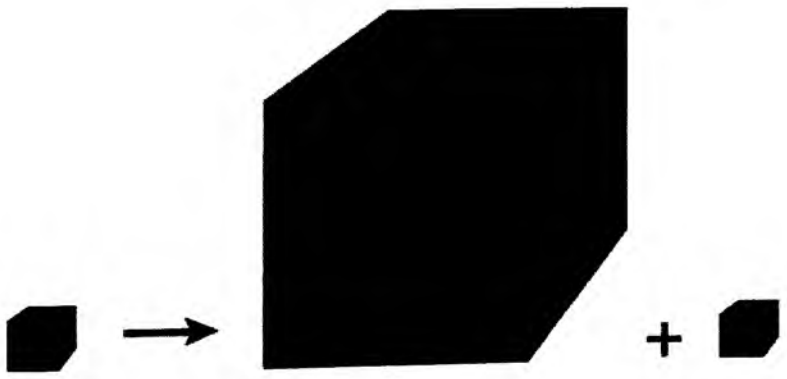

Fig. 41: Schematic illustration of theoretical and practical composition of gas hydrates from Hydrate Ridge. The gas to water volumetric ratios measured on 34 subsamples of methane hydrates from Hydrate Ridge is given. Pore water contamination of 2-14 Vol.% in residual hydrate waters was estimated by chloride determinations.

Composition of Water and Gas of Gas Hydrates

Composition of water
Water from hydrate degassing was filtered through 0.2 µm membrane filters, subsampled and fixed with zinc acetate for hydrogensulfide determinations. The remaining water was stored cool for the pending chlorinity measurements on board. Subsamples were taken for shore-based ICP and isotopic ($\partial^{18}O$, ∂D) analyses.
Gas hydrates exclude all ions upon formation, thus the chlorinity of gas hydrate water reflects the amount of pore water and/or sea water that accompanies gas hydrates in our measurements. Therefore, pore-water contamination can be estimated by the observed chlorinity concentration in dissociated gas hydrate residual water. In addition, H_2S concentrations in residual hydrate waters reflect the contamination of solely adjacent pore water and dissolved gas from mixed-H_2S-CH_4-hydrates.

In Fig. 42 results of sulfide (a) and chloride (b) concentration in rising order are illustrated. Chloride concentrations vary from 10 to 75 mM. This corresponds to 2-14 Vol.% of sea or pore water mixed with the residual hydrate water assuming that the pristine gas hydrate-derived water was salt free. H_2S ranges from 300-3000 µM. No correlation between these two parameters was observed. Consequently, the relative orders of samples in (a) and (b) are not the same. Since the H_2S-to-Cl ratio in most cases is neither constant, as in normal sea water, nor does it represent interstitial water, a random mixture of adhering moisture during sampling is the most likely explanation for sea salt in hydrate water (Suess et al, submitted). 300-800 µM H_2S observed in almost pure hydrate waters is considered as background value of dissolved gas from mixed-H_2S-CH_4-hydrates, assuming that the sea water is sulfide-free.

Chloride anomalies measured in pore waters after recovery of hydrate-bearing sediments are believed to be a reliable method of estimating gas hydrate amounts (e.g., Kvenvolden and Kastner, 1990; Froelich et al., 1995; Kastner et al., 1995; Yuan et al., 1996). This method was critically assessed in Chapter 13 (3.3) since we observed again positive chloride anomalies in interstitial waters after the first identification during SO143 (Rickert et al., 1999; Suess et al., in press). Another serious question has been raised concerning the effects of selective filtration/adsorbtion on some chemical elements during squeezing (Cave et al., 1998). These problems seem to require a reassessment of the chloride anomaly technique.

Matsumoto et al. (2000) proposed deviations in $\partial^{18}O$ of pore waters from baseline values - which also need a critical raassessment - as an independent technique in estimating gas hydrate amounts in sediments. Our large set of samples and future $\partial^{18}O$ and ∂D isotope data of pore water - both with positive and negative chloride anomalies - and hydrate waters with variable contamination of sediment and/or sea water signals will improve the ability to estimate the amount of gas hydrate trapped in sediments and to quantify the potential importance and risks of marine gas hydrates for human welfare.

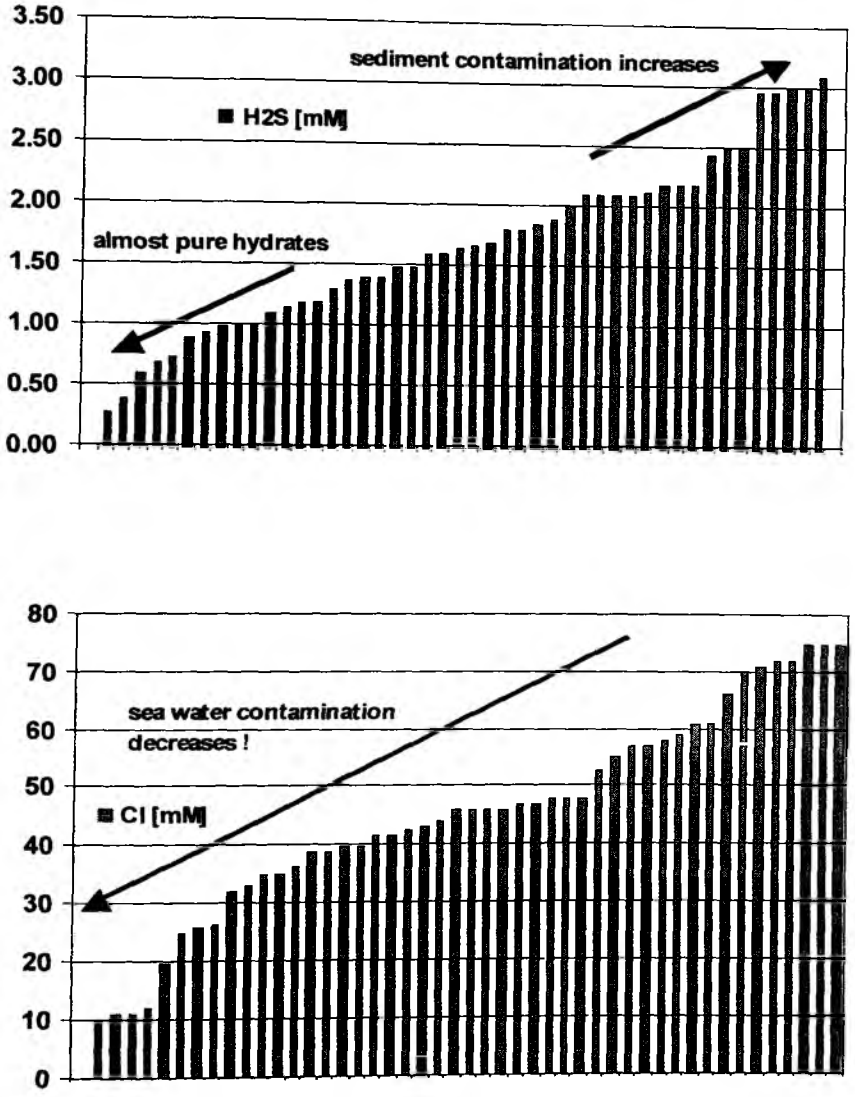

Fig. 42: Sulfide (a) and chloride (b) concentration of hydrate samples. The order of samples differs in (a) and (b). Chloride and sulfide concentrations reveal no correlation.

Composition of gas

Molecular compositions of hydrocarbons and carbon isotope composition of methane is widely used for a genetic classification of hydrogen gases (Rosenfield and Silverman, 1959; Schoell, 1980; Rice and Claypool, 1981). Schoell (1980) and Whiticar et al. (1986) have shown additionally that the hydrogen isotope composition in combination with the carbon isotope composition characterizes different pathways of microbial methane formation: CO_2 reduction and fermentation. To address these important topics we collected gas in headspace vials and water samples for chemical and isotopic analyses in home laboratories using an apparatus for a controlled degassing for pieces of hydrate (Fig. 43).

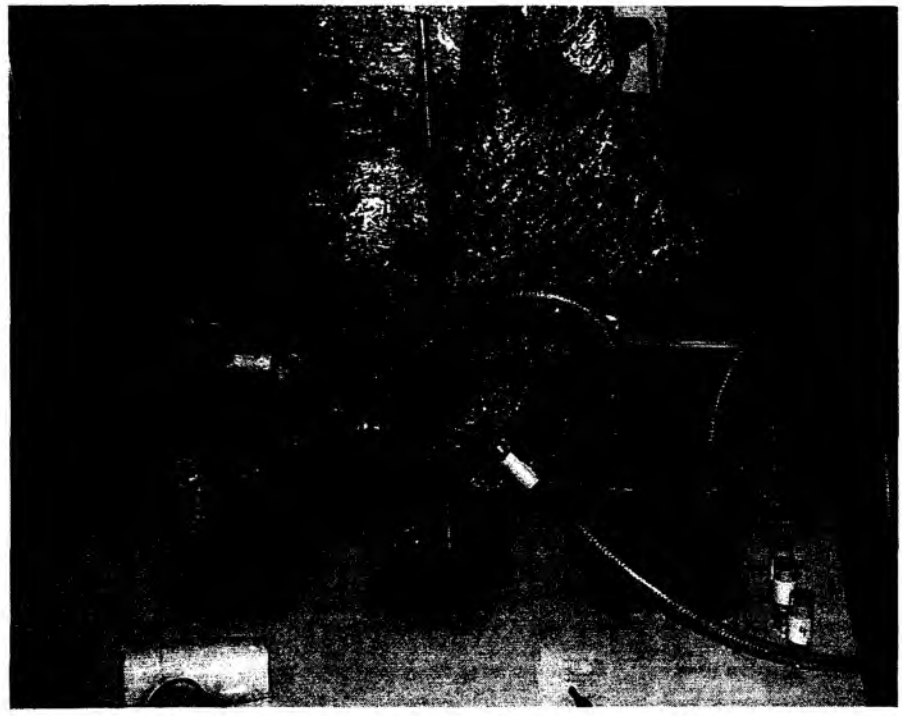

Fig. 43: Controlled degassing of gas hydrates for chemical and isotopic analyses of the gas and water phase.

10.5 Carbonates

B. Teichert, B. Bock, G. Bohrmann, C. Jung

Authigenic carbonates are widely distributed at the sediment surface along Cascadia accretionary prism (e.g. Kulm et al., 1986). These carbonate structures are prominent features associated with fluid venting, which is well known to occur in this area. Recent studies have discovered a great variety of authigenic carbonates (Greinert, 1999; Greinert et al., in press). During the TECFLUX I cruises a large collection had been sampled. In ongoing studies, a classification will be developed which will help to achieve new insights into their specific diagenetic formation environments. Most rock samples on this cruise were collected using ROPOS's manipulator arms (dives 560, 561, 562, 563, 564, 565, 567, 570, 571, 574). But TV-G 36, 65, 66, 73, 82 and 99 and also OFOS 39 provided additional samples. The carbonate samples were visually pre-classified into the rock types listed in Tab. 8.

Massive carbonate concretions were observed in many places and form specimen up to 40 cm in diameter. Generally, they are well rounded to subrounded and are classified as **mudstones**. These mudstones are characterized by a dense homogenous matrix of terrigenous sediment (e.g. quartz, feldspar, and clay minerals) which is cemented by micritic carbonate. The surface of theses rocks often show yellow, brown or black coatings on their surface, most probably caused by Mn or Fe oxide or hydroxide precipitation due to exposure for longer time on the seafloor. Such mudstones often represent the relief of bioturbation casts.

Tab. 8: List of all carbonate rocks and their sample sites.

ROPOS dive/ Station No. SO148	Sample No.	Device	Carbonate types					Sand-stone
			Mud-stone	Chemoherm Carbonate		Gashydrate Carbonate		
				Breccia	Aragonite	Aragonite	Unconsolid. Breccia	
559	1	ROPOS		x				
	2	ROPOS		x				
	8	ROPOS		x				
	9	ROPOS	x					
560	1	ROPOS				x		
561	1	ROPOS	x					
	4	ROPOS		x				
562	1	ROPOS		x				
563	5	ROPOS				x		
564	1	ROPOS		x				
	2	ROPOS	x					
565	7	ROPOS		x				
	8	ROPOS		x				
567	1	ROPOS		x				
570	1	ROPOS			x			
	3	ROPOS		x				
	4	ROPOS		x				
	6	ROPOS		x				
	9	ROPOS			x			
571	2	ROPOS		x				
	3	ROPOS		x				
574	2	ROPOS						x
	7	ROPOS						x
36		TV-G	1	2		9	5	
39		OFOS			1			
65		TV-G	9	9			12	
66		TV-G	9	1				
73		TV-G	2				10	
82		TV-G					16	
99		TV-G	1				11	

Chemoherm Carbonates

Chemoherm carbonates are either breccia type rocks or rocks in which aragonite encrustations occur. **Breccias** are of variable size up to 40 cm in diameter. The surface shapes of such rocks are irregular and in most cases very rough. Based on their composition polymict lithologies occur that show ruditic components of matrix-like intraclasts (565-7, 565-8, 36).

Carbonate minerals are calcite Mg-calcite and aragonite. Light to medium grey calcitic clasts dominate the rock. Clasts of 1-2 cm in diameter are either rounded or angular. The cement consists of whitish-yellowish or pinkish aragonite of pure carbonate composition. Thick cement layers were observed, however, open cavities were also observed in many cases. These features are responsible for the high porosity. The amount of aragonite in the samples is variable. In parts where dissolution features are developed, the calcitic components are preferentially dissolved and often soft like in sample 565-7, 36, 65. Other components are clam shells (mostly *Calyptogena* and *Acharax*) and gastropod shells. Sample 562-1 is rich in small, rounded glauconite grains up to 1 mm in diameter.

One sample that should be mentioned separately is 571-3 (Fig. 44B). The upper very porous and fragile part cropped out of the sediment, before the sample was recovered by the ROPOS arm. Its porous structure seems to be a network created by constant fluid outflow. A *Calyptogena* shell is also incorporated prooving the occurrence of chemosynthetic organisms. The lower part of the sample was covered by soft sediment. It is not fully consolidated yet and is composed of calcareous, only slightly cemented fragments.

Three pieces of pure **aragonite** specimen were sampled at the pinnacle to the west of Hydrate Ridge summit (570-1, 570-9; Fig. 44C) and the SE Knoll. Sample sizes vary up to 40 cm in diameter. The surface is often slimy or 'chalk-like' (570-1, 570-9). The specimen are highly porous and irregularly shaped. Probably these samples are also strongly influenced by constant fluid flow. Some open pore spaces show a yellowish coating (570-1, 570-9). This can also be seen in the breccia-type chemoherm carbonate 570-3. Sample 39 is massive and has angular edges. Several different cement generations follow each other. They are separated by a thin brownish 'skin' of unknown composition.

Gashydrate Carbonates

Gas hydrate-related carbonates include two different types: pure aragonite layers and carbonate-cemented breccia (Bohrmann et al., 1998).
The **aragonite** samples show a distinct platy or crusty shape and are sometimes found together with gas hydrate in TV-grabs (36). Some samples show their precipitation directly in gas hydrate layers forming pseudomorphic textures of the hydrates. The aragonite crusts of Site 36 were typically whitish to yellowish, with only few grey parts.

In sample 560-1 (Fig. 44A) no internal layering could be recognized. The yellow aragonite shows a porous texture. This specific sample was remarkable because it was covered with living bacteria. The relationship between the bacteria and the precipitation of aragonite will be investigated in future studies.

Sample 563-5 was sieved from a sediment sample taken directly above a bubbling vent site where the formation of gas hydrate could be proved by digging with ROPOS. The aragonites consist of several yellowish, bodroydal thin crusts up to 1 cm. This could document the starting formation of larger aragonite crusts like sample 560-1.

Unconsolidated **breccia** were only found in TV-grab samples and occur associated with gas hydrates (36, 73, 82, 99). Their shape is irregular and their color ranges from light to medium grey. Due to many calcitic clasts (sometimes polymict (36)) including clam and gastropod shells (especially in TV-G 82) they have an irregular and sharp-edged surface. The different components are held together by a sticky, muddy sediment. Sometimes channel-like parts are better cemented (82 (Fig. 44), 99). This might be an indication of migrating fluids.

At one location, the NW-Knoll, two sandstones were sampled. These samples are poorly cemented and fragile.

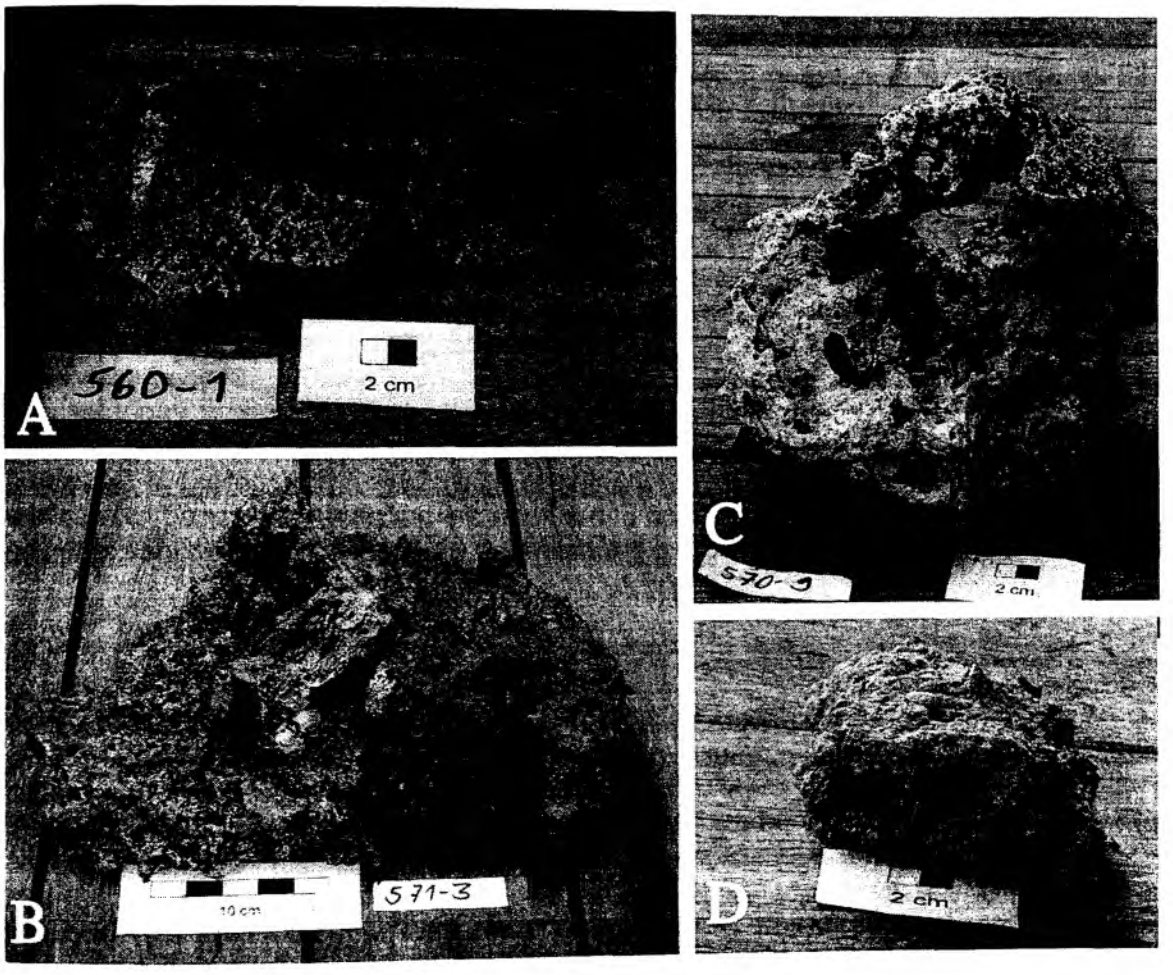

Fig. 44: Photographs of carbonate rocks recoverd during SONNE Cruise 148.

11 MICROBIAL ECOLOGY

11.1 Characterization of *Beggiatoa* filaments in Respect to Sulfide Gradients

H. Sahling, D. Rickert

Objectives

The mat-forming bacteria *Beggiatoa* sp. contributes significantly to the biomass at seeps and gas hydrate deposits at the Cascadia margin. During cruise SO143 it was observed that these sulfur-oxidizing bacteria are indicative of a very high flux of hydrogen sulfide. Therefore, one major goal during this cruise was to characterize the *Beggiatoa* filaments in terms of width and length as well as their depth distribution in the sediment and in relation to the sulfide concentrations in the porewater.
Sulfur-oxidizing, mat-forming bacteria are known to store nitrate in their vacuoles. For the process of sulfide oxidation this nitrate can be used as electron acceptor when oxygen is not available. Therefore, we wanted to study the nitrate content of *Beggiatoa* filaments. Due to the high concentration of nitrate in the bacteria we planned to measure nitrate in the porewater after destroying the cells with ultrasonic. The basic idea is to use nitrate as a tracer for the biomass of nitrate storing bacteria.

Methods

Six cores from three stations were used for the investigations of *Beggiatoa* biomass in relation to the sulfide concentrations in the sediments: MUC 63F, 90D, 90B, 90E, 91A, 91C. Subsamples of the sediment with *Beggiatoa* filaments were collected with syringes (one end cut open, 20 and 50 ml) vertically from the sediment surface. The sediment around the syringes was then sliced in 1 cm depth intervals up to a depth of 8 cm. The pore water of the sediment sections was extracted by squeezing (MUC 63F) or centrifugation (others). Before centrifugating, the tubes with sediment and bacterial filaments were treated with ultrasonic for 30 min in ice water to destroy the cells and release the nitrate. For comparison, sediment samples were frozen to analyze the nitrate concentration in the home lab. The extracted pore water was analyzed for nitrate concentration on board and will be analyzed for hydrogen sulfide at GEOMAR.
The sediment in the syringes was carefully washed from base to top to determine the maximum depth of penetration of the bacterial filaments. The sediment where filaments were present was collected in depth intervals and preserved for later biomass determination. Before preservation, the length of a certain number of filaments was determined and the filaments transferred into a vial with 0.5 ml sea water. The filament length was determined with an ocular micrometer under a dissecting microscope with a resolution of about 0.4 mm. The diameter of the filaments was determined earlier (approx. 50 µm). The biovolume of the filaments was calculated applying the formula for cylindrical bodies. The proportion of the vacuole, the compartment which stores nitrate in the bacterial cell, was assumed to be 70 %. Similar values have been reported from species investigated elsewhere. The extracted filaments (about 20 to 30 cm) in 0.5 ml sea water were treated with ultrasonic for 30 min (on ice). The nitrate concentration was determined using the autoanalyzer (see Chapter 13).

Results and Discussion

Despite the fact that bacterial filaments were present in the sediment the nitrate concentrations of the pore water extracted on board do not indicate significant input of bacterial nitrate. This may be explained by incomplete destruction of the cell membranes or by inadequate extraction of the porewater applying the centrifugation technique.

Bacterial filaments were never found deeper than 3 cm in the sediment. Filaments penetrating that deeply had filament length of 7 to 10 mm. The longest filaments with up to 15 cm were collected from the sediment surface. Since the filaments are very fragile it cannot be ruled out that longer filaments exist. Their orientation in the sediment is more horizontal than vertical. Due to the sampling with syringes filaments get artificially transported into the sediment.
The nitrate concentration in the vacuoles of the bacterial filaments can be as high as 230 mM but varies with location, filament abundance and depth in the sediment (Tab. 9). A model of spatial segregation of the nitrate metabolism with nitrate accumulation at the sediment surface and the consumption in deeper sediment depth cannot be proven with the available data.

Tab. 9: Nitrate concentrations in the vacuoles of *Beggiatoa* filaments.

Station	Description	Filament	Depth / cm	Nitrate concentration in vacuole /mM
MUC 63F	single layered bacterial filaments	white filaments	0-1	228
			0-1	231
			0-1	232
ROPOS 570, SS4	bunch of orange filaments	orange filaments		146
				144
				156
		Thioploca-like		ca. 300-500
MUC 90D	thin layer of filaments	white filaments	0-0.5	60
			0-0.5	215
			0.5-2	174
			0.5-2	190
			2-3	192
MUC 90B	thick multi layer patch of filaments	white filaments	Surface	65
MUC 90E	thin layer of filaments	white filaments	0-1	105
MUC 91A	very thin layer of filaments	white filaments	Surface	146
MUC 91C	hardly any filaments	white filaments	1-2	58

11.2 MICROBIAL SULFATE REDUCTION AND METHANE OXIDATION

A. Boetius, T. Treude

The major aim of this study was the investigation of microbial sulfate reduction (SRR) and methane oxidation (MOx) in methane enriched surface sediments of Hydrate Ridge. Samples were obtained from the sediment cores which were retrieved by TV-guided multicorer hauls (Tab. 10). Both radioactive tracers $^{35}SO_4$ and $^{14}CH_4$ were injected into 6 replicate core subsamples (inner diameter 3.5 cm) and incubated at *in situ* temperature for 24 hrs. After incubation, the upper 10 cm of the sediment cores were split into 1 cm intervals and mixed with zinc acetate (20% w/w) or sodium hydroxide (2.5% w/w), respectively, to stop the bacterial activity. These samples will be analyzed in the home laboratory. A series of slurry experiments with ^{14}C-labeled tracers were carried out to investigate the incorporation of different inorganic (CO_2) and organic carbon molecules (methane, acetate, methanol, methylamine) by the sulfate reducing bacteria. From each of the slurries, subsamples were taken to analyze sulfate and sulfide concentrations as well as CO_2, methane and acetate concentrations. Further subsamples were taken from cores and slurries

- to determine the total number of bacteria
- to quantify different taxonomic groups of bacteria by fluorescence *in situ* hybridization (FISH)
- to attempt cultivation of bacteria involved in sulfate reduction and methane oxidation.

Tab. 10: Station list. Subsamples for total bacterial biomass and FISH were taken at each of the stations.

Station	Location	Sediment horizon (cm)	Parameters	Method
148-12	thick *Beggiatoa* mat, gashydrates >13cm	1-5/8-12	SSR, MOx, incorp. rates	slurry
148-14	thin *Beggiatoa* mat	0-10 (cm-layers)	SSR, MOx	whole core injection
148-19	medium *Beggiatoa* mat, gashydrate >13cm	0-10 (cm-layers)	SSR, MOx	whole core injection
148-28	thin *Beggiatoa* mat	0-1/1-5/8-12	cultivation	slurry
148-29	medium *Beggiatoa* mat	0-1/1-5/8-12	cultivation SSR, MOx, incorp. rates	slurry
148-38	*Calyptogena* field 3-4 clams per core	0-10 (cm-layers)	SSR, MOx	whole core injection
148-44	*Calyptogena* field 1-2 clams per core	0-2/2-6/6-12	cultivation SSR, MOx, incorp. rates	slurry
148-51	Reference (few *Acharax*)	0-10 (cm-layers)	SSR, MOx	whole core injection
148-52	thick *Beggiatoa* mat, gashydrates >13cm	1-5/8-12	SSR, MOx	slurry

Sites with highest methane enrichment were indicated by the presence of white and orange mats of giant sulfur-oxidizing bacteria (*Beggiatoa*) covering the seafloor. These patches of bacterial mats varied in size from a few centimeters up to several tens of

meters at the southern Hydrate Ridge. The thinnest mats consisted of single vertically oriented white *Beggiatoa* filaments which extended 2-3 cm into the sediment. The thickest mats (0.5 - 2 cm thickness) were bright orange with strongly tangled filaments which were easily resuspended from the sediment surface in large aggregates. The suction sampler of the ROPOS was used to obtain quantitative samples of these surficial *Beggiatoa* mats (Tab. 11). For this purpose, a 40 x 40 cm metal frame with scales on each side was set on a mat and photographed before and after sampling of a patch of about 10 x 10 cm within the frame. The sample was sucked into one of the jars of the ROPOS rosette sampler and the bacterial filaments were retained on a 20 µm gauze. After recovery of ROPOS, the contents of each jar were carefully concentrated by centrifugation at slow speed and washed several times with bottom water to remove sediment particles. Replicate subsamples of the *Beggiatoa* filaments were fixed in formaldehyde or deep frozen for later analyses of size and total biomass, for the measurement of C, N, S, for the quantification of protein, carbohydrate and lipid content as well as for stable isotope measurements.

Tab. 11: ROPOS samples of *Beggiatoa* mats. Pictures were taken before and after sampling the inner frame area with the suction sampler.

Dive no.	Station	Date	Jar	Sample description
559	4	24-Jul	2	orange mat
			3	filter test
			4	orange mat
			5	filter test
			6	filter test
560	10	25-Jul	2	orange mat
			3	white mat
			4	white mat
			5	white mat
			6	orange mat
561	17	26-Jul	2	white mat
			4	white mat
562	23	27-Jul	8	white mat
563	30	28-Jul	6	white mat
			8	orange mat
565	41	30-Jul	7	white filaments on carbonate rock

12 MACROFAUNAL ECOLOGY

12.1 Respiration Studies

H. Sahling

Objectives

The animals at the cold seeps and gas hydrate deposits are exposed to significant concentrations of hydrogen sulfide. It is likely that they experience suboxic conditions temporarily. To study the influence of hydrogen sulfide on the metabolism of the dominant species it was the main objective during this cruise to collect animals and maintain them for studies in a respiration system on shore.
The closed flow-through system is run by Dr. Raymond Lee, Washington State University, Pullman, WA and can measure and control O_2, H_2S, pH, CO_2, NH_4, and temperature.

Species Collected

Species were collected with the suction sampler of ROPOS and with the multicorer. Living species of the chemoautotrophic vesicomyid bivalves (*Calyptogena kilmeri*, *C. pacifica*, *Vesicomya stearnsi*), provannid gastropods (*Provanna lomana*, *P. laevis*), and polynoid polychaets were successfully maintained alive for a period of about a week.

12.2 Experimental Studies in a Flume

L. Thomsen and V. Karpen

It is known from permeable sediments that the bottom flow conditions can change pore water release. As gas hydrate sediments are coarse it was hypothesized that the tidal cycle with its changing bottom flow conditions has an impact on the efflux of fluids from the sediments.
Additionally, the importance of the *Calyptogena* community on the fluid flow was studied. Therefore, 26 cores obtained with the multicorer from both vent sediments and reference stations were transferred to the large sea water flume of the Friday Harbor laboratories (San Juan Islands) after the cruise. The MUC cores were placed into a test section with 50 x 50 cm surface area. The sediment community was allowed to adjust to the flume conditions for 24 hours before experiments started. Seep fluid generated from overlying water of the cores was inserted at 5 cm sediment depth and the efflux was visualized by means of an *In Situ Schlierenoptic* (Karpen, 1999). Under different flow conditions no significant differences in fluid flow could be detected. The sediments consisted of a cohesive surface layer, sometimes covered by a white layer of *Beggiatoa* mats, which prevented an increase of pore water flow under increased flow conditions. The *Calyptogena* communities clearly showed the tendency that the clams placed themselves on point sources of seepage (3-5 below each clam). But no correlation with the flow conditions and fluid flow could be detected. On the other hand, as already pointed out by other studies, differences in sea water level inside the flume (e.g. pressure differences) had a significant impact on fluid release and will be further studied. In general, the *Calyptogena* community survived for about 5 days in the flume.

13 PORE WATER INVESTIGATIONS

13.1 Pore Water Chemistry

D. Rickert, A. Heuser, B. Bock, B. Domeyer

Introduction

The objective of the geochemistry program during SO148 was to confirm and complete the data collected at Hydrate Ridge during SO143 cruises last summer (Bohrmann et al., 2000). Of special interest was to combine geochemical, micro- and macro-biological investigations on identical core samples from the Southern Summit to improve our understanding of the mechanisms and geochemical consequences of hydrate formation and decomposition at active vent sites and the complex interplay of biological activity and pore water chemistry. The necessity of such investigation erose from the dramatic differences in pore water chemistry, and the occurence of different seep biota on smallest geographical scales. Microbial investigations are described in more detail in Chapter 11, macrofaunal studies are reported in Chapter 12.
The composition of pore fluids associated with gas hydrates is strongly affected by hydrate formation and in turn controls the stability and formation rate of hydrates. An increase in pore water salinity through hydrate formation were to the first time discovered during SO143 (Rickert et al., 1999; Suess et al., 1999; Suess et al., in prep.). Samples showed chloride concentrations from 580 mM to 840 mM. Therefore, field work during SO148 aimed towards the discovery of Cl anomalies in sediments interlayered with gas hydrates. The magnitude of salt-enrichments are used to decipher the conditions and mechanisms of hydrate formation as well as for more plausible estimates of gas hydrate volumes within sediments than estimates based on chloride anomalies (e.g., Kvenvolden and Kastner, 1990; Froelich et al., 1995; Kastner et al., 1995; Yuan et al., 1996).
We also studied the physico-chemical behavior of gas hydrates on samples taken with the TV-guided grab from Southern Hydrate Ridge. Results of physical and chemical properties of ex situ gas hydrates are discussed in more detail in Chapter 10.4.
Besides the extensive pore water program water samples from the overlying water column of near bottom water were investigated with CTD water samplers, VEnt SamPlers (VESP) (Linke et al., 1994), and samples taken during ROPOS dives. A detailed description of the CTD deployments is given in Chapter 9, preliminary results of VESP operations are given in Chapter 6. ROPOS dives are documented in Chapter 5.

Methods

Sediments
Sediments were taken with piston corers and gravity corers. Surface sediments with almost undisturbed surfaces were taken with a video-guided multicorer.

Pore waters were separated from the sediments by squeezing them in the ship's cold room at 4 °C and 3 atm using argon gas. The types of analyses performed on the pore waters of the cores are listed in Tab. 13a.

CTD, VESP and ROPOS samples
Water samples collected with CTD, VESP or ROPOS were filtered whenever sediment resuspension contaminating the samples was visible. Usually samples were directly analyzed for oxygen, nutrients, chloride and total alkalinity using standard analytical

methods (Tab. 12). A synopsis of water samples (CTD, VESP, ROPOS), numbers, subsampling, and geochemical analysis performed on board is listed in Tab. 13b.

Tab. 12: Techniques used for pore water analyses. For modifications see text.

Constituent	Method	Reference
Alkalinity	Titration	Ivanenkov and Lyakhin (1978)
pH		Dickson (1993)
Ammonium	spectrophotometry	Grasshoff et al. (1983)
Phosphate	autoanalyzer	Grasshoff et al. (1983)
Silicate	spectrophotometer	Grasshoff et al. (1983)
Nitrate	autoanalyzer	Grasshoff et al. (1983)
Chloride	Mohr ($AgNO_3$)titration	Gieskes et al (1991)
Hydrogen sulphide	spectrophotometry	Grasshoff et al. (1983)

Tab. 13a: Number of samples taken from cores and analyses performed[1]

ANALYSIS / STATION	PO_4 [µM]	NO_3 [µM]	NH_4 [µM]	H_2S [mM]	Cl [mM]	TA [mM]	SiO_2 [mM]	pH sedi-ment	core depth [cm]	number of samples
Hydrate Ridge										
Southern summit										
12-1G TV-MUC	x	x	x	x	x	x	x	x	8	9
14-1C TV-MUC	x	x	x	x	x	x	x	x	16	13
19-2H TV-MUC	x	x	x	x	x	x	x	x	19	14
29-1D TV-MUC	x	x	x	x	x	x	x	x	19	14
44-1D TV-MUC	x	x	x	x	x	x	x	x	19	14
51-1B TV-MUC	x	x	x	x	x	x	x	x	16	13
63-1D TV-MUC	x	x	x	(x)[2]	x	x	x	x	13	11
63-1F TV-MUC	x	x	x	(x)[2]	x	x	x	x	19	14
85-1 SL	x	x	x	(x)[2]	x	x	x		209	9
86-1 SL	x	x	x	(x)[2]	x	x	x		248	20
95-1D TV-MUC	x	x	x		x	x	x	x	16	13
105-1 KOL					x			x	234	23
SE Patch										
75-1B TV-MUC	x	x	x	(x)[2]	x	x	x	x	19	14
total of samples										181

[1]for all MUCs oxygen of bottom water was measured (titration)
TA, Cl, Ca, Mg = titration
PO_4, NO_2, NO_3, NH_4 = autoanalyser
H_2S, SiO_2 = spectrophotometer
[2]samples were fixed with zinc acetate and measured in home laboratories

Analytical methods

The analytical techniques used on board to determine the various dissolved constituents are listed in Tab. 12. Modifications of pore water analyses were necessary for samples with high sulphide contents. Different procedures which are briefly summarized in the subsequent section were evaluated during SONNE Cruises 143 (Rickert et al., 1999).

Spectrophotometric methods

Concentrations of dissolved nitrate, nitrite, phosphate and ammonia were determined using an autoanalyser employing standard photometric procedures (Grasshoff et al., 1983). In order to remove the H_2S in samples containing high concentrations of sulphide, 1-5 ml were acidified with 30% suprapure HCl (10 µl/ml sample), and left

Tab. 13b: Water samples taken from CTD, VESP and ROPOS and types of analyses performed[1]

ANALYSIS / STATION	PO_4 [µM]	NO_3 [µM]	NH_4 [µM]	H_2S [mM]	Cl [mM]	TA [mM]	SiO_2 [mM]	Ca [mM]	Mg [mM]	O_2 [mM]	number of samples
Hydrate Ridge											
Northern summit											
34-1 CTD										x	12
42-1 VESP	x	x	x		x	x	x			x	2
47-1 CTD										x	12
48-1 ROPOS	x	x	x		x	x	x			x	4
55-1 VESP	x	x	x		x	x	x			x	3
59-1 CTD										x	11
61-1 CTD										x	13
71-1 CTD											13
97-1 CTD										x	3
Southern summit											
2-1 CTD										x	16
8-1 CTD										x	13
15-1 CTD										x	12
27-1 CTD										x	12
30-1 ROPOS	x	x	x		x	x	x			x	2
36-1 TVG				x	x	x	x				3
40-1 CTD										x	14
54-1 CTD										x	13
57-1 TVG				x	x	x	x				3
58-1 TVG				x	x	x	x				5
66-1 TVG				x	x	x	x				6
72-1 CTD										x	14
74-1 ROPOS										x	2
81-1 ROPOS										x	1
82-1 TVG											12
99-1 TVG											17
SE Knoll											
7-1 CTD										x	11
22-1 CTD										x	11
41-1 ROPOS	x	x	x		x	x	x			x	3
Daisy-Bank											
77-1 CTD										x	8
78-1 CTD										x	9
79-1 CTD										x	11
"R1-structure"											
60-1 ROPOS	x	x	x		x	x	x			x	6
Deep Sea											
87-1 CTD										x	14
									total of samples		291

uncapped for 48 hours in the cold room. An alternative method of sulphide removal involves bubbling nitrogen gas through an acidified aliquot of the sample. Silicate was measured after the elimination of sulphides using the standard manual molybdenum blue method (Grasshoff et al., 1983).
The method for sulphide determination described by Grasshoff et al. (1983) has been adapted for pore waters with sulphide concentrations in millimolar amounts. For reliable and reproducible results, a pore water sample was diluted with oxygen-free artificial sea water (35 g NaCl/1 litre MilliQ) and a zinc acetate gelatine solution, which fixed the sulphide. After dilution, the sulphide concentration should be lower than 50 µM. For example, 8.9 ml of oxygen-free artificial seawater and 1 ml of zinc acetate gelatine solution were added to a 100 µl sample to produce a total dilution of 1:1000.

Titration of Cl
Chloride titration and the precipitation of AgCl is largely affected by H_2S concentrations >> 1 mM through additional Ag_2S precipitation that enhances the amount of total silver nitrate added. Additionally, the reliable detection of the titration endpoint is more difficult to achieve in the presence of black Ag_2S precipitate. Samples should be pretreated with a 1:1 addition of 0.01 N suprapure HNO_3 rather than HCl and degassed overnight in the cold room in open vials.
The subsequent titration with silver nitrate is standardized against IAPSO sea water or a 1:1 dilution of IAPSO sea water for samples containing sulphide.

pH/Total Alkalinity (TA)
pH electrodes were used for the determination of pH at 4°C in the cold room and were calibrated using buffers prepared with artificial seawater (Dickson, 1993). BIS and 2-Aminopyridine were used as buffers in the neutral pH range (pH 7 to 9). The temperature dependent slope and intercept of the electrode were determined from the potential measurements (E) in the two standard buffer solutions for which a pH is defined as a function of temperature and salinity.
In comparison to our pH determinations from the last cruise, samples were stored in closed vials before the measurements were performed almost immediately after core processing in order to avoid elevated pH values due to degassing of CO_2 and H_2S from the sample (Rickert et al., 1999). Additionally pH was determined in the sediment instead of using squeezed pore waters where a loss of CO_2 and H_2S leads to a significant increase in pH (Fig. 49).
Measurements of total alkalinity were made by direct titration of 1 ml of pore water with 0.02 N HCl in an open cell (Ivanenkov and Lyakhin, 1978). This method is especially suited for samples containing H_2S and high TA values as CO_2 and H_2S are removed during the titration by a continuous stream of pure argon through samples and standards. A mixture of methylene blue and methyl red was used as indicator and the titration was completed when the yellow-green colour of the solution turned light pink (pH at the end point is 5.4-5.5). During this expedition, the time lag between pore water squeezing and alkalinity determination was shortened in comparison to our previous expeditions (SO 143). Total alkalinity (TA) of anoxic samples was determined within less than 2 hours after pore water retrieval this cruise since the data from Wallmann et al. (1999) imply that up to 10 % of the total alkalinity might be lost during that time span.

Home laboratory analyses
Acidified subsamples (10 µl/ml sample) were prepared for ICP analyses (Na, K, Li, Mg, Ca, Sr and Mn). Subsamples of pore water for sulphate, DIC and $\partial^{13}C$ of $\sum CO_2$ as well as $\partial^{18}O$ and ∂D determinations were taken and subsets will be analyzed in the shore-

based laboratory. Sediment squeeze cakes will be used for C,N,S, and $CaCO_3$ determinations with a Carlo Erba Element Analyser.

Results and Discussions

Altogether, 10 multicores (TV-MUC), 2 gravity cores (SL) and 1 piston core (KOL) were recovered and pore waters analyzed for their constituents. A summary of cores, amount and distribution of samples as well as geochemical analyses performed on board is given in Tab. 14. Selected depth profiles of chemical constituents in pore waters are illustrated in Fig. 44 & 45 and described in the following section.

Sulphide gradients and related vent fauna
Hydrates are rapidly dissolved by methane-poor sea water due to their high solubility (~ 10-100 mM, Egeberg and Dickens, 1999; Egorov et al., 1999). The released methane is oxidized by aerobic and anaerobic bacteria and the reaction products induce a series of redox and precipitation processes. The main biogeochemical reactions at surface-near hydrate deposits occur in the following sequence (e.g., Wallmann et al., 1997; Boetius et al., 2000):

(1) methane release at the gas hydrate surface

$$CH_4 \bullet H_2O(s) \rightarrow CH_4 + H_2O$$

(2) anaerobic methane oxidation in adjacent anoxic sediments

$$CH_4 + SO_4^{2-} \rightarrow HCO_3^- + HS^- + H_2O$$

(3) carbonate precipitation induced by the production of carbonate alkalinity during anaerobic methane oxidation

$$Ca^{2+} + 2HCO_3^- \rightarrow CaCO_3(s) + CO_2 + H_2O$$

(4) pyrite formation caused by sulfide released during anaerobic methane formation

$$2FeOOH + 2HS^- + 4H^+ \rightarrow FeS_2(s) + Fe^{2+} + +4H_2O$$

(5) oxidation of released sulfide with nitrate and oxygen in suboxic and oxic surface sediments as well as in benthic macrofauna bearing endosymbiotic bacteria

$$HS^- + 2O_2 \rightarrow SO_4^{2-} + H^+$$
$$HS^- + 8/5NO_3^- + 3/5H^+ \rightarrow SO_4^{2-} + 4/5N_2 + 4/5H_2O$$

Video surveys and biological sampling revealed a clear zoning around outcropping gas hydrates (Bohrmann et al., 2000). On top of these hydrates and in the immediate vicinity, bacterial mats are abundant and composed primarily of sulfide oxidizing *Beggiatoa* sp. (Boetius et al., 2000). In the surrounding areas, *Calyptogena* sp. communities are dominant followed by an extended zone with abundant *Acharax* sp. The composition of pore waters is strongly correlated with the composition of the vent fauna (Fig. 45).

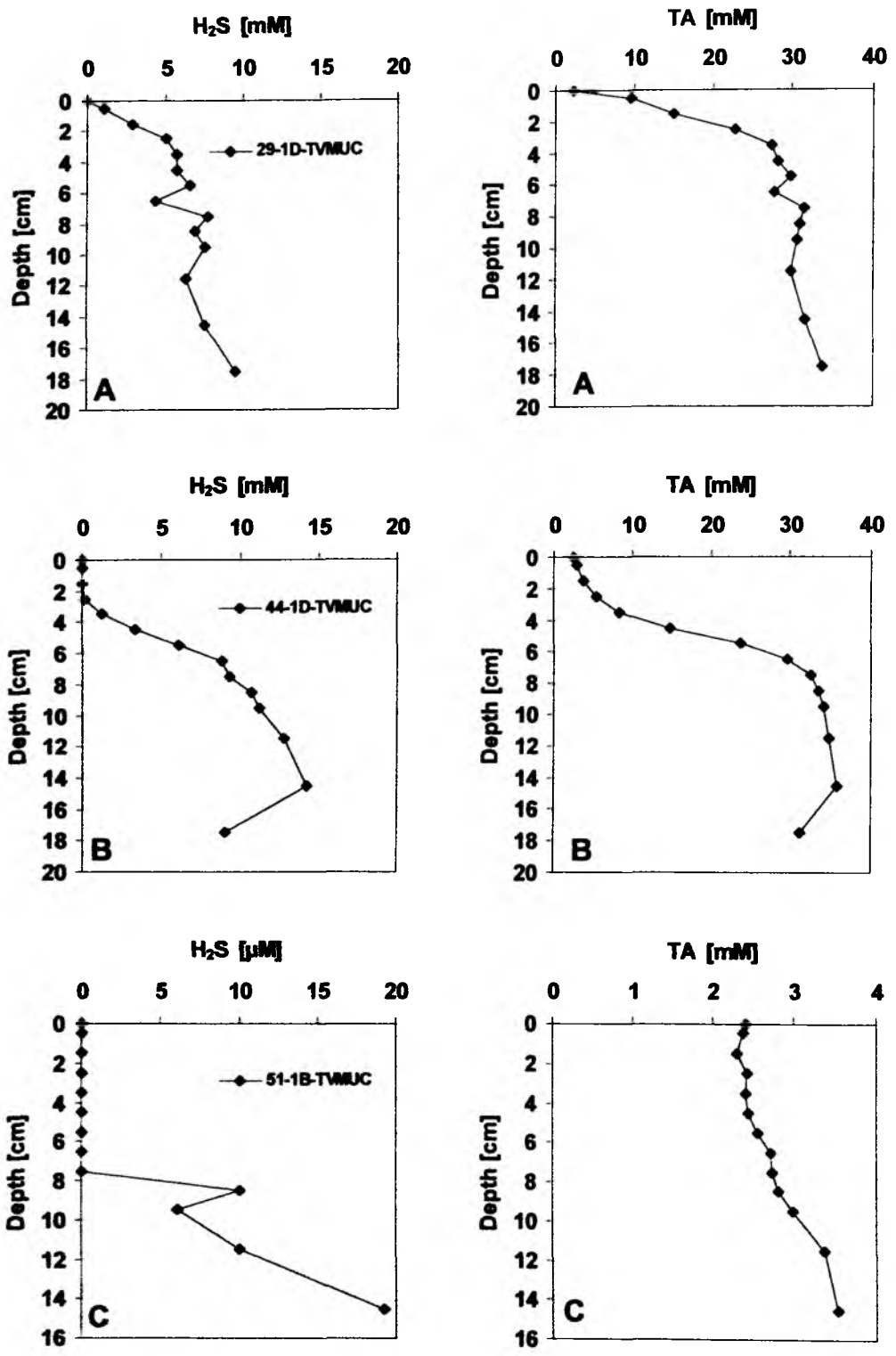

Fig. 45: Depth profiles of H_2S and TA in relation to overlying bacterial mats (A), *Calyptogena* sp. communities (B) and *Acharax* sp. (C) or methane discharge of different extent. Note the different penetration depths of H_2S as well as different concentration units for H_2S.

The lowest sulfide concentrations are found in sediments populated by *Acharax* sp. As these large clams live as in-fauna digging and ventilating extended burrows down to sediment depth of approximately 1 m, the low sulfide contents could either be produced by ventilation (bioirrigation) or could indicate a low supply of methane from deeper layer. The sulfide contents are significantly higher below *Calyptogena* sp. colonies. These clams live within the top 10 cm of the surface sediment and only affect the upper layers by bioirrigation and sulfide oxidation. Finally, the highest sulfide concentrations were detected below bacterial mats that are confined to the sediment-water interface. Possibly, the biological zoning reflects the thickness of the sedimentary veneer covering the underlying gas hydrates that increases from bacterial mats to *Acharax* sp. In turn, the location of hydrate deposits within the surface sediments could also be controlled by the biological populations or by the methane supply from deeper strata. As a direct consequence of methane oxidation hydrogen carbonate concentrations increase with depth according to Equation 3 (Fig. 45).
A better understanding of microbiological processes responsible for both production of the methane in hydrate deposits and removal of methane via anaerobic oxidation, requires improved knowledge of processes in the sulfate reduction zone, identifiaction of the class of microbes responsible for methanogenesis and oxidation, and research on associated biomarkers.

Nitrate-Storing *Beggiatoa* sp. in Bacterial Mats

Anomalously high nitrate concentrations (up to 3 mmol/l) in pore waters derived from squeezed sediments recovered below bacterial mats extended from a few millimetres above the surface to 3-4 cm below the surface (Fig. 46). An approximately two orders of magnitude increase in nitrate concentration compared to a reference location on Southern Hydrate Rdige (095-1B-TVMC) was determined. Phosphate, ammonia, and silicic acid concentrations in the first sediment segments were also elevated compared to the reference location reflecting the presence of bacteria which are confined to the sediment-water interface. The bacterial mats are believed to consist of *Beggiatoa* sp. (Bohrmann et al., 2000; Boetius et al., 2000). During this cruise, H. Sahling (Chapter 11) observed bacteria during ROPOS dive 570 which are likely *Thioploca* sp. This observation, however, needs further microbial investigations. Either bacteria sp. are able to store and use nitrate to oxidize the sulfide, as it was observed for other large, vent-forming bacteria in upwelling areas (e.g. Gallardo, 1977; Jannasch et al., 1989; Jørgensen, 1977; Fossing et al., 1995; Schulz et al., 1999). In order to use nitrate as a tracer for the biomass of nitrate-storing bacteria, nitrate concentrations measured after squeezing the sediment needed to be more seriously evaluated since the extent of destruction of bacteria cells, hence, nitrate release in the pore water is critically dependent on the squeezing technique used. Therefore, we first determined the time needed to completely destroy pure bacteria cells in a salt solution using ultrasonic treatment and ice cooling (see Chapter 11). After approximately 30 minutes the nitrate concentration in the solution remained constant indicating that the cells were completely destroyed. The nitrate concentrations in the vacuoles varied between 50-500 mM/vacuole of the cells (Tab. 9 in Chapter 11).
This ultrasonic treatment was also applied for the sediments which were subsampled in centrifuging tubes. After pretreatment a centrifuge was used to extract the pore water from the sediments instead of using the squeezing technique. Nitrate, however, could not be detected in pore water of ultrasonically treated and centrifuged sediment samples. Obviously ultrasonics is not able to completely destruct the bacteria cells surrounded by sediment particles. In home laboratories further improvements or alternatives to completely extract nitrate from the cells will be examined.

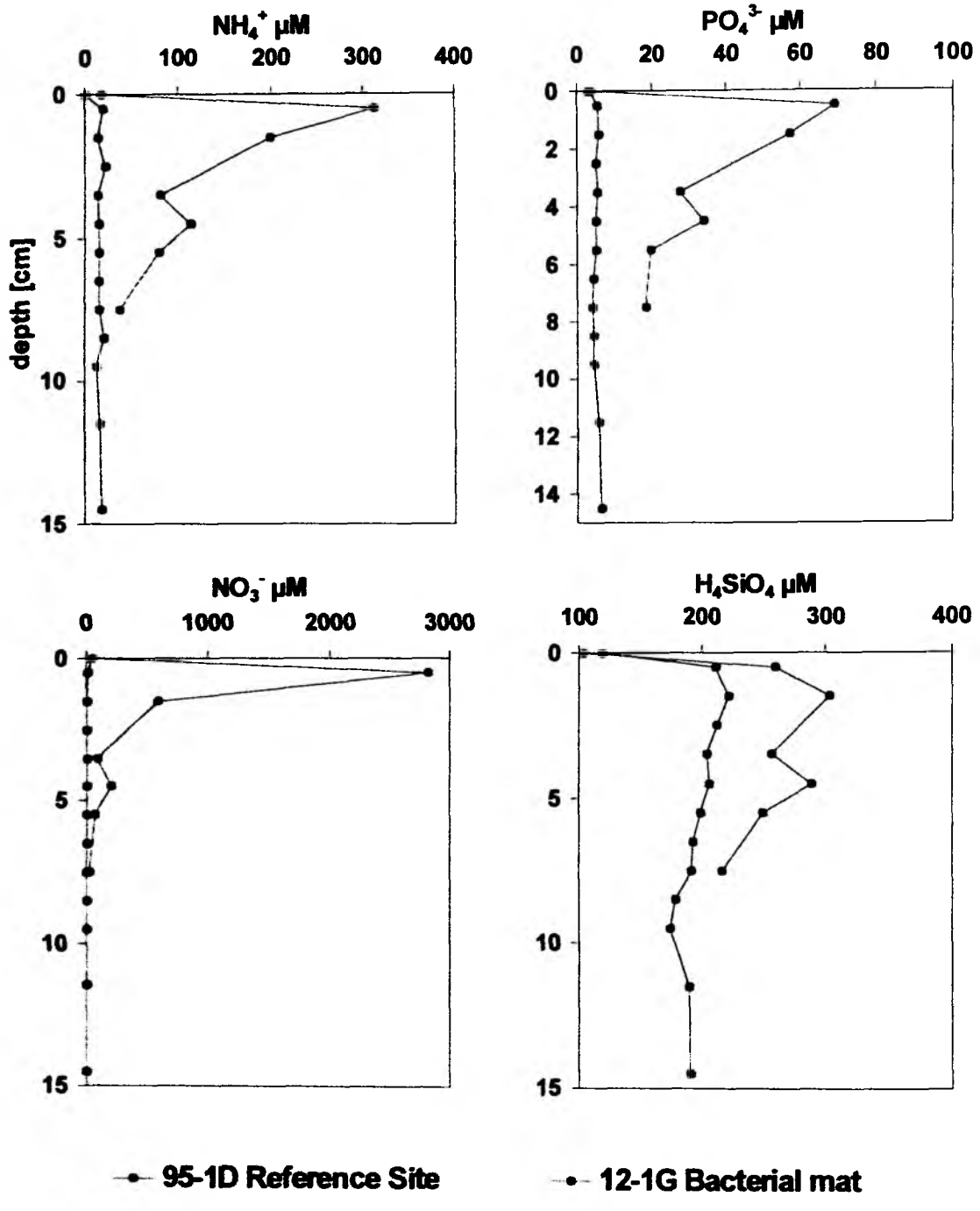

Fig. 46: Pore water chemistry of 95-1D-TVMC (reference site) and 12-1D-TVMC (bacterial mat site). Squeezing of bacteria during core processing causes anomalies in all nutrient contents. A quantitative estimate of these anomalies in particular those of nitrate may be useful to quantify the biomass of bacteria in the sediment (see Chapter 11).

Salt anomalies related to gas hydrate formation

The composition of fluids associated with gas hydrates is strongly affected by hydrate formation and in turn controls the stability and formation rate of hydrates. Thus, the pore water surrounding massive layers of gas hydrate recovered at Hydrate Ridge show variable degrees of salt exclusion (positive chloride anomalies in Fig. 47).

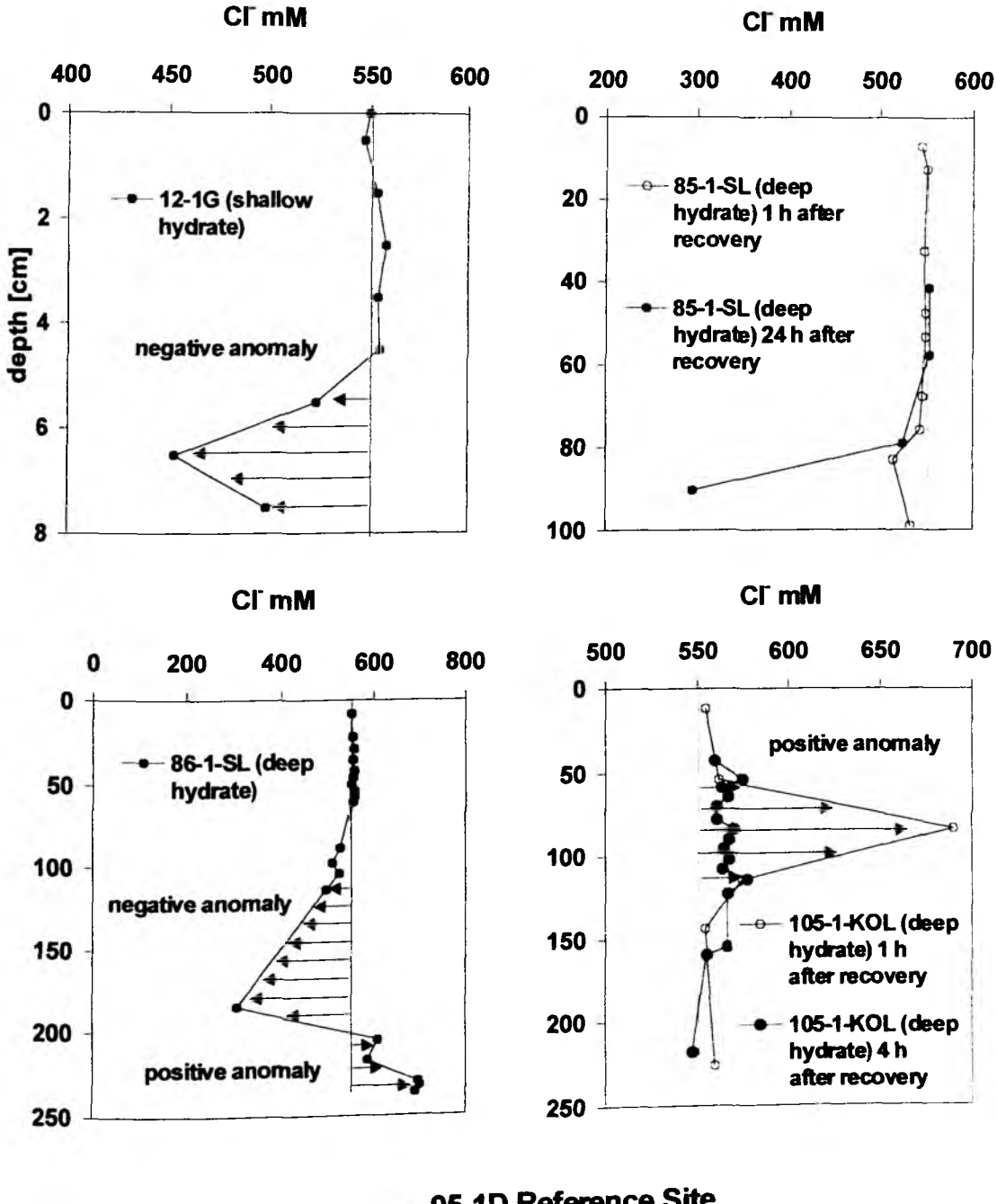

Fig. 47: Chloride concentrations in 4 sediment cores taken at Hydrate Ridge. Low concentrations are an artifact induced through gas hydrate dissociation after core retrieval, whereas high concentrations reflect the true conditions and indicate salt exclusion during hydrate formation. 85-1-SL and 105-1-KOL were sampled twice to monitor the dilution of pore water after 1 h of core recovery and complete dissociation of gas hydrates.

An increase in salinity was observed in all contact zones of pore water and hydrate, where it was possible to separate the hydrate layers *immediately* from the sediment before dissociation could commence. Samples separated in that way showed chloride concentrations up to 700 mM (86-1-SL & 105-1-KOL). The magnitude of salt-enrichment is about 1.5 times the seawater salinity and somewhat lower than observed on SO143/1b cruise (Rickert et al., 1999; Suess et al., in press). Contracting the stability field of hydrate under constant P-T-conditions through salt exclusion (Sloan Jr., 1998) could lead to dissociation of hydrate at depth intervals where otherwise gas hydrates would be stable. Such a negative feed-back mechanism could limit the formation rates and the abundance of gas hydrates. More specifically, it may cause hydrate-free layers sandwiched between hydrate-bearing zones, a mechanism explaining the double-BSRs (Mienert and Posewang, 1997). Furthermore, modeling the salinity profile could yield a time constraint on the formation and destruction of hydrates that could be used to decipher the dynamics of near-surface hydrates (Rickert et al, in prep.). The salt enrichments observed at Hydrate Ridge may be comparable to brine formation through build-up of sea-ice. That mechanism has been studied at high latitudes and leads to the precipitation of a well-studied sequence of evaporite minerals (Sonnenfeld, 1984). This sequence is determined by the mineral solubility and usually starts with the precipitation of calcium carbonates. Interestingly, near-surface gas hydrates are always associated with $CaCO_3$ precipitates (Bohrmann et al., 1998). It is possible that brine formation plays a key role in the genesis of these characteristic minerals. Undisturbed hydrate samples from the seafloor recovered with the proposed autoclave technology could yield other evaporite minerals such as halite and late state potassium minerals that could be used to decipher the conditions and mechanisms of hydrate formation.
In most samples, however, negative anomalies, i.e. Cl concentrations lower than those observed in pore waters of the reference locations on Hydrate Ridge (e.g. 95-1D-TVMC) were observed due to the dissociation of gas hydrates and release of fresh water which dilutes the pore water during core recovery (12-1G-TVMC; 85-1-SL; 86-1-SL). Although quantification of gas hydrate abundance from negative chloride anomalies is conceptually simple (e.g., Hesse and Harrison, 1981; Suess et al., in prep.), the method is not straightforward because

1. *in situ* pore water chemistry prior to gas hydrate dissociation is unknown. Estimates of gas hydrates made by this method, therefore, are entirely dependent on assumed *in situ* concentrations of Cl-, commonly assumed similar to that of seawater (e.g., Kvenvolden and Kastner, 1990; Froelich et al., 1995; Kastner et al., 1995; Yuan et al., 1996)
2. such an assumption neglects *in situ* advection and diffusion of excluded ions and results in overestimation of gas hydrate abundance (Ussler and Paull, 1995)
3. estimates depend critically on the extent of gas hydrate dissociation. This is illustrated in Fig. 46 for cores 85-1-SL and 105-1-KOL. Depending on the time-span between core recovery and squeezing chloride anomalies vary from positive anomaly (105-1-KOL) to negative anomalies with various extents (85-1-SL).

From the degree of Cl-dilution 1h after recovery (Cl ~ 510 mM) it can be estimated that ~ 5 Vol.% of the sediment in the depth interval 82-84 cm consists of gas hydrate. Using the value measured 4 h after recovery, i.e. ~ 290 mM for depth interval 87-94 cm, ~50 Vol.% gashydrate can be estimated. Hereby it is assumed that the total porosity including the volume of interstitial water of the sediment plus a variable volume of solid hydrate is almost constant (~ 0.6) and that the *in situ* chloride concentration equals that of sea water (~ 551 mM at Hydrate Ridge). A more rigorous estimate requires the exact porosity values as well as the *in situ* value of chloride in addition to an estimation of

respective transport processes. It is possible that the *in situ* value of chloride might even exceed those of 700-800 mM measured this and on previous cruises (Rickert et al., 1999; Suess et al., in press). This will enable us to better quantify the volume of hydrate in these sediments.

pH in Pore Water vs. Sediment

Replicate measurements of pore water samples over a time span of several hours revealed that the total alkalinity of anoxic pore water samples is not constant but decreases in time (Wallmann et al., 1999). The two most important reactions that cause alkalinity reduction are carbonate precipitation and sulfide oxidation. Carbonate precipitation is induced by a loss of CO_2 and H_2S from the pore waters to the atmosphere and the resulting shift in the dissolution/precipitation equilibrium:

$$Ca^{2+} + HCO_3^- \rightarrow CaCO_3(s)\downarrow + CO_2(g)\uparrow + H_2O$$

In contact with air, sulfide is oxidized by molecular oxygen:

$$HS^- + 2O_2 \rightarrow SO_4^{2-} + H^+$$

Both the decrease in dissolved HS- and the production of H+ significantly reduce the total alkalinity. The sulfide oxidation rate and its impact on total alkalinity were tested on board using a 30 mM solution of Na_2S in 0.5 M NaCl (Wallmann et al., 1999). The initial pH was adjusted to 7.1 with concentrated HCl and the solution was titrated repeatedly at room temperature (24 - 25°C). The data depicted in Fig. 47 clearly show that the total alkalinity is significantly reduced within a few hours. The simultaneous increase in pH indicates that the H_2S loss to the atmosphere proceeds more rapidly than the oxidation reaction.

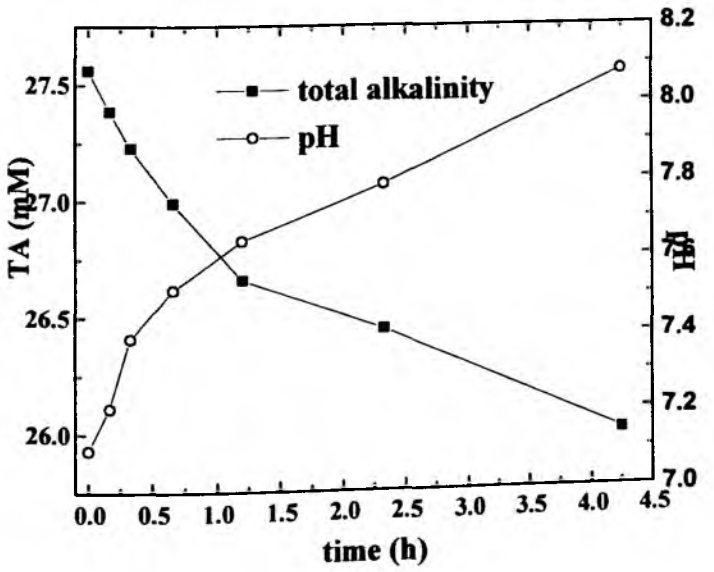

Fig. 48: Oxidation of a sulfide solution (~30 mM (H_2S in 0.5 M NaCl) in contact with air at room temperature (Wallmann et al., 1999).

During the GELOVANY 99 expedition (Wallmann et al., 1999), total alkalinity of anoxic samples was determined within two hours after pore water retrieval. The data in Fig. 48 imply that up to 10 % of the total alkalinity might be lost during this short time interval. As the samples were stored at 4°C, the oxidation reaction probably proceeded at a lower rate, so that the real loss was somewhat lower than implied by the experimental data obtained at room temperature.
During SO148 expeditions, the time lag between pore water squeezing and alkalinity determination was considerably shortened in comparison to our previous cruise (SO143; GELOVANY 99) Results, however do not indicate significant differences (see also Rickert et al., 1999). Maximum alkalinity values in the range of 30-35 mM were determined in both cruises. As the samples were stored at 4°C, the oxidation reaction probably proceeded at a lower rate. pH and total alkalinity values along with total sulfide, boron, sulfate, silica, and phosphate concentrations are used to determine the total inorganic carbon concentrations in pore water samples. For this determination the accuracy of both determinations is of prime importance. Therefore pH determinations were performed exclusively in sediment samples during this cruise instead of using pore water samples. The duration of the potential measurements from which pH was calculated using BIS and AMPY (see methods) was reduced from 15 to 5 minutes during this cruise. Moreover, the subsamples were only briefly stored in closed vials before the pH was determined to minimize degassing of CO_2 and H_2S. Throughout our pH determinations in highly anoxic samples the pH was significantly lower than on the last cruise. In Fig. 49 the consequence of changing pH for the calculation of total CO_2 ($\_CO_2$) is illustrated.

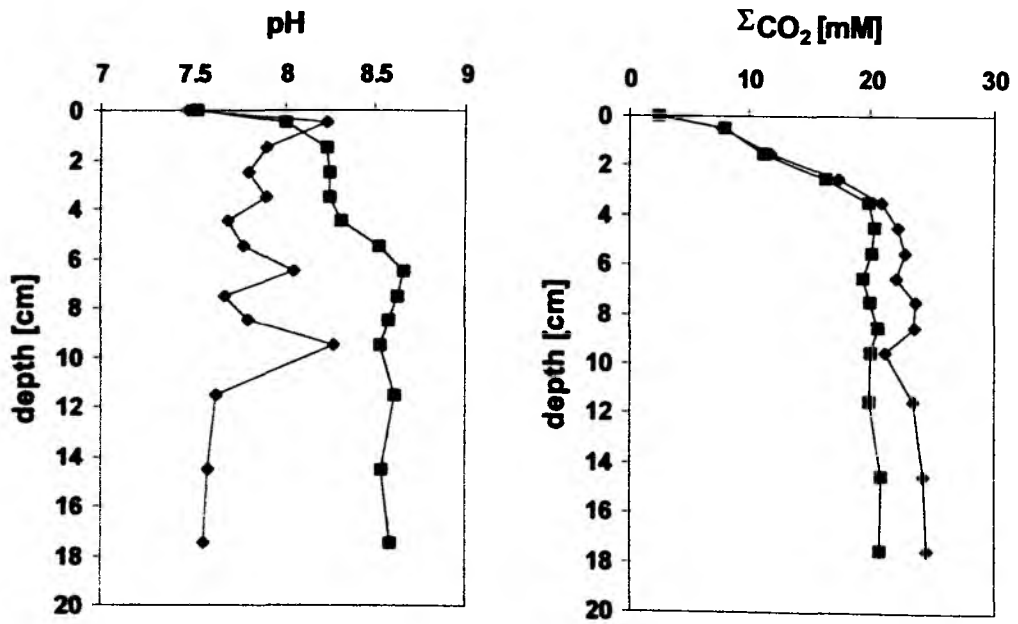

• 29-1D (pH in sediment; SO-148/1)

▪ 105-2F (pH in pore water; SO-143/2)

Fig. 49: Comparison of calculated total CO_2 ($\sum CO_2$) values as a function of pH measured either in sediment or in pore water in sediments underlying bacterial mats.

For a bacterial mat site core 29-1D (SO148/1) and 105-2F (SO143/2) were chosen. We calculated total CO_2 concentration with values of total alkalinity, sulfide, boron, sulfate, silica, phosphate, and ammonia measured for 29-1D and used pH values determined for 29-1D in the sediment and 105-2F in the pore water. H^+ values differ by almost one order of magnitude. Total CO_2 concentrations show variations of up to 5 mM among the cores. The higher the pH the lower is the P_{CO2} value. Thus saturation with respect to calcite and aragonite decreases.

Summarizing these and previous investigations (Wallmann et al., 1999) we recommend to shorten the time lag between core recovery, pore water squeezing and alkalinity or pH determination to minimize artifacts resulting from ex situ degassing of CO_2 and H_2S.

13.2 Methane and Ethane in Sediment Cores

K. Heeschen, A. Voorhees

Objectives

TECFLUX'99 investigations showed a high variability for CH_4 concentrations and other pore water species among samples taken a few meters apart, and even within a single multicorer deployment. Possible explanations include diffusive flow versus locally concentrated venting along faults, gas hydrate occurrence, and different biological communities. Therefore, one of the main goals of the TECFLUX'2000 investigation was to take samples for pore water chemistry and methane measurements from the same core. In addition, the headspace samples taken this year were analyzed for both, methane and ethane. For the locations of the cores see Tab. 7, for those analyzed for hydrocarbons see Tab. 14. Chosen were multicores from sites with different biological communities at Southern Hydrate Ridge and one core from a zone of high reflectivity in the side-scan sonar from the E-Basin. In addition one deep core from both locations was sampled for hydrocarbons.

Method and Sampling

Two different methods were used for measuring the methane content of sediment samples. In both cases samples for the analysis of the gases were taken first. For the onboard methane measurement, 3 ml of sediment were taken in syringes from the same core as all pore water chemistry samples. The sediment was then extruded into 20-ml vials and mixed into a slurry with 5 ml of 1 M KOH for faster equilibration and to avoid biological activity. The vials were immediately sealed with black rubber stoppers and crimped tightly (so called headspace analysis). In order to establish equilibrium between the slurry and the gas phase the vials were shaken for 24 - 48 hours. 100 µl subsamples of the gas phase were taken with gas tight syringes and detected using a gas chromatograph (Shimadzu) equipped with a flame ionization detector (FID). Recalculation from nl/ml sediment to nl/g or nmol/g sediment will be performed after the determination of physical properties on shore. The standards used where 10100 ppm CH_4 and 100 ppm C_2H_6, 1002 ppm CH_4 and 10 ppm CH_4.

At some cores (see Tab. 14) 150 g of sediment were taken and put into Zip-lock bags stored in liquid nitrogen for degassing on shore. The gas will be taken to measure the methane content and the stable carbon isotopic ratio in CH_4 using a Gas Chromatography-Combustion-Isotope Ratio Mass Spectrometry (GC-IR-MS).

To minimize mixing effects in the core liner, only cores without visible degassing were taken. The same criteria were used for sampling the bottom water from the multicorer (TV-MUC). The bottom water was sampled with glass syringes, which were also used for the water column sampling from the rosette (for methods see Chapter 9). The water samples were taken before the cores were removed from the instrument to avoid mixing between sediment and water. Methane concentrations in sediments and bottom water were determined on the multicores listed in Tab. 14:

Tab. 14: Sediment samples taken for the determination of methane concentrations and $\partial^{13}C_{CH_4}$.

Station no.	Core No.	Bottom water sample	# of headspace analysis	Location
14-1 TV-MUC	C	x, core C	12	bacterial mats at SHR
19-2 TV-MUC	H	x, core G	13	transition between *Calyptogena* sp. field and bacterial mats, SHR
29-1 TV-MUC	D	non	samples taken for isotope analysis	
44-1 TV-MUC	D	x, core C	12	*Calyptogena* sp. field at Southern Hydrate Ridge
75-1 TV-MUC	B	x, core D	13	bacterial mats at site of high reflectivty in the E-Basin
76-1 SL			samples taken for isotope analysis	site of high reflectivity in the E-Basin
86-1 SL			9	Southern Hydrate Ridge
105-1 KL			6	Southern Hydrate Ridge

Preliminary Results

Methane profiles from the multicores are shown in Fig. 50. Like last year (Bohrmann et al., 2000) the sediments underlying bacterial mats showed the steepest rise (14-1 TV-MUC), whereas in sediments underneath *Calyptogena* sp. fields the methane concentration did not increase noticeably above 7 cm depth (44-1 TV-MUC). The core taken in the transition zone between bacterial mats and a *Calyptogena* sp. field at Southern Hydrate Ridge (19-1 TV-MUC) showed intermediate methane values in the upper 7 cm. The profile of a core from the E-Basin patch (75-1 TV-MUC) with a small bacterial community at the surface showed about the same shape and concentration for methane in the upper 10 cm as core 19-1 TV-MUC. However, the ethane values were

substantially different. The ethane values at the head of the E-Basin patch were as low as those of the *Calyptogena* sp. site at Southern Hydrate Ridge, but stayed low with increasing depth. The sediments of the transition site showed the highest amounts of ethane below 3 cm. Ethane profiles from the transition zone and the bacterial mat site showed similar gradients in the upper 3 cm, although the transition zones gradient is shifted by 1 cm. Relating to their ethane concentrations below the depth influenced by the biological community only the 3 cores from Southern Hydrate Ridge could be grouped together. The core from the E-Basin patch showed distinctly lower C_2H_6 values. These 2 groups were even more obvious in the C1/C2 ratio shown in Fig. 50, with values of up to 1800 for 75-1TV-MUC and ratios below 500 for Southern Hydrate Ridge. In the upper 6 cm, the cores from the bacterial mat at Southern Hydrate Ridge and the E-Basin patch showed equal distributions. The decline for methane as well as ethane in the deepest samples taken at each core probably were due to degassing while sampling and thus were an artifact.

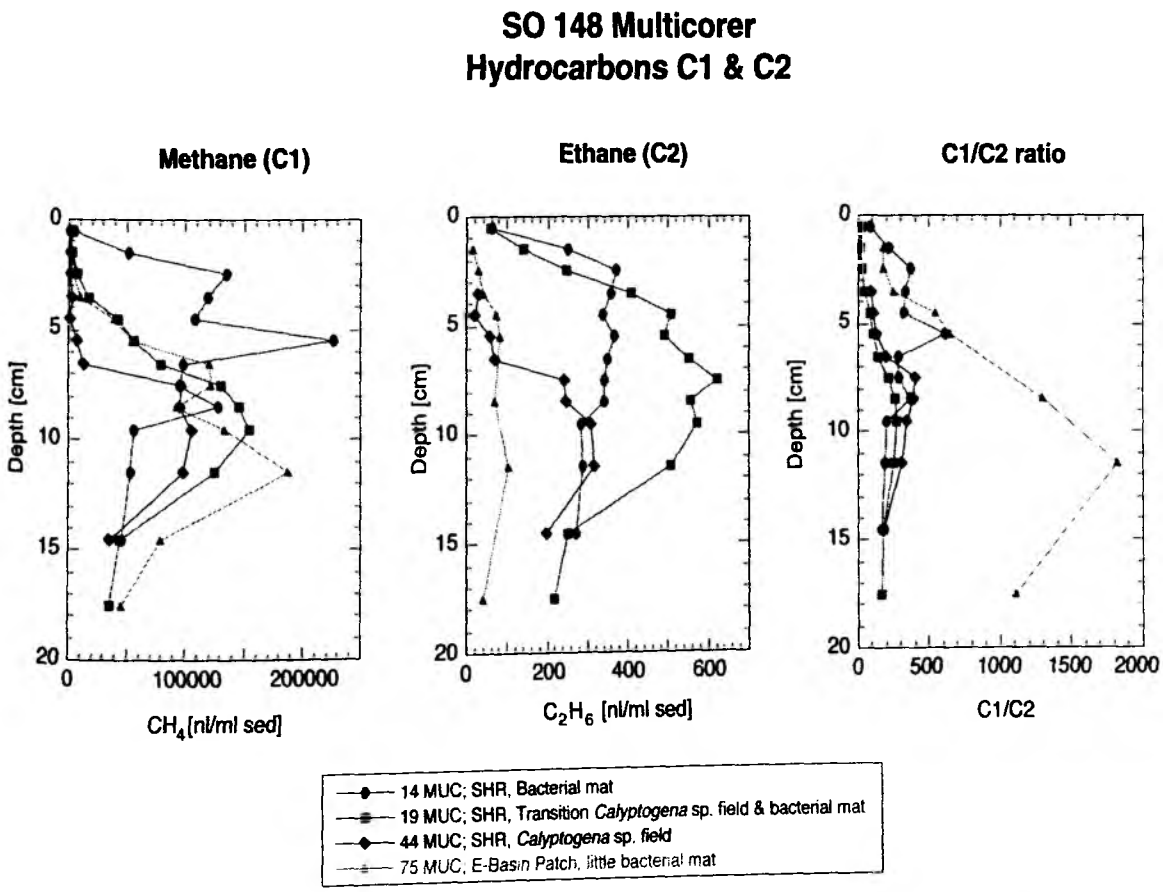

Fig. 50: Concentrations of methane and ethane as well as their ratio in multicores from different settings.

The C1/C2(+C3) ratio is known to be a good indicator to distinguish between biogenic and thermogenic sources. The ratio for the former typically is 10^3 to 10^5, whereas the latter shows ratios below 50 (Gamo et al., 1992). Thus 75-1 TV-MUC may be of biogenic origin and the cores from Southern Hydrate Ridge reveal a mixture of thermogenic and biogenic sources, similar to ODP cores at Hydrate Ridge (Kastner et al., 1998). However, the preferential oxidation of methane also leads to lower C1/C2 (+C3) ratios (Gamo et al., 1992; Whiticar, 1999). Lower C1/C2 ratio (as low as 20; 19-2 TV-MUC) in

the upper core, where the oxidation should be highest, support this idea. Gamo et al. (1992) showed a positive correlation between CH_4 concentrations and C1/C2 ratios, and consequently favored preferential methane oxidation over thermogenic origin to explain the low C1/C2 ratios. Their sediment samples were collected from a cold seepage zone in the Nankai Trough. The correlation between CH_4 values and C1/C2 ratios was also found for the SO148 TV-MUC data discussed here (R= 0.7). Within the core from E-Basin with higher C1/C2 ratios would be less oxidized than those from Southern Hydrate Ridge. Since, unlike the oxidation rate, the measured methane concentrations are about the same, the source gas at the Eastern Basin had a higher C1/C2 ratio to start with or the source at Southern Hydrate Ridge could be bigger. However, the occurrence of gas hydrate at Hydrate Ridge as well as E-Basin could also alternate the C1/C2 ratio, since the gas hydrates stored high amounts of methane. The one of E-Basin is less solid than that from Hydrate Ridge – which was observed in the deep coring. A stronger decomposition of gas hydrates during recovery could have increased the C1/C2 in these samples, too.

The two deep cores on SO148 sampled for methane at Southern Hydrate Ridge reveal higher concentrations than the short cores from the multicorer (TV-MUC). The highest concentrations should indicate a gas hydrate zone. Within this zone the C1/C2 ratio is elevated by 400, which was probablay due to gas hydrate decomposition during recovering. The determination of CH_4 and C_2H_6 and the C1/C2 ratio in core 76-1 SL from the patch of high reflectivity in the E-Basin will be done on shore.

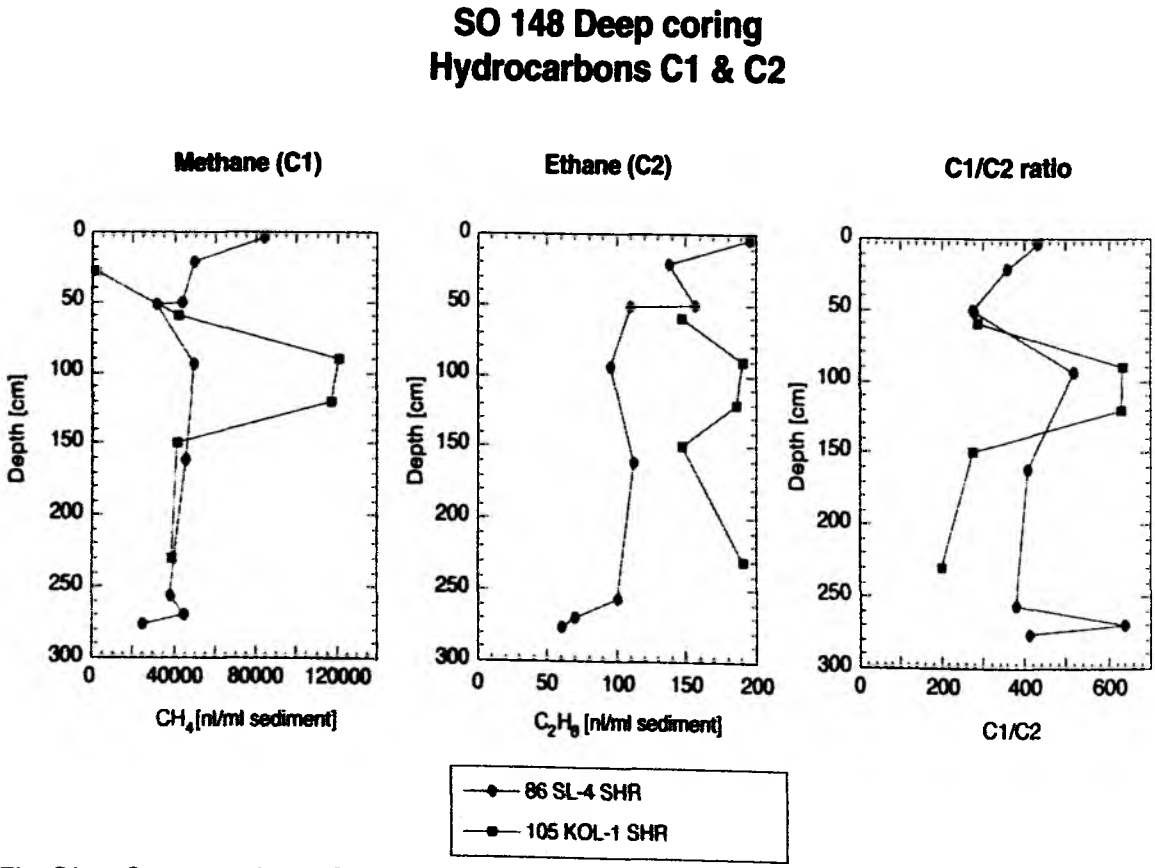

Fig. 51: Concentrations of methane and ethane and their ratio in cores from the SO148 deep coring program.

To compare the 4 bottom water samples with the sediment samples, the concentration of both needs to be recalculated into nmol/L. Highest concentrations were found in the bottom water of core 19-1 with 47900 ppm CH_4 and 87.06 ppm C_2H_6. The C1/C2 ratio of 551 reflects what was found deeper in the sediment core. Hence pumping of bottom water into the core is not a reason for lower C1/C2 ratios in the upper cm of the cores. The same is true for the bottom water of 14-1 TV-MUC with 7821 ppm CH_4 and 51.21 ppm C_2H_6 (C1/C2: 418). The water from 44-1 TV-MUC, collected at a *Calyptogena* sp. field, showed intermediate CH_4 concentration (927 ppm). C_2H_6 was not determined. The sample from E-Basin only showed 49.96 ppm CH_4 and no C_2H_6, which is not found to be typical for bottom water overlying bacterial mats at Southern Hydrate Ridge. Since the shape of the sediment profile for methane was not typical for those areas, either, the bacterial mat community probably was rather small and influences from other processes might have been stronger.

14 AUTOCLAVE TOOLS

14.1 Autoclave piston corer (AKL)

H. Kudrass

The autoclave piston corer (AKL) was lost during its first employment during the SONNE Cruise 143 in 788 m water depth on the Southern Hydrate Ridge (44°34,12 'N, 125°08,86'W) on 30 August 1999. The 5 m long version of the corer had penetrated by about 3 m into the gashydrate bearing sediments. During the pull-out, the wire connecting the piston of the AKL to the ship's wire was unexpectedly torn out from its socket at a tension of 5 tonnes and the AKL had to be left at the seafloor. The relatively high pull-out forces were thought to be caused by the injection of sea water through the penetrating core barrel into sediment with free methane and consequent freezing of the core barrel by formation of gashydrate. The corer was inspected with the OFOS and TV-grab and was found stuck in a vertical position. A recovery by a chain loop attached to the TV-grab failed. Therefore it was planned to recover the prototype from the seafloor during SONNE cruise 148 using ROPOS.

ROPOS dives during the first leg of SO148 had observed the AKL and had found that the corer was almost lying at the seafloor with the core barrel almost completely covered by mud. The salvage of the AKL was done in three carefully prepared steps on 7 August starting at 6:00 am.

During the first step, a 22 m thick and 1200 m long steel wire was hooked to a 500 kg dummy weight, which was lowered to the position of the lost instrument. The wire was then fed out by slowly moving the ship in northern direction, thus laying the wire in several slings at the seafloor. The end of the wire was then connected to a nylon rope (Meteorleine) and by moving the ship further to the north the 850 m long rope was fed out thus lowering the end of the steel wire to the seafloor. The end of the rope was attached to a surface buoy. This part of the operation took a period of about 4 hours.

During the next step, the ROPOS was lowered to the position of the AKL with a basket containing a 100 m long spectra rope attached to the cage of the ROPOS. We first inspected the distance of the AKL to the dummy weight at the end of the steel wire. As the distance between the weight and the AKL was much less than 100 m, we could deploy the basket with the rope between the AKL and the dummy weight. Then the ROV took the carabiner hooks attached to both ends of the rope and hooked them in a large loop of the steel wire at the dummy weight and to the AKL top end. This operation took about five hours. The ROPOS spend then another hour to inspect the time-lapse camera before returning to the ship.

During the final step, the ship took the end of the Meteorleine at the buoy, heaved the end of the steel wire to the deck, attached the steel wire to the main winch (W 6) and lifted the AKL from the seafloor. Twisted turns in the first one hundred meter of the steel wire caused much work at the deck. The final recovery from the seafloor was relatively easy and maximum pull out force was only about 3.5 tonnes, much less than the abnormal pull - out forces during the loss in 1999. This part of the operation lasted 3 hours and the successful salvage of the AKL was finished at 6:37 pm.

During the last 10 meters before reaching the sea surface bubbling of gas was observed from the AKL. Except some unprotected iron parts of hydraulic houses and wires the corer was well preserved. Both valves of the pressure chamber were closed, the top end

by the piston and the base end by the conical valve. The pressure chamber contained the 5 m - long core liner with a 2-3 m long core containing two layers of 5 cm - and 10 cm - thick gas hydrate.

Generally the AKL has performed according to expectations and the prototype seems to be a reasonable tool for coring and preserving gashydrate from the seafloor with *in situ* pressure and temperature conditions. Some details, however, have to be amended. Simple tools have to be developed to easily recover the core liner from the pressure chamber. The release mechanism for the core barrel is difficult to remove, which is necessary to remove the core liner on deck. Therefore the connection between release - pressure chamber has to be redesigned and reconstructed. Furthermore, stainless steel has to replace several small parts which were heavily corroded.

14.2 Pressure Conservation Mechanism (PCM)

G. Hohenberg

Synopsis

Gas hydrates collected with the aid of autoclave samplers, e. g. with a piston corer, have to be stored at constant pressure and temperature for several weeks or months to guarantee their analysis and evaluation in laboratories aboard the research vessel or on land under autochthonous conditions. Previous experiences gained with the storage of gas hydrates under low temperature and high pressure during the SONNE Leg 143-3 had the following consequences:

After some months of storage under *in situ* conditions, i. e. with a temperature of about 2 to 4 °C and a pressure of 100 bar in sea water, the autochthonous gas hydrate was conserved only at a very limited scale. It has to be assumed that a large amount of the methane from the hydrates was dissolved in the ambient sea water, although not in total. This can be concluded from the tests being performed aboard the research vessel this year. Gas hydrates in contact with water disintegrate very rapidly when the pressure is released – contrary to gas (endothermic dissociation with a big thermal capacity of the water). After opening the pressure mechanism this was observed for several minutes leading to the conclusion that as a consequence of the opening and the following pressure release a large amount of the sampled gas hydrates had disintegrated. This was especially kept in mind during the SONNE Leg 148-2. Here, in two subsequent tests with different methods the storage of gas hydrates was investigated.

A. The storage of gas hydrates in a pressure tank after dissolving external methane bubbles rising in sea water within a period of 24 hours.

- The water after being treated in this kind was filled against a pressure of 17 bar into the pressure tank No 1 to the sampled gas hydrates that had to be stored and conserved. Then the pressure was increased to 80 bar.

Test Procedure

- On August 5th, 2000 at 10 p.m. filling sea water into a accumulator unit (to 90 % of its volume)
- Connection to a gas bottle and addition of CH_4 (ascending as bubbles in the accumulator unit) until a pressure of 17 bar was obtained (It was impossible to get higher values with the pressure reducer used)

- Examining the lines and connecting elements – no leakages
- Loss of CH_4 within 24 hours: about 30 bar, that corresponds with 300 liters of methane under normal pressure. Corresponding to the solving capacity diagram for CH_4 in water at the existing pressure 4 liters of methane could have been dissolved at the maximum. The difference, i. e. about 296 liters CH_4, can be assumed to have been bound to gas hydrates in a volume of about 1.8 liters of water. That means that in the accumulator unit gas hydrates had been generated.
- 24 hours later in the night of August 7 at station 66 gas hydrates were taken onboard with the aid of a TV-grab.
- Putting hydrates into a liner and shutting the liner with a cover
- Forwarding the liner to the cold-storage room
- Filling the hydrates into the pressure chamber No. 1 of the PCM
- Shutting the pressure chamber
- Generating a pressure of about 17 bar in the chamber by connecting it with a cylinder containing CH_4
- Connection of the accumulator unit and decanting the gas containing water from the chamber under pressure, and increasing the pressure up to 80 bar by compressed air
- Maintenance of the 80 bar pressure with compressed air on the water surface in the accumulator unit

B. Storage of hydrates in a pressure chamber after dissolving CH_4 in sea water by addition of gas hydrates for a period of 24 hours

- Decanting the saturated sea water against a pressure of 17 bar into the pressure chamber No 2 to the hydrates that have to be stored. Increasing the pressure to 80 bar.

Test Procedure

- On August 8 at station 73 pouring the gas hydrates out of the TV-grab into liners, tilting a ladies' stocking over and then putting them into the accumulator unit; filling the accumulator unit with sea water
- Connecting a gas cylinder and adding CH_4 on the top of the accumulator unit until 17 bars are reached
- On August 9 at station No. 82 gaining hydrates with a TV-grab
- Putting hydrates into a liner and shutting the liner with a cover
- Forwarding the liner to the cold-storage room
- Filling the hydrates into the pressure chamber No. 2 of the PCM
- Shutting the pressure chamber
- Generating a pressure of about 17 bar in the chamber 2 by connecting it with a cylinder containing CH_4
- Connection of the accumulator unit and decanting the gas containing water from the chamber under pressure, and increasing the pressure up to 80 bar by compressed air
- Maintenance of the 80 bar pressure with compressed air on the water surface in the accumulator unit

Results and discussion

The pressure chambers were opened after about 2 months under constant pressure with a basically other procedure than during leg SO143-3 where some valves where opened and the gas expanded. This time at first the water was decanted from the hydrates out of

the pressure chambers No 1 and 2 to prevent an accelerated degassing of the hydrates in the depressurized water during slowly opening the chambers. So it can be evaluated with a high degree of reliability if the gas hydrates could have been conserved.
For the opening procedure described an auxiliary equipment is necessary that was not aboard RV SONNE on leg SO148-2. This equipment will be manufactured by us and handed over to Dr. Bohrmann in time.

First of all, a qualified procedure for a long-time storage of gas hydrates has to be developed. When we succeed in storing the hydrates being sampled by a TV-grab without considerable losses then we can try to put samples out of the autoclave into the PCM. Later on a laboratory transfer chamber will be projected to transfer autoclave samples under their autochthonous pressures. The technology needed therefore was already developed within the frame of the HYACE project.

15 REFERENCES

Boetius, A., Ravenschlag, K., Schubert, C.J., Rickert, D., Widdel, F., Gieseke, A., Amann, R., Jørgensen, B.B., Witte, U. and O. Pfannkuche (2000) A marine microbial consortium apparently mediating anaerobic oxidation of methane. Nature 407: 623-626.

Bohrmann, G., Greinert, J., Suess E. and M. Torres (1998) Authigenic carbonates from Cascadia Subduction Zone and their relation to gas hydrate stability. Geology 26(7): 647-650.

Bohrmann, G., Linke, P. , Suess, E. and O. Pfannkuche (2000) RV SONNE cruise report SO 143. Geomar Report 93: 217pp.

Boulegue, J., Lijama, J.T., Charlou, J.L. and J. Jedwab (1987) Nankai Trough, Japan Trench and Kuril Trench: Geochemistry of fluids sampled by submersible „Nautile". Earth Planet. Sci. Lett. 83: 363-375.

Bralower, T.J.; Thomas, D.J., Zachos, J.C., Hirschmann, M.M., Röhl, U., Sigurdsson, H., Thomas, E. and D.L. Whitney (1997) High-resolution records of the late Paleocene thermal maximum and circum-Caribbean volcanism: Is there a causal link? Geology 25: 963-967.

Brooks, J.M., Field, M.E., and M.C. Kennicutt (1991) Observations of gas hydrates in marine sediments, offshore Northern California. Mar. Geol. 96, 103-109.

Brown, K.M., Sauter, A.W. and L.M. Dorman (1995) Diffusive flux measurement in convergent margin and ridge flank environments: A new sea-floor fluid flux meter system. EOS, Transactions AGU 76: 563.

Caress, D.W. and D.N. Chayes (1996) Improved processing of Hydrosweep DS multibeam data on the R/V Maurice Ewing. Mar. Geophys. Res. 18: 631-650.

Carson, B., Seke, E., Paskevich, V. and M.L. Holmes (1994) Fluid expulsion sites on the Cascadia accretionary prism: Mapping disgenetic deposits with processed GLORIA imagery. Journal of Geophysical Research, 99: 11959-11969.

Cave, M., Griffault, L. and S. Reeder (1998) The extraction and charakterization of pore water from low permeability argillaceous rock samples. 23rd General Assembly of EGS, Nice, Abstr. SE406.

Dickens, G.R., Paull, C., Wallace P. and ODP Leg 164 Scientific Party (1997) Direct measurement of in situ methane quantities in a large gas-hydrate reservoir. Nature 385: 426-428.

Dickens, G.R. (1999) Carbon cycle: The blast in the past. Nature 401: 752-753.

Dickson, A.G. (1993) pH buffers for sea water media based on the total hydrogen ion concentration scale. Deep Sea Res. I 40: 107-118.

Egeberg, P.K. and G.R. Dickens (1999) Thermodynamic and pore water halogen constraints on gas hydrate distribution at ODP Site 997 (Blake Ridge). Chem. Geol. 153: 53 –79.

Egorov, A.V. and A.N. Rozhkov (1997) The scale of upward diffusional flux in bottom sediments of the Baltic Sea in the regions of the gas craters and geocacoustical anomalies. In: Geodekayn, A.A., Romankevitch, E.A. and V.Ya. Trotsuik (eds.), Geochemistry of the Baltic Sea's waters and sediments in the in the region of the gas craters and geoacoustic anomalies occurrence, Moscow, IO RAS, 135-147 (in Russian).

Egorov, A.V., Crane, K., Vogt, P.R. and A. N. Rozhkov (1999) Gas hydrates that outcrop on the sea floor: stability models. Geo-Marine Letters 19: 68-75.

Fossing, H., Gallardo, B.B., Jørgensen, B.B., Huttel, M., Nielsen, L.P., Schulz, H., Canfield, D.E., Forster, S., Glud, R.N., Gundersen, J.K., Kuver, J., Ramsing, N.B., Teske, A., Thamdrup, B. and O. Ulloa (1995) Concentration and transport of nitrate by the mat-forming sulphur bacterium Thioploca. Nature 374: 713-715.

Froelich, P.N., Kvenvolden, K.A., Torres, M.E., Waseda, A., Didyk, B.M. and T.D. Lorenson (1995) Geochemical evidence for gas hydrate in sediment near the Chile triple junction. In: Lewis, S.D., Behrmann, J.H., Musgrave, R.J. and S.C. Cande (eds.) Proc. ODP, Sci. Res. Ocean Drilling Program, TX, 141, 279-286.

Gallardo, V.A. (1977) Large benthic microbial communities in sulphide biota under Peru-Chile subsurface countercurrent: Nature 268: 331-332.

Gamo, T., Hitoshi, S., Ishibashi, J., Shitashima, K. and J. Boulegue (1992) Methane, ethane and total inorganic carbon in fluid samples taken during the 1989 Kaiko-Nankai project. Earth Planet. Sci. Lett. 109: 383-390.

Gieskes, J.M., Gamo, T. and H. Brumsack (1991) Chemical methods for interstitial water analyses on Joides Resolution, Ocean Drill. Program, Texas A&M Univ., College Station.

Ginsburg, G.D., Guseynov, R.A., Dadashev, A.A., Ivanova, G.A., Kazantsev, S.A., Solov'yev, V.A., Telepnev, E.V., Askeri-Nasirov, R.Y., Yesikov, A.D., Mal'tseva, V.I., Mashirov, Y.G. and I.Y. Shabayeva (1992) Gas Hydrates on the Southern Caspian. Int. Geol. Rev. 34(8): 765-782.

Ginsburg, G.D., Soloviev, V.A., Cranston, R.E., Lorenson, T.D. and K.A. Kvenvolden (1993) Gas hydrates from the continental slope, offshore Sakhalin Island, Okhostk Sea. Geo-Marine Letters 13: 41-48.

Grasshoff, M., Ehrhardt, K. and K. Kremling (1983) Methods of seawater analysis, 2nd edition, Verlag Chemie, Weinheim: 419pp.

Greinert, J. (1999) Rezente submarine Mineralbildungen: Abbild geochemischer Prozesse an aktiven Fluidaustrittsstellen im Aleuten- und Cascadia-Akkretionskomplex. GEOMAR Report 87: 196pp.

Greinert, J., Bohrmann, G. and E. Suess (in press) Gas hydrate-associated carbonates and methane venting at Hydrate Ridge: Classification, distribution and origin of authigenic lithologies. In: Paull, C. and W. Dillon (eds.) Natural Gas Hydrates: Occurrence, Distribution, and Dynamics, Washington, American Geophysical Union, Monograph Series.

Hesse, R. and W. E. Harrison (1981) Gas hydrates (clathrates) causing pore water freshening and oxygen isotope fractionation in deep-water sedimentary sections of terrigenous continental margins. Earth Planet. Sci. Lett. 55: 453-462.

Hyndman, R.D. and E.E. Davis (1992) A mechanism for the formation of authigenic carbonates along the Cascadia continental margin: Implications for the global Ca-cycle. Paleography Paleoclimatology 71: 97-118.

Ivanenkov, V.N. and Y.I. Lyakhin (1978) Determination of total alkalinity in seawater. In: Bordovsky, O.K. and V.N. Ivanenkov (eds.) Methods of hydrochemical investigations in the ocean, Nauka Publ. House, Moscow: 110-114 (in Russian).

Jannasch, H.W., Nelson, D.C. and C.O. Wirsen (1989) Massive natural occurrence of unusually large bacteria (Beggiatoa sp.) at the hydrothermal deep-sea vent site. Nature 342: 834-836.

Jørgensen, B.B. (1977) Bacterial sulfate reduction within reduced microniches of oxidized marine sediments. Mar. Biol. 41: 7-17.

Karpen, V. (1999) Experimentelle Untersuchungen von Austauschprozessen in der Sediment-Wasser-Grenzschicht. Diplomarbeit, Christian-Albrechts-Universität Kiel.

Kastner, M., Kvenvolden, K.A., Whiticar, M.J., Camerlenghi, A. and T.D. Lorenson (1995) Relation between pore fluid chemistry and gas hydrates asociated with bottom simulating reflectors at the Cascadia Margin, Sites 889 and 892. In: Carson, B., Westbrook, G.K., Musgrave, R.J. and E. Suess (eds.) Proc. ODP, Sci. Results 146: College Station, Texas: 175-187.

Kastner, M., Kvenvolden, K.A. and T.D. Lorenson (1998) Chemistry, isotopic composition, and origin of a methane-hydrogen sulfide hydrate at the Cascadia subduction zone. Earth Planet. Sci. Lett. 156: 173-183.

Katz, M., Pak, D., Dickens, D. and K. Miller (1999) The source and fate of massive carbon input during the latest Paleocene Thermal Maximum. Science 286: 1531-1533.

Kennett, J.P. and L.D. Stott (1991) Abrupt deep-sea warming, palaeooceanographic changes and benthic extinctions at the end of the Palaeocene. Nature 353: 225-229.

Kennett, J.P., Cannariato, K.G., Hendy, I.L. and R.J. Behl (2000) Carbon isotopic evidence for methane hydrate instability during Quaternary interstadials. Science 288: 128-133.

Kulm, L.D., Suess, E., Moore, J.C., Carson, B., Lewis, B.T., Ritger, S.D., Kadko, D., Thornburg, T.M., Embley, R., Rugh, W., Massoth, G., Langseth M. and G. Cochrane (1986) Oregon margin subduction zone: Venting, Fauna and Carbonates. Science 231, 561-566.

Kvenvolden, K.A. and L. A. Barnard (1983) Gas hydrates of the Blake Outer Ridge, Site 553, Deep Sea Drilling Project Leg 76. In: Sheridan, R.E., Gradstein, F.M., et al. Init. Repts. DSDP, 76: Washington (U.S. Govt. Printing Office): 353-365.

Kvenvolden, K.A. (1988) Methane hydrate-a major reservoir of carbon in the shallow geosphere? Chem. Geol. 17: 41-51.

Kvenvolden, K.A. and M. Kastner (1990) Gas hydrates of the Peruvian outer continental margin. In: Suess, E., von Huene, R. et al. Proc. ODP, Sci. Results, 112: College Station, TX (Ocean Drilling Program): 55-63.

Kvenvolden, K.A. (1993) Gas hydrates – Geological perspective and global change. Rev. Geophys. 31: 173-183.

Lammers, S. and E. Suess (1994) An improved head-space analysis method for methane in seawater. Mar. Chem. 47: 115-125.

Linke, P., Suess, E., Torres, M., Martens, V., Rugh, W.D., Ziebis W. and L.D. Kulm (1994) *In situ* measurement of fluid flow from cold seeps at active continental margins. Deep-Sea Research, 41, 721-739.

Linke, P., Pfannkuche, O., Torres, M.E., R.W. Coller, Witte, U., McManus, J., Hammond, D.E., Brown, K.M., Tryon, M.D. and K. Nakamura (1999) Variability of benthic flux and discharge rates at vent site determined by in situ intruments. EOS 80(46): 509.

Lorenson, T.D. and T.S. Collett (2000) Gas content and composition of gas hydrate from sediments of the southeastern North American continental margin. In: Paull, C.K., Matsumoto, R., Wallace, P.J., et al. Proc. ODP, Init. Repts., 164: College Station, TX (Ocean Drilling Program): 37-46.

MacDonald, I.R., Guinasso, N.L.J., Sassen, R., Brooks, J.M., Lee, L. and K.T. Scott (1994) Gas hydrate that breaches the sea floor on the continental slope of the Gulf of Mexico. Geology 22: 699-702.

MacKay, M.E., Moore, G.F., Cochrane, G.R., Moore, J.C. and L.D. Kulm (1992) Landward vergence and oblique structural trends in the Oregon margin accretionary rism: Implications and effect on fluid flow. Earth Planet. Sci. Lett. 109: 477-491.

MacKay, M.E., Jarrard, R.D., Westbrook, G.K. and R.D. Hyndman (1994) Origin of bottom simulating reflectors: Geophysical evidence from the Cascadia accretionary prism. Geology 22: 459-462.

MacKay, M.E. (1995) Structural variation and landward vergence at the toe of the Oregon accretionary prism. Tectonics 14: 1309-1320.

Matsumoto, R. and W.S. Borowski (2000) Gas hydrate estimates from newly determined oxygen isotopic fractionation (_GH-IW) and _^{18}O anomalies of the interstitial waters: LEG 164, Blake Ridge. In: Paull, C.K., Matsumoto, R., Wallace, P.J., et al. Proc. ODP, Sci. Results, 164: College Station, TX (Ocean Drilling Program): 59-66.

Matsumoto, R., Uchida, T., Waseda, A., Uchida, T., Takeya, S., Hirano, S., Yamada, K., Maeda, Y. and T. Okui (2000) Occurrence, structure, and composition of natural gas hydrates recovered from the Blake Ridge, Nortwest Atlantic. In: Paull, C.K., Matsumoto, R., Wallace, P.J., et al. Proc. ODP, Sci. Results, 164: College Station, TX (Ocean Drilling Program): 13-28.

Mienert, J. and J. Posewang (1997) Flach- und Tiefwassergashydrate in Sedimenten polarer Kontinentalränder des Nordatlantiks. Geowissenschaften 15(9): 287-291.

Moore, C. and P. Vrolijk (1992) Fluids in accretionary prisms. Revue Geophys. 30: 113-135.

Moore, W.S. (1996) Large groundwater inputs to coastal water revealed by ^{226}Ra enrichments. Nature 380: 612-614.

Norris, R. and U. Röhl (1999) Carbon cycling and chronology of climate warming during the Paleocene/Eocene transition. Nature 401: 775-778.

Paull, C.K., Matsumoto, R., Wallace, P.J., et al. (1996) Proc. ODP, Init. Repts., 164: College Station, TX (Ocean Drilling Program).

Rice, D.D. and G.E. Claypool (1981) Generation, accumulation, and resource potential of biogenic gas. AAPG Bull. 65: 5-25.

Rickert, D., Heuser, A., Domeyer, B. and B. Heitmann (1999) Pore water chemistry. In: Bohrmann, G., Linke, P. and O. Pfannkuche (eds.) RV SONNE Cruise Report SO143 TECFLUX-I-, GEOMAR Report 93: 65-74, 120-128, 184-194.

Rickert, D., Suess, E., Linke, P. and M. Haeckel (in prep.) Gas hydrate formation in sediments of the Cascadia margin: formation rate, salt exclusion, and fluid-flow rates. A model approach. Geochim. Cosmochim. Acta.

Rosenfield, W.D. and S.R. Silverman (1959) Carbon isotope fractionation in bacterial production of methane. Science 130: 1658-1659.

Rothwell, R.G., Thomsen, J. and G. Kähler (1998) Low-sea-level emplacement of a very large Late Pleistocene 'megaturbite' in the western Mediterranean Sea. Nature 392: 377-380.

Sassen, R. and I.R. MacDonald (1994) Evidence of structure H hydrate, Gulf of Mexico continental slope. Org. Geochem. 22: 1029-1032.

Sassen, R., MacDonald, I.R., Guinasso Jr., N.L., Joye, S., Requejo, A.G., Sweet, S.T., Alcala-Herrera, J., DeFreitas, D.A. and D.R. Schink (1998) Bacterial methane oxidation in sea-floor gas hydrate: significance to life in extreme environments. Geology 26(9): 851-854.

Schoell, M. (1980) The hydrogen and carbon isotopic composition of methane from natural gases of various origins. Geochim. Cosmochim. Acta 44: 649-661.

Schulz, H.N., Brinkhoff, T., Ferdelman, T.G., Hernadéz Mariné, M., Teske, A. and B.B. Jørgensen (1999) Dense populations of a giant sulfur bacterium in Namibian shelf sediments. Science 284: 493-495.

Shipley, T.H. and W.B. Didyk (1982) Occurrence of methane hydrates offshore southern Mexico. In: Watkins, J. S., Moore, J.C., et al. Init. Rep. DSDP, 66: Washington (U.S. Govt. Printing Office): 547-555.

Sloan Jr., E.D. (1998) Physical/chemical properties of gas hydrates and application to world margin stability and climate change. In: Henriet, J.-P. and J. Mienert (eds.) Gas Hydrates: Relevance to world margin stability and climate change, Geological Society 137: 31-50.

Sonnenfeld, P. (1984) Brines and Evaporites. Academic Press.

Spieß, V. (1993) Digitale Sedimentechographie - Neue Wege zu einer hochauflösenden Akustostratigraphie. Berichte, Fachbereich Geowissenschaften 35: p. 199.

Suess, E., Carson, B., Ritger, S.D., Moore, J.C., Kulm, L.D. and G.R. Cochrane (1985) Biological communities at vent sites along the subduction zone off Oregon. In: M.C. Jones (ed.) The hydrothermal vents of the Eastern Pacific: An overview, Bulletin of the Biological Society of Washington, 6: 475-484.

Suess, E., von Huene, R., et al. (1988) Proc ODP, Init. Repts. 112, College Station, TX (Ocean Drilling Program): 1015 pp.

Suess, E. and G. Bohrmann (1997) FS-Sonne Cruise Report SO 110, GEOMAR Report 59: 181pp.

Suess, E., Torres, M., Bohrmann, G., Collier, R.W., Greinert, J., Linke, P., Rehder, G., Trehu, A., Wallmann, K., Winckler, G. and E. Zuleger (1999) Gas hydrate destabilization: enhanced dewatering, benthic material turnover and large methane plumes at the Cascadia convergent margin. Earth and Planetary Science Letters 170: 1-15.

Suess, E. and J. Thiede (1999) Gashydrate im Geosystem, Forschungszentrum Jülich Gmbh, Projektträger BEO, Jülich Warnemünde: 64 pp.

Suess, E. et al. (in prep.) Extreme salt and isotope fractionation documented above marine gas hydrates.

Suess, E., Torres, M., Bohrmann, G., Collier, R.W., Rickert, D., Goldfinger, C., Linke, P., Heuser, A., Sahling H., Heeschen, K., Jung, C., Nakamura, K.-i., Greinert, J., Pfannkuche, O., Trehu, A., Klinkhammer, G., Whiticar, M., Eisenhauer, A., Teichert, B. and M. Elvert (in press) Sea floor methane hydrates at Hydrate Ridge, Cascadia Margin. In: Paull, C. and W. Dillon (eds.) Natural Gas Hydrates: Occurrence, Distribution, and Dynamics, American Geophysical Union, Monograph Series, Washington.

Tilbrook, B.D. and D.M. Karl (1994) Dissolved Methane Distributions Sources, and Sinks in the Western Bransfield Strait. Antarctica. J. Geophys. Res. 99C(8): 16383-16393.

Torres, M.E., Brown, K.M., Collier, R.W., DeAngelis, M.A., Hammond, D., McManus, J., Rehder, G. and A. Trehu (1998) Geochemical observations on Hydrate Ridge, Cascadia Margin during R/V Brown-ROPOS cruise, August 1998. Oregon State University COAS-Data Report 171, Ref. 98-4.

Torres, M., Bohrmann, G., Brown, K., deAngelis, M., Hammond, D., Kllinkhammer, G., McManus, J., Suess, E. and A. Trehu (1999) Atlantis Geochemical observations on Hydrate Ridge, Cascadia margin during R/V-ATLANTIS-cruise AT 3-35b, July 1999: Oregon State University, COAS-Data Report 174.

Tréhu, A., Torres, M., Moore, G., Suess, E. and G. Bohrmann (1999) Temporal and spatial evolution of a gas hydrate-bearing accretionary ridge on the Oregon continental margin. Geology 27(10): 939-942.

Tryon, M., Brown, K., Torres, M., Trehu, A., McManus, J. and R.W. Collier (1999) Measurements of transience and downward fluid flow flux near episodic methane gas vents, Hydrate Ridge, Cascadia. Geology, 27(12): 1075-1078.

Ussler, W. III. and C.K. Paull (1995) Effects of ion exclusion and isotope fractionation on pore water geochemistry during gas hydrate formation and decomposition. Geo-Mar. Let. 15: 37-44.

Vogt, P.R., Cherkashev, G., Ginsburg, G., Ivanov, G., Milkov, A., Crane, K., Lein, A., Sundvor, E., Pimenov, N. and A. Egorov (1997) Haakon Mosby Mud Volcano provides unusual example of venting. EOS 78(48): 549.

Von Huene, R., Aubouin, J., et al. (1985) Init. Repts. DSDP, 84: Washington (U.S. Govt. Printing Office).

Wallmann, K., Linke, P., Suess, E., Bohrmann, G., Sahling, H., Schlüter, M., Dählmann, A., Lammers, S., Greinhert, J. and N. von Mirbach (1997) Quantifying fluid flow, solute mixing, and biogeochemical turnover at cold vents of the eastern Aleutian subduction zone. Geochimica et Cosmochimica Acta 61(24): 5209-5219.

Wallmann, K., Bollwerk, S., Kolevica, A. and Y. Shulga (1999) Pore Water Geochemistry. In: Biebow, N., Lüdmann, T., Karp, B. and R. Kulinich (eds.) KOMEX V and VI Cruise Reports, GEOMAR Report 88: 153-173.

Weiss, R.F. (1970) The solubility of nitrogen, oxygen and argon in water and seawater. Deep-Sea Res. 17: 721-735

Westbrook, G.K., Carson, B., Musgrave, R.J. and E. Suess (1995) Proc. ODP, Init. Rep. 146 (Pt. 1): College Station, TX (Ocean Drilling Program), 477 pp.

Whiticar, M.J., Faber E. and M. Schoell (1986) Biogenic methane formation in marine and freshwater environments: CO_2 reduction vs. acetate fermentation - Isotope evidence. Geochimica et Cosmochimica Acta 50: 693-709.

Whiticar, M.J. (1999) Carbon and hydrogen isotope systematics of bacterial formation and oxidation of methane. Chem. Geol. 161: 291-314.

Wiesenburg, D.A. and N.L. Guinasso Jr. (1979) Equilibrium solubilities of methane, carbon monoxide, and hydrogen in water in sea water. Journal of chemical and engineering data 24(4): 356-360.

Woodside, J.M., Ivanov, M.K., Limonov, A.F. and Shipboard Scientists of the Anaxiprobe Expeditions (1998) Shallow gas and gas hydrates in the Anaximander Mountains region, eastern Mediterranean Sea. In: Henriet, J.-P. and J. Mienert (eds.) Gas Hydrates: Relevance to world margin stability and climate change, Geological Society 137: 177-193.

Yefremova, A.G. and B.P. Zhizchenko (1974) Occurrence of crystal hydrates of gases in the sediments of modern marine basins. Doklady Akademii Nauk SSSR 214(5): 1179-1181.

Yuan, T., Hyndman, R.D., Spence, G.D. and B. Desmons (1996) Seismic velocity increase and deep-sea gas hydrate concentration above a bottom simulating reflector on the Northern Cascadia continental slope. J. Geophys. Res. 101: 13655-13671.

Zachos, J.C., Lohmann, K.C., Walker, J.C.G. and S.W. Wise (1993) Abrupt climate change and transient climates during the Oaleogene: A marine perspective. Geology 101: 191-213.

Zhou, Y., Goldfinger, C., Johnson, J.E., Torres, M.E., Trehu, A.M., Clague, D., Paull, C. and G. Bohrmann (1999) Distribution and morphology of venting-related carbonates near Hydrate Ridge, Oregon Margin, based on sidescan sonar and multibeam imagery. EOS transactions, 80(46), Fall Meet. Suppl.: F510.

Zonenshayn, L.P., Murmaa, I.O., Baranov, B.V., Kuznetsov, A.P., Kuzin, V.S., Kuz´min, M.I., Avdeyko, G.P., Stunzhas, P.A., Lukashin, V.N., Barash, M.S., Valyashko, G.M. and L.L. Demina (1987) An underwater gas source in the Sea of Okhotsk West of Paramushir Island. Oceanology 27(5): 598-602.

Appendix

SONNE 148 **Station list**

			Time (UTC)					Begin / on seafloor		End / off seafloor			
2000	St.No. SO148/	Instrument	Begin	on sea-floor	off sea-floor	End	Duration hh:mm	Latitude N°	Longitude W°	Latitude N°	Longitude W°	Water depth (m)	Recovery Remarks
23. 7.	1	ROPOS-558	1:28	1:43	3:03	3:29	2:01	48°18.078	125°53.067	48°19.566	125°53.374	780	test dive
23. 7.	2	CTD-1	3:54	4:34		5:41	1:47	44°34.170	125°08.890	44°34.160	125°08.850	777	24 bottles
24. 7.	3	OFOS-1	7:35	7:41	13:00	13:08	5:33	44°34.261	125°08.978	44°37.920	124°42.886	132	
24. 7.	4	ROPOS-559	15:55	16:03	22:25	22:29	6:34	44°34.261	125°08.978	44°34.107	125°09.050	758	5 samples
25. 7.	5	OFOS-2	0:30	0:47	2:25	2:52	2:22	44°34.053	125°08.465	44°33.981	125°09.446	811	
25. 7.	6	TV-MUC-1	3:22			4:12	0:50						not deployed
25. 7.	7	CTD-2	4:42	5:21		6:37	1:55	44°35.670	125°10.330	44°35.700	125°10.300	1158	17 bottles
25. 7.	8	CTD-3	8:16	8:46		9:48	1:32	44°33.010	125°07.040	44°32.980	125°07.030	1004	22 bottles
25. 7.	9	OFOS-3	10:40	11:41	14:09	14:13	3:33	44°33.215	125°11.487	44°31.729	125°13.027	996	
25. 7.	10	ROPOS-560	15:24	15:52	21:49	22:22	6:58	44°34.171	125°08.720	44°34.195	125°08.829	725	6 samples
25. 7.	11	TV-MUC-2	23:15	23:52		0:17	1:02	44°34.175	125°08.750	44°34.225	125°08.135	776	4 cores
26. 7.	12	TV-MUC-3	0:55	1:31		1:56	1:01	44°34.233	125°08.835	44°34.235	125°08.844	775	3 cores, 10-18 cm
26. 7.	13	ISSO-1	4:15	4:40		5:29	1:14	44°34.180	125°08.834			775	deployed 3 times
26. 7.	14	TV-MUC-4	6:00	7:04		7:33	1:33	44°34.178	125°08.864	44°34.218	125°08.804	777	4 cores, 12-16 cm
26. 7.	15	CTD-4	8:45	9:15		10:18	1:33	44°32.750	125°08.040	44°32.760	125°08.020	968	23 bottles
26. 7.	16	OFOS-4	11:32	11:48	14:57	15:21	3:49	44°40.138	125°06.507	44°40.120	125°03.254	620	
26. 7.	17	ROPOS-561	15:36			23:09	7:33	44°40.161	125°05.822	44°40.166	125°05.875	?	4 samples
27. 7.	18	LANDER I	0:15	0:46	0:54	1:18	1:03	44°34.229	125°08.824	44°34.226	125°08.806	776	deployed
27. 7.	19-1	TV-MUC-5	3:00	3:24	3:34	4:00	1:00	44°34.222	125°08.796	44°34.228	125°08.791	776	3 cores, 10-14 cm
27. 7.	19-2	TV-MUC-6	4:24	4:40	4:43	7:02	2:38	44°34.197	125°08.793	44°34.104	125°08.807	777	6 cores, 20-26 cm
27. 7.	20	ISSO-2	6:15					44°34.173	125°08.807			776	not deployed
27. 7.	21	OFOS-5	8:08	8:26	9:45	10:02	1:54	44°34.124	125°08.754	44°26.994	125°01.752	744	
27. 7.	22	CTD-5	10:52	11:30		12:12	1:20	44°26.990	125°01.890	44°26.990	125°01.810	620	22 bottles
27. 7.	23	ROPOS-562	15:30	15:30	22:57	23:00	7:30	44°40.194	125°05.854	44°40.165	125°05.885	587	
28. 7.	24	LANDER II	0:30	0:51		3:13	2:43	44°39.945	125°05.732			609	not deployed
28. 7.	25	LANDER II	5:10	5:40		7:10	2:00	44°34.197	125°08.895			777	not deployed
28. 7.	26	OFOS-6	8:05	8:33	10:42	11:07	3:02	44°27.145	125°02.546	44°26.894	125°01.819	636	
28. 7.	27	CTD-6	12:00	12:34		13:43	1:43	44°32.350	125°08.950	44°32.350	125°08.960	980	22 bottles
28. 7.	28	TV-MUC-7	14:30	14:50	15:22	15:47	1:17	44°34.235	125°08.842	44°34.196	125°08.816	777	4 cores, 11-17cm
28. 7.	29	TV-MUC-8	16:00	16:25	16:54	17:21	1:21	44°34.232	125°08.613	44°34.222	125°08.834	777	7 cores, 20-26 cm
28. 7.	30	ROPOS-563	17:55	18:06	21:45	22:10	4:15	44°34.195	125°08.849	44°34.195	125°08.824	760	7 samples
28. 7.	31	CTD-7	23:06	23:41		0:46	1:40	44°34.780	125°11.560	44°34.810	125°11.580	1161	22 bottles
29. 7.	32	ISSO-3	1:30	1:50		2:56	1:26	44°34.252	125°08.877			779	deployed 2 times
29. 7.	33	ROPOS - 564	15:20	15:44	22.08	22:34	7:14	44°40.180	125°05.918	44°40.181	125°05.893		2 samples
29. 7.	34	CTD-8	23:39	0:06		0:50	1:11	44°40.490	125°08.020	44°40.610	125°08.020	752	20 bottles
30. 7.	35	LANDER II	1:30	1:52	2:00	2:29	0:59	44°40.046	125°06.062	44°40.039	125°06.029	607	deployed
30. 7.	36	TV-G - 1	3:45	4:06	4:17	5:30	1:45	44°34.098	125°08.873	44°34.190	125°08.847	786	gas hydrates, carbonates
30. 7.	37	TV-MUC-9	5:45		6.09	6:57	1:12	44°34.194	125°08.837	44°34.195	125°08.838	788	2 cores, 12-16 cm
30. 7.	38	TV-MUC-10	7:00	7:16	7:18	7:50	0:50	44°34.202	125°08.838	44°34.186	125°08.847	787	4 cores, 15-19 cm
30. 7.	39	OFOS-7	9:12	9:30	11:42	12:02	2:50	44°24.196	125°00.205	44°24.197	125°01.720	676	
30. 7.	40	CTD-9	13:23	13:59		15:16	1:53	44°34.220	125°13.060	44°34.210	125°13.010	1350	24 bottles
30. 7.	41	ROPOS - 565	16:29	17:02	22:21	23:15	6:46	44°27.061	125°01.694	44°27.012	125°01.921		8 samples
30. 7.	42	LANDER I	23:57			0:38	0:41						recovery
31. 7.	43	CTD-10	1:09	1:42		2:42	1:33	44°33.480	125°06.560	44°33.500	125°06.530	1036	22 bottles
31. 7.	44	TV-MUC-11	3:25	3:49	4:22	4:47	1:22	44°34.265	125°08.817	44°34.185	125°08.834	776	5 cores, 15-19 cm
31. 7.	45	ISSO-4	5:35	5:45		6.15	0:40	44°34.187	125°08.810			776	
31. 7.	46	OFOS-8	7:51	8:10	11:44	11:45	3:54	44°38.102	125°04.935	44°38.498	125°08.802	941	
31. 7.	47	CTD-11	12:49	13:18		14:06	1:17	44°40.170	125°09.020	44°40.180	125°09.020	851	24 bottles
31. 7.	48	ROPOS - 566	15:10	15:38	22:01	22:30	7:20	44°40.136	125°05.911	44°40.135	125°05.882		4 samples
31. 7.	49	LANDER I	23:52	0:19	0:52	1:19	1:27	44°39.891	125°06.114	44°39.873	125°06.097	601	deployed

SONNE 148 **Station list**

2000	St.No. SO148/	Instrument	Time (UTC) Begin	on sea-floor	off sea-floor	End	Dura-tion hh:mm	Begin / on seafloor Latitude N°	Longitude W°	End / off seafloor Latitude N°	Longitude W°	Water depth (m)	Recovery Remarks
01. 8.	50	CTD-12	1:48	2:15		3:00	1:12	44°40.960	125°07.003	44°40.990	125°07.004	706	20 bottles
01. 8.	51	TV-MUC-12	4:06	4:36		5:00	0:54	44°34.191	125°08.865	44°34.198	125°08.858	775	6 cores, 12-16 cm
01. 8.	52	TV-MUC-13	5:20	6:26		7:25	2:05			44°34.201	125°08.808	777	4 cores, 13-18 cm
01. 8.	53	OFOS-9	8:04	8:26	11:54	12:35	4:31	44°34.368	125°00.781	44°34.241	125°00.237	1027	
01. 8.	54	CTD-13	13:31	14:01		14:59	1:28	44°31.760	125°10.120	44°31.830	125°10.008	1062	23 bottles
01. 8.	55	LANDER II	16:13			16:35	0:22	44°39.920	125°06.180				recovery
01. 8.	56	TV-G-2	17:48	18:07		20:02	2:14	44°34.200	125°08.920	44°34.160	125°08.810	779	not deployed
01. 8.	57	TV-G-3	20:36	20:53	21:40	21:43	1:07	44°34.185	125°08.867	44°34.154	125°08.807	777	gas hydrates
01. 8.	58	TV-G-4	22:38	22:56	23:38	0:40	2:02	44°34.154	125°08.900	44°34.172	125°08.831	776	gas hydrates
02. 8.	59	CTD-14	2:06	2:33		3:29	1:23	44°41.640	125°06.004	44°41.670	125°06.004	774	20 bottles
05. 8.	60	ROPOS - 567	15:12	15:38	22:49	23:17	8:05	45°35.872	125°09.376	45°36.789	125°09.918	632	7 samples
06. 8.	61	CTD-15	5:58	6:32		7:31	1:33	44°39.480	125°10.010	44°39.520	125°10.000	1009	22 bottles
06. 8.	62	OFOS-10	8:31	8:53	12:00	12:26	3:55	44°34.503	125°00.014	44°34.303	124°59.791	904	
06. 8.	63	TV-MUC-14	13:23	13:45	13:53	14:25	1:02	44°34.188	125°08.813	44°34.197	125°08.812	776	3 cores, 15-28 cm
06. 8.	64	ROPOS - 568	15:25	16:04	0:39	1:08	9:43	44°34.192	125°08.800	44°34.198	125°08.846	758	no samples
07. 8.	65	TV-G-5	2:03	2:18	4:45	5:15	3:12			44°34.197	125°08.830	777	carbonates
07. 8.	66	TV-G-6	5:52		6:31	8:10	2:18			44°34.207	125°08.845		gas hydrates, carbonates
07. 8.	67	CTD-16	9:10	9:42		10:43	1:33	44°36.490	125°09.050	44°36.480	125°09.030	1027	24 bottles
07. 8.	68	ISSO-5	11:28	11:50		12:45	1:17	44°34.176	125°08.823	44°34.165	125°08.829	776	
07. 8.	69	ROPOS - 569	16:08	18,3	21:41	22:27	6:19	44°34.199	125°08.855	44°34.204	125°08.822	760	no samples
08. 8.	70	OFOS-11	3:33	3:58	7:07	7:27	3:54	44°39.148	125°03.004	44°39.270	125°06.909	1062	
08. 8.	71	CTD-17	8:24	9:02		10:20	1:56	44°38.800	125°10.650	44°38.800	125°10.630	1351	22 bottles
08. 8.	72	CTD-18	11:12	11:57		13:19	2:07	44°33.200	125°13.300	44°33.200	125°13.320	1591	23 bottles
08. 8.	73	TV-G-7	14:00		14:30	15:15	1:15			44°34.188	125°08.825	777	gas hydrates, carbonates
08. 8.	74	ROPOS - 570	15:59	16:42	23:34	0:41	8:42	44°34.181	125°08.849	44°34.113	125°09.160	764	9 samples
09. 8.	75	TV-MUC-15	1:59	2:26	2:35	3:10	1:11	44°34.266	124°59.942	44°34.311	124°59.976	797	3 cores, 23-24 cm
09. 8.	76	SL-1	4:15	4:38		5:33	1:18			44°34.288	124°59.983	887	477 cm
09. 8.	77	CTD-19	7:12	7:28		7:48	0:36	44°38.560	124°45.370				14 bottles
09. 8.	78	CTD-20	8:41	9:00		9:28	0:47	44°37.680	124°50.650	44°37.670	124°50.630	410	14 bottles
09. 8.	79	CTD-21	10:28	10:49		11:33	1:05	44°36.700	124°56.150	44°36.700	124°56.170	714	20 bottles
09. 8.	80	SL-2	13:55	14:10		14:31	0:36			44°36.782	124°55.951	776	50 cm
09. 8.	81	ROPOS - 571	15:31	15:49	22:32	23:12	7:41	44°34.097	125°09.176	44°34.208	125°08.803	760	3 samples
09. 8.	82	TV-G-8	23:50	0:09	0:21	1:19	1:29	44°34.440	125°08.870	44°34.220	125°08.790	777	gas hydrates, carbonates
10. 8.	83	OFOS-12	3:40	3:59	8:53	9:12	7:41	44°24.120	125°00.464	44°23.899	125°00.896	667	
10. 8.	84	OFOS-13	9:39			9:55	0:16						cable problem
10. 8.	85	SL-3	13:20	13:53		14:20	1:00	44°34.208	125°08.834	44°34.212	125°08.872	777	209 cm
10. 8.	86	SL-4	15:09	15:29		16:21	1:12	44°34.216	125°08.812	44°34.217	125°08.816	777	248 cm
10. 8.	87	CTD-22	20:19	20:44		22:06	1:47	44°43.500	125°22.500	44°43.500	125°22.510	2843	20 bottles
10. 8.	88	TV-MUC-16	23:48	0:18	0:58	1:30	1:42	44°34.220	125°08.800	44°34.286	125°08.801	777	not deployed
11. 8.	89	TV-MUC-17	1:32			1:54	0:22						not deployed
11. 8.	90	TV-MUC-18	4:37	5:01	5:03	5:40	1:03	44°34.201	125°08.826	44°34.200	125°08.830	777	4 cores
11. 8.	91	TV-MUC-19	5:44	6:05	6:08	6:40	0:56	44°34.200	125°08.820			778	3 cores
11. 8.	92	TV-MUC-20	6:44	7:04	7:08	8:00	1:16	44°34.212	125°08.821	44°34.208	125°08.809	777	8 cores
11. 8.	93	TV-MUC-21	8:07	8:29	8:30	9:10	1:03	44°34.164	125°08.845	44°34.182	125°08.822	776	5 cores
11. 8.	94	TV-MUC-22	9:12	9:34	9:47	10:20	1:08	44°34.199	125°08.835	44°34.202	125°08.805	776	7 cores
11. 8.	95	TV-MUC-23	10:30	10:50	10:54	11:15	0:45			44°34.145	125°08.855		5 cores
11. 8.	96	CTD-23	12:29	13:01		14:08	1:39	44°42.700	125°04.950	44°42.760	125°04.830	1184	24 bottles
11. 8.	97	ROPOS - 572	15:01	15:32	17:22	17:56	2:55	44°39.841	125°06.139	44°40.166	125°05.936	591	3 samples
11. 8.	98	ROPOS - 573	20:05	20:40	23:24	0:06	4:01	44°34.199	125°08.878	44°34.195	125°08.822	763	no samples
12. 8.	99	TV-G-9	0:35		1:35	2:50	2:15	44°34.172	125°08.851	44°34.187	125°08.824	772	gas hydrates, carbonates

SONNE 148			Station list										
			Time (UTC)					Begin / on seafloor		End / off seafloor			
2000	St.No. SO148/	Instrument	Begin	on sea-floor	off sea-floor	End	Duration hh:mm	Latitude N°	Longitude W°	Latitude N°	Longitude W°	Water depth (m)	Recovery Remarks
12. 8.	100	OFOS-14	3:34	4:13	10:43	11:05	7:31	44°34.309	125°08.629	44°34.154	125°08.883	778	
12. 8.	101	CTD-24	11:54	12:21		13:09	1:15	44°35.960	125°03.340	44°36.000	125°00.320	1007	24 bottles
12. 8.	102	ISSO-6	14:00	14:45		16:15	2:15	44°34.181	125°08.818	44°34.220	125°08.890	776	dropped 6 times
12. 8.	103	ROPOS - 574	17:24	18:01	21:14	22:22	4:58	44°43.782	125°13.729	44°43.771	125°13.679	938	9 samples
12. 8.	104	ISSO-7	22:45	23:16		0:44	1:59	44°43.760	125°13.730	44°43.600	125°13.990	965	dropped 7 times
13. 8.	105	KOL-1	2:19			3:40	1:21	44°34.127	125°08.797			777	234 cm
13. 8.	106	CTD-25	5:03	5:27		6:23	1:20	44°34.820	125°13.760	44°34.830	125°13.710	949	21 bottles

Abbreviations: CTD (Conductivity temperature depth)
ISSO (in-situ Schlieren-optic)
KOL (Piston Corer)

OFOS (Ocean floor observation system)
ROPOS (The remotely operated platform for ocean sciences)
SL (Gravity Corer)
TV-G (TV-Grab sampler)
TV-MUC (TV-Multicorer)

Annotations: all Lat./Long. positions are ssbl positions
= ssbl positions, except CTD, ROPOS-558, TV-G 82, TV-MUC 11 and 14, KOL 105